THE DEVELOPMENT OF SATELLITE DERIVED NITRATE AND STRATIFICATION INDICES FOR THE SOUTHERN BENGUELA ECOSYSTEM

Madoda Brian Khumalo

A thesis presented for the degree of Master of Science

Department of Oceanography
Faculty of Science
University of Cape Town
South Africa

UNIVERSITY OF CAPE TOWN
IYUNIVESITHI YASEKAPA • UNIVERSITEIT VAN KAAPSTAD

Abstract

An earth observation based study was conducted in the southern Benguela upwelling system, aimed at developing remotely sensed proxies to determine ecological conditions conducive to the formation of harmful algal blooms (HAB) which are endemic to the system. The aim of this study was to identify the relationship between nutrient availability, turbulence and phytoplankton community assemblages using remotely sensed data. Certain phytoplankton functional groups are adapted to a particular environment within an ecological space conceptually based on the nutrient availability and turbulence (Margalef, 1978). Two proxies, representing the nutrient availability, and turbulence or stratification, were created using satellite-derived surface nitrate (NO_3) concentrations and the 12ºC isotherm (Iso_{12}) depths, and used to define the ecosystem state through Margalef's Mandala (Margalef, 1978). The approach involved the development of robust algorithms using *in situ* data collected in the greater St Helena Bay region to estimate the surface NO_3 concentrations and the depth of the Iso_{12} for the southern Benguela, using remotely sensed sea surface temperatures (SST) and wind data. The derivation of the nutrient proxy was based on a model initially developed by Dugdale et al., (1989) then modified by Silió-Calzada et al., (2008) for use in the Benguela. The turbulence proxy was derived using a simple linear regression model to estimate the depth of the Iso_{12} which was utilized as a proxy for the thermocline depth in the system. The performance of the nutrient and turbulence proxies were assessed on local, meso- and synoptic scales for their ability to resolve the event and seasonal scale variations in the inner shelf environment of the southern Benguela. The derived NO_3 and Iso_{12} products were sufficiently able to resolve the event and mesoscale variability of the system in 2005, 2006 and 2007. The performance of the products at capturing the annual and intra-seasonal variability of the system was satisfactory, displaying an ability to resolve the ecosystem upwelling variability. Using the NO_3 and Iso_{12} products as the nutrient and turbulence proxies was satisfactory as a first attempt at using earth observation to classify the ecosystem according to Margalef's Mandala (Margalef, 1978). The proxies were able to model the ecosystem inner-shelf environment for multiple years and thus create the ability to hypothesize ecosystem sub-habitats occupied by particular life forms of phytoplankton. There were however two concerns that needed further consideration in the approach: 1).The large warm bias discovered between the *in situ* and remotely sensed temperatures which had a

direct influence on the validity of the algorithms in the ecosystem and 2.) The temporal and spatial disconnects between the physical forcing and biological response of the ecosystem and subsequent impact upon the utility of the remotely sensed proxies.

Acknowledgements

I would like to thank my supervisor, Dr. S. Bernard for the invaluable assistance, travel opportunities, ideas and support which made the completion of this dissertation a possibility. A further equally important hand of gratitude must go towards two people in the Marine Remote Sensing Unit at the CSIR, without whom, this study would not have been possible: Mr C. Whittle for the extraction and help with the MODIS and QuickScat data sets which were central to this project and always being on hand for any problems I encountered; and Mr Andy Rabagliati for organizing the MERIS data .

A further large appreciation is reserved for Drs. G. Pitcher and T. Probyn for allowing me the use of their *in situ* data set. My appreciation is also extended to my financial supporters, the National Research Fund and the Applied Center for Climate and Earth Systems Science programs.

A final thank you is reserved for: my friends and family, for their tireless motivation and support during this project and last but not least I would like to thank my mother for all of her financial and emotional support during the duration of this project.

Contents

CHAPTER 6 : Algorithm Validation (Seasonal Scale Variability)

CHAPTER 7: Conclusions

List of Figures

Chapter 1:

Chapter 2:

Chapter 3:

Chapter 4:

Chapter 5:

Chapter 6:

Appendix I:

List of Tables

List of Symbols

Symbol	Description	Unit
Chl a	Chlorophyll a Concentration	mg/m^3
T	Temperature	ºC
SST	Sea Surface Temperature	ºC
T_{up}	Temperature of Upwelled Water	ºC
δT	Difference between SST and T_{up}	ºC
NO_3	Nitrate Concentration	µmol/l
Depth	Water Depth	M
$Iso_{temperature}$	Isotherm Depth	M
T	Time	Days
$Wind_{rs}$	V-component Vector	m/s
C_d	Drag Coefficient	
ρ_a	Density of Air	kg/m^3
U_{10}	Scalar Wind Speed	m/s
M	Ekman Mass Transport	m^3/s
f	Coriolis Parameter	

Chapter 1- General Introduction

1.1 INTRODUCTION

Large marine ecosystems (LME) are vast regions of ocean space which require monitoring, assessment and management due to their importance in controlling the structure and functioning of phytoplankton communities (Sherman, 2006). The southern Benguela ecosystem, being a sector of one of these LMEs, suffers from the frequent occurrence of HABs of predominantly dinoflagellates. HABs are known to occur in the southern Benguela ecosystem more frequently and reach concentrations far higher than explained by local growth, showing the importance of advection, physical concentration mechanisms and other forms of physical-biological interaction (Pitcher and Nelson, 2006). The negative consequences associated with HABs in the system, such as hypoxic conditions from large biomass degradation and shellfish poisoning from toxins which affect the ecosystem health and fishing communities, need careful understanding and ultimately prediction mechanisms. HAB detection and operational forecasting is a necessary requirement in the effective coastal management of the southern Benguela (Bernard et al, 2006), and developing mechanisms to quantitatively understand the physical-biological couplings through which the system operates is critical.

The southern Benguela is a wind-driven upwelling system along the South African west coast (Hutchings et al., 2009). The system is marked by a strong seasonality of upwelling, due to the seasonal changes in the equatorward winds responsible for surface divergence along the coast. Upwelling results in nutrient rich waters being brought up into the euphotic zone where phytoplankton can consequently thrive due to high nutrient and light availability. A recurring theme of studies in the southern Benguela is the succession of phytoplankton leading to HABs, where much of the work on succession is based on an initial study done by Margalef (1978). Margalef's proposal was to identify the relationship between nutrient availability, turbulence and phytoplankton community assemblages. This implied that certain phytoplankton groups are adapted to a particular environment within an ecological space in a system based on the nutrient availability and turbulence.

In this thesis, an attempt is made at using earth observation derived nutrient and turbulence proxies developed for the southern Benguela to define the ecological niche for key phytoplankton functional types based on Margalef's Mandala (Margalef, 1978), to aid in the characterisation and prediction of HABs.

The potential for accurate forecasts and HAB characterization requires the understanding of multiple ecological components: how they manifest individually and how they act in unison to potentially yield HABs in the system. Due to the lack of ability in producing good biological models that aid in HAB forecasting, the collection of real time observations are used in the place of the biological models (Bernard et al, 2006).

The need for an ideal observation framework which utilizes (amongst other things) high resolution synoptic satellite data, led to the development of this project, which introduces a simplified analysis of the biological and physical real-time observations using earth observation techniques, in an attempt to identify sub-habitats in which particular life forms of phytoplankton can be predicted using an 'ecological window' approach hypothesized in the mandala. The core part of the study was the use of *in situ* data, collected in the late austral summer/early autumn off Lambert's Bay in the greater St Helena Bay region in 2005, 2006 and 2007, to develop algorithms producing nutrient and turbulence proxies

The analyses of the processes involved with detailed phytoplankton characterisation during bloom formation: their relative cell counts; toxicity or transport prediction are beyond the scope of this project. However the geophysical aspects which create a suitable environment for the possibility of HAB formation and residence are analyzed, with a clear understanding that the dominant processes before and during bloom formation are not mutually exclusive.

1.2 NEW PRIMARY PRODUCTION: THE ROLE AND EFFECT ON PHYTOPLANKTON GROWTH IN MARINE ECOSYSTEMS.

Apart from their importance in the functioning of the marine food web and ecosystem, phytoplankton play a fundamental role in the earth's climate. They are central to the functioning of the "biological carbon pump (BCP)" that fixes atmospheric carbon dioxide (CO_2) in surface waters and exports it as particulate organic carbon (POC) into the deep ocean. For this reason greater importance is being placed on understanding the global carbon system and the vital role the ocean plays in regulating the climate system. As CO_2 concentrations increase in the atmosphere due to large anthropogenic forces, the scientific community predict increased sea and air temperatures (Crowley, 2000, Falkowski et al., 2000) and the effect the ocean has on carbon sequestration is now perceived to be more important than ever. Currently CO_2 concentrations in the atmosphere are at ~380 parts per million (ppm), the most in the past 740 thousand years (Hoegh-Guldberg et al., 2007). If it were not for the ocean the current concentrations would be estimated to be remarkably higher at 450 ppm (*ibid*). The ocean acts as a "carbon sink" and the resultant uptake, storage and release capacity of CO_2 make it a major component in the global carbon cycle (Sarmiento and Siegenthaler, 1992), approximately 16 and 50 times larger than the terrestrial and atmospheric biospheres respectively (Berger et al., 1989, Raven and Falkowski, 1999, Sabine et al., 2004, Fung et al., 2005). The effects the marine ecological system has on atmospheric CO_2 concentrations cannot be quantified with absolute certainty as our complete understanding of the systems are at their infancy stage (Gazeau et al., 2007). However our understanding of ocean chemistry allows for the development of models to try and simulate the ocean uptake and the release of CO_2.

The ocean's ability to uptake and release CO_2 is primarily altered through changes in surface productivity (Broeker, 1982, Field et al., 1998) for which phytoplankton are responsible for. Phytoplankton share an intimate link with important marine nutrient cycles of nitrogen (N), phosphorus (P), silicon (Si) and most importantly carbon (C) itself. The transfer of C from the atmosphere to the ocean is facilitated by the uptake of CO_2 along with N, P and Si by phytoplankton in well lit surface waters, and the re-mineralization of those elements in deeper waters controls the oceanic distribution of those elements. This process mentioned earlier is

known as the BCP (Eppley and Peterson, 1979, Ducklow et al., 2001), which can be sub-divided into an interrelated biogeochemical and physical system of production and export.

In a simplified model the process of the BCP begins with the production of organic material in the euphotic zone, supported by the consumption of the major inorganic macronutrients (ammonia (NH_4), nitrate (NO_3), phosphate (PO_4) and silicate ($Si(OH)_4$)) amongst other trace elements (Koeve, 2001). Due to the nature of the process, not all of the surface POC is exported to the lower depths but a major portion remains and is recycled within the food web above the mixed layer. This recycled production is termed regenerated production and is primarily driven by NH_4 produced inside the euphotic zone (Dugdale and Goering, 1967, Eppley and Peterson, 1979). Recently the regeneration of NO_3 into the euphotic zone by nitrification has taken particular significance where Yool et al., 2007 performed the first synthesis of open-ocean measurements of the specific rate of surface nitrification which contributes to the global BCP. During the export process through the water column the POC is also predominantly consumed and regenerated, and only a fraction of the initial POC transported to deeper water is either dissolved or re-mineralized. Over a specific period deep sea nutrient rich sediments eventually transfer their nutrients back into the euphotic layer via the upwelling of deep water, and this yields new nutrients and thus new production, and it is termed 'new' due to the fact that the input is from an external source outside the system (i.e. euphotic layer) (Eppley and Peterson, 1979). The efficiency of the BCP is wholly dependent on the fraction of POC that escapes regeneration within the mixed layer and finds its way into deep ocean sediments (Dugdale et al., 1992, Berger et al., 1998, Kurz and Maier-Reimer, 1993, Sarmiento et al., 2004), thus playing a vital role in the ocean's ability to act as a CO_2 "sink" or "source".

The importance of the BCP in ocean and atmosphere CO_2 exchanges, results in a need to describe the temporal and spatial variability of total production in an attempt to find the regions of the oceans where the CO_2 exchanges were and still are significant to the sustainability of ocean and climate systems.

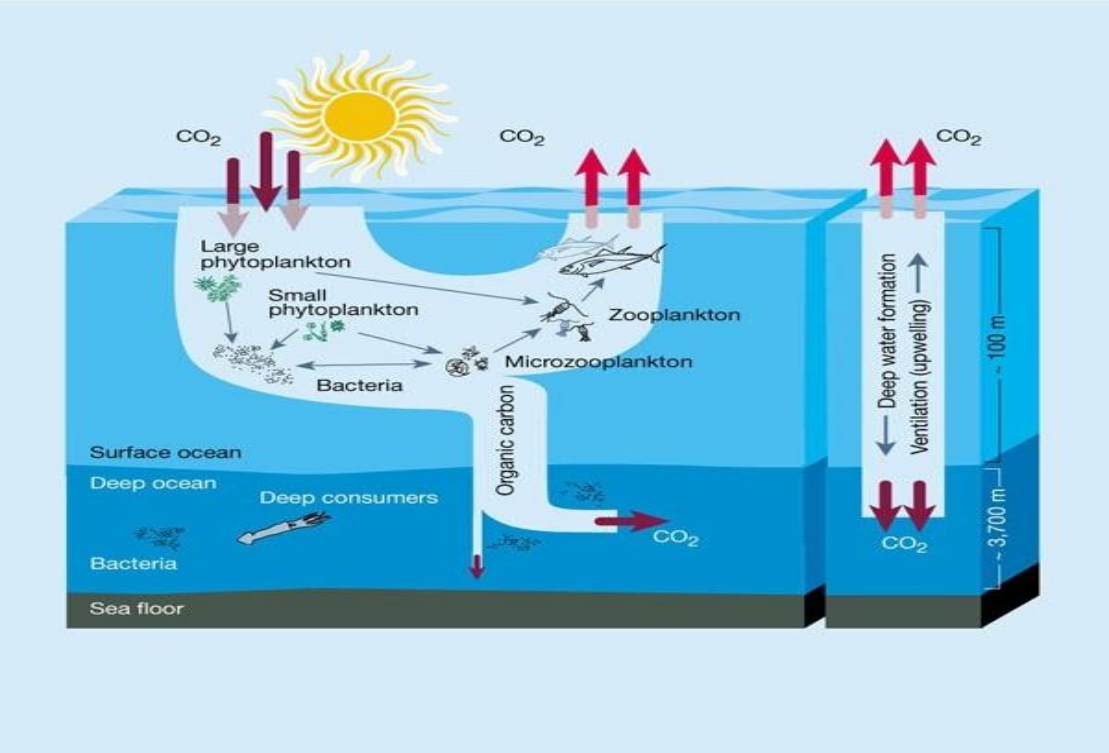

Figure 1.1 A simplified illustration of the BCP (from the Antarctic Climate and Ecosystems Cooperative Research Centre (www.acecrc.org.au/Research)).

1.2.1 Nitrogen Cycling

The growth of phytoplankton in water environments is determinate on photosynthesis which is limited to the euphotic zone due to its dependence on light. Phytoplankton use solar radiation as an energy source to convert dissolved inorganic carbon (DIC) to organic carbon and nutrients such as NO_3 and PO_4 are required for growth. It has been established that in both freshwater and marine environments these macronutrients can act as a limiting substrate which control new primary production, with determination of the most limiting factor found using the equation below:

$$106CO_2 + 16NO_3^- + PO_4^{3-} + 78H_2O + 18H^+ \leftrightarrow C_{106}H_{175}O_{42}N_{16}P + 138O_2 \qquad (1.1)$$

the ratio at which nutrients are taken up is termed the Redfield ratio C:N:P, 106:16:1 (Redfield et al., 1963).

The concept of new and regenerated production as two fractions of total production established by Dugdale and Goering (1967), has offered insight into the functioning of ocean pelagic ecosystems, where according to biological oceanographers the macronutrient, NO_3 demand by phytoplankton is greater, and thus the limiting factor in productivity (Smith and Kalf, 1983; Codispoti, 1989). Geologists however offer a different perspective to those of their oceanographic scientific counterparts, where another macronutrient, PO_4 is deemed the true limiting factor in production, but not discounting the ability of NO_3 in acting as a limiting factor too at any location and time (Codispoti, 1989).

For the purposes of this study, new and regenerated production will be defined according to Dugdale and Goering, (1967) where new and regenerated production are fractions comprising of the total production. This leads to a convenient means of directly partitioning total production between new and regenerated moieties based on the relationship between the oxidation state and origin of N (Probyn, 1992). This allows for oxidized N (predominantly NO_3) can be classified as new production which can in turn be stoichemetrically related to C (*ibid*). The accepted assumption holds prominent significance in highly productive eastern boundary currents (i.e. Benguela) where phytoplankton growth is most typically limited by N

(Chapman and Shannon, 1985). As mentioned earlier $Si(OH)_4$ may contribute as a limiting or co-limiting factor in coastal upwelling systems and may shape the community dynamics of diatoms (Kudela et al., 2005). In a number of instances the changes in the ratio of ambient concentrations of $Si(OH)_4$ to N have been implicated in the formation of dinoflagellate blooms (Hodgkiss and Ho, 1997, Anderson et al., 2002, 2008). This leads to compelling evidence that the global increase in different phytoplankton blooms may be related to a declining ratio between $Si(OH)_4$ and N due to eutrophication, which leads to the favouring of species that do not require $Si(OH)_4$ (Smayda, 1990). This classification of new production does recognize that there are other sources of new production such as N fixation from the atmosphere but due to their lack of importance in the global ocean and upwelling systems they are not considered in this thesis.

In the marine environment N is found in organic (eg. urea, amino acids) and inorganic (eg. NO_3, NO_2, NH_4) forms both arriving from a variety of sources. According to Eppley and Peterson, (1979), the primary sources for new production are vertical and horizontal inputs (i.e. upwelling and eddy diffusion), with most of the new production coming from wind-driven upwelling (Chavez and Toggweiler, 1995).

Newly upwelled waters cause a typical signal change in the inorganic as well as their organic constituents in the euphotic zone, exhibiting concentrations typically higher than those of pre-upwelled waters. Typical NO_3 surface concentrations vary within the oceans, with temperate to high latitudes presenting concentrations of between ~1 and ~35 µmol/l and tropical oceans < 0.05 µmol/l (Kamykowski and Zentara, 1985). The relative concentrations of both the organic and inorganic fraction of N are a vital component in phytoplankton productivity. The subject of whether or not phytoplankton growth rates being primarily based on regenerated or new N has overarching consequences on the nature of the phytoplankton assemblage and thus the possibility of bloom formation.

1.2.2 Cell Growth and the Kinetics of Nutrient Growth

The f-ratio (Eqn. 1.2) first defined in Eppley and Peterson (1979), was an attempt to articulate the paradigm initially discussed in Dugdale and Goering (1967), of determining the fraction of primary production that is available for consumption at higher levels.

$$f = \frac{new\ production}{new + regenrated\ \ production}$$

$$\cong \frac{NO_3^-\ uptake}{(NO_3^-\ +\ NH_4^+\ +\ NO_2^-\ + DON)uptake}$$

$$\cong \frac{NO_3^-\ uptake}{CO_2\ uptake} \text{ x } \left(\frac{C}{N}\right)_{\text{plankton}} \qquad (1.2)$$

The significance of the f-ratio is that it creates the ability to characterize ecosystem functioning. If the f-ratio is between 0.1 and 0.5, the system would be regarded as having phytoplankton production being primarily based on regenerated N, and an f-ratio of between 0.5 and 0.9, being based primarily based on new N. Immediately after upwelling in the Benguela as well as with other upwelling ecosystems there is a lag phase which is then followed by a period of exponential phytoplankton growth in response to favourable light and nutrients (Eppley and Thomas, 1979). The resultant high f-ratio (>0.6) illustrates significant NO_3 uptake which is usually at least, conceptually associated with diatom dominated communities due to their high growth rates (Probyn, 1992, Collos et al., 2005). This is articulated in the "shift up" hypothesis first described in Dugdale et al., 1990 and later in Kudela and Dugdale, (1996) where the "physiological description of the ecological events within the phytoplankton community during upwelling are: as the water ages, the NO_3 utilization is predicted to increase in a non-linear way until maximum uptake is reached". Eventually the supply of NO_3 in the system cannot support the NO_3 requirements of the diatom community thus resulting in NO_3 usage decreasing ("shift down") (Kudela and Dugdale, 1996).

1.3 PHYTOPLANKTON

Phytoplankton are at the base of all euphotic marine food chains and they support a vast and varied food web of secondary production and predators. In studies conducted in phytoplankton ecology it has been established that the development of blooms is linked to upwelling events and that blooms are not only confined to upwelling systems but occur worldwide (Kudela et al., 2005). Key to forecasting and understanding the bloom formation processes is a detailed knowledge of the influence physical characteristics of the water have on phytoplankton taxonomy and succession.

Semina (1997) created a concise history of the global distribution of species-specific phytoplankton biogeography, and found that species distribution is largely defined by the surface physical-chemical conditions of the water. The works done by Semina (1997) were built on the understanding first presented by Cleve (1900) and refined in Gran (1902) and countless others that: phytoplankton communities and species associations characterize water masses and current systems (Ramsfjell, 1960, Smayda, 1980). On the temporal scale the chemical characteristics of the water affect the community succession pattern at size, mixed species/class level (Smayda, 1990). The establishment and the general acceptance that physical-chemical conditions dictate phytoplankton distribution was elaborated by Longhurst (1998 a&b) in a classification scheme by diving the ocean into 4 biomes.

1.3.1 Harmful Algal Blooms

Smayda and Reynolds (2001) evaluated the habitat preferences of dinoflagellate species and their adaptive strategies, with a comparison between Margalef's well-known mandala (Margalef, 1978) and Reynolds Intaglio. The study proposed that along an onshore-offshore mixing-nutrient gradient there are nine different phytoplankton habitats and that the associated dinoflagellate types have distinctive morphotype features linked to those habitats. Furthermore Reynolds Intaglio provided a greater reliability to actual *in situ* dinoflagellate assemblages than the mandala did. The most important outcome of the study was that the correlation between the turbulence and nutrient levels presumed to be of utmost importance

in the mandala are not the essential interaction in the selection of life-forms and their succession (Smayda and Reynolds, 2001). The attempt at forecasting HABs using *in situ* and earth observation techniques is the central pillar of this thesis and is built on the premise established by the mandala, which is based on using the chemical properties of the watermass in an attempt at predicting phytoplankton assemblage and their potential blooms. An opposing view suggested in Smayda and Reynolds (2001), is a focus on the HAB forming phytoplankton life-forms and their habitat preferences rather than the current ecological investigative approaches supported by the mandala.

Using a simplistic approach, the understanding and the construction of reasonably accurate forecasting techniques for HABs is not only linked to a detailed knowledge of phytoplankton class spatial distribution but also an equally important understanding of the temporal distribution (i.e. succession). The classical view in flagellate ecology is that watermass stratification is essential in the potential formation of blooms (Smayda, 2002). Kierstead and Slobodkin, (1953) showed that theoretically in stratified waters below the "critical patchsize" the rate of horizontal diffusion will exceed flagellate growth rates and hinder bloom development. This was essentially articulated in Margalef's seminal paper in 1978 which highlighted the critical influence that turbulence has on blooms. Phytoplankton biomass in the ocean is related to the survival of the phytoplankton populations as the result of the temporary equilibrium between success in remaining afloat and the inevitable sinking (Margalef, 1978). The mandala hypothesizes that phytoplankton can be controlled by physical-chemical factors (temperature, salinity and/or nutrients) but this does not explain why not all phytoplankton thrive according to these factors. Too much importance has been afforded to grazing, biogeochemical interactions and other phenomena but the composition of phytoplankton is related to the turbulence and nutrient availability, with the large diatoms thriving in high nutrient, high turbulence environments and the smaller dinoflagellates having success in low nutrient, low turbulence environments (*ibid*).

Aforementioned in this section is that Smayda and Reynolds (2001), have a modified approach to the mandala. Margalef's model essentially combines the interactive effects of habitat mixing and nutrient conditions on the selection of phylogenetic morphotypes and their seasonal succession; whereas the Reynolds Intaglio is based on HAB dinoflagellate ecophysiology and their adaptive abilities in varying habitats. Both the approaches can be employed when investigating the potential for HABs in a specified area.

Successional patterns are difficult to predict in upwelling systems such as the Benguela due to both temporal and spatial fluctuations in the wind. According to Margalef, (1978) the general succession of phytoplankton functional groups are based on an ecological place which is defined by a continuum from r-selected (diatoms) to K-selected (dinoflagellate) organisms, which is largely controlled by turbulence, which provides a proxy for nutrient and light availability. The seasonal succession of microplankton follows a general pattern of diatom dominance in spring, progressive contribution of heterotrophic organisms in summer and dinoflagellates in late summer/autumn (Margalef, 1978). While the difficulties and inefficiencies of the mandala are rightly highlighted in Smayda and Reynolds, (2001) and elaborated on in Kudela et al., (2010), the adhering to the premise of the mandala within the scope of this thesis is continued, with an appreciation that the classic paradigm of flagellate ecology may be a little "out-dated".

With that in mind an approach will be used to predict the succession of phytoplankton, where during and immediately after the active phase of an upwelling cycle diatoms have fast growth rates (Dugdale et al., 1995). The nutrient depletion in the euphotic zone during the subsequent quiescent period leads to a community succession in the phytoplankton, from diatoms to dinoflagellates (Johnson et al., 2007). During this time due to the low nutrient concentrations, diatom growth is limited, so dinoflagellates are able to out-compete their larger counterparts for scarce nutrients due to their greater motility. This is over simplifying a complex and deeply researched area of phytoplankton community and succession structures which are also controlled by a limiting nutrient such as $Si(OH)_4$ that acts as a limiting substrate for diatom growth (Kudela et al, 2010), in the production of protective glass-like frustules. Diatoms use their frustules as ballast which leads to greater sinking rates for the species.

Smayda and Reynolds, (2001) generally classified dinoflagellate species as the main group forming HABs in coastal upwelling systems and their respective proliferations can manifest in different ways within a system. In the Benguela, red tides are common and are usually attributed to members of the *Dinophyceae* family which are non-toxic (Pitcher and Calder, 2000). The spatial extent at which blooms occur in the ecosystem vary with most blooms occurring to the west of Cape Agulhas in the southern Benguela, and commonly from January to May (*ibid*).

In the Benguela as well as other eastern boundary systems there are generally 2 main types of HABS which occur: toxic and non-toxic, and they are mainly caused by monospecific dinoflagellate-dominated blooms (Steidinger and Haddad, 1981, Pitcher and Calder, 2000).

Non-Toxic

In the Benguela the phenomenon of HABs tends to be localized (Tyrrell and Lucas, 2002) and its occurrence is normally dictated by the physical retention mechanisms of the area, for example the occurrence of HABS in the greater St Helena Bay region (Pitcher and Calder, 2000). The upwelling of low oxygen bottom water, which is endemic to the Benguela, onto the continental shelf creates an opportunity where the degradation of organic matter can further reduce the dissolved oxygen in the water (Pitcher and Probyn, 2011). The excess surface derived primary production and poor ventilation post upwelling phase, leads to waters characterized by oxygen depletion in the mixed and bottom layers, due to the decay of dinoflagellate-dominated blooms (*ibid*). This could lead to the potential death of vertebrates and invertebrates due to hypoxia in the bottom layers (Steidinger and Haddad, 1981).

Zhang et al., (2010) define hypoxia as regions where dissolved oxygen < 62.5 µmol/kg. The study of coastal hypoxia is becoming increasingly important as human impact on the environment is growing. As mentioned above coastal upwelling systems such as the Benguela are known examples of natural hypoxia and low coastal rainfall adjacent to eastern boundary systems means that they are seldom affected by human riverine input but rather natural cycles of large amounts of decaying biomass.

Toxic

Toxicity in phytoplankton blooms is caused by dinoflagellates which produce low molecular weight, nonproteinaceous endotoxins (Steidinger and Haddad, 1981). The toxins accompanying phytoplankton taxonomy in blooms differ between upwelling systems. In the California and the Iberian Upwelling Systems there are 2 major types of toxins: paralytic shellfish poisoning (PSP) and amnesic shellfish poisoning (DSP) (Kudela et al., 2005). DSP is commonly caused by a diatom of genus *Pseudo-nitzschia* (*ibid*). The toxic events that cause PSP are commonly associated with the dinoflagellate *Alexandrium catenella*, which produces neurotoxins and several derivatives of the molecule that causes PSP (Pitcher et al., 2008). Due to the fact that PSP predominantly affects filter feeders, toxins can accumulate

and kill higher level consumers as well (Steidinger and Haddad, 1981). In the Benguela however *Alexandrium Catenella* is only confined to the southern part of the system, mainly in the St Helena Bay region where the detection of PSP toxins is common in shellfish (Pitcher et al., 2008). In the northern Benguela another dinoflagellate, *Karlodinium micrum,* is linked with toxins which lead to fish mortalities (Kudela et al., 2005).

1.4 GEOGRAPHICAL LOCATION

1.4.1 Eastern Boundary Currents

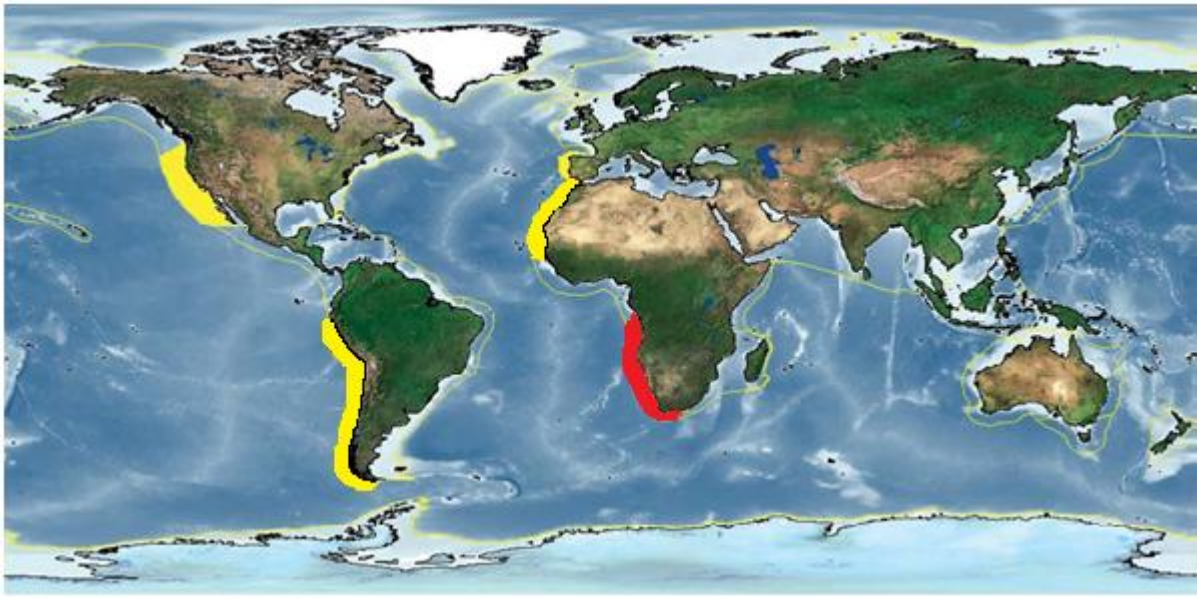

Figure 1.2 Map of major ocean ecosytems. Eastern boundary systems are highlighted in yellow. The Benguela region is highlighted in red. (Figure adapted from Kudela et al., (2005)).

The Benguela is one of the four major productive upwelling zones in the world's oceans. These four areas: Canary, California, Benguela and Humboldt (Iberian is sometimes included as a fifth) make up a very small fraction of the ocean (<1%) but account for 5% of all marine primary production and 17% of the world's fish catch (Pauly and Christensen, 1995). Eastern boundary current regions are a vital part of pelagic fisheries (mainly sardines and anchovies) (Carr, 2002) and their value cannot be over-estimated.

Amongst the four areas the Benguela is the most productive zone, so it is important to understand the ecosystem (Demarcq et al., 2003) for commercial and sustainability reasons. The ecosystem stretches in a generally north-south orientation along the south-western coast of Africa and extends from southern Angola (~17°S) to the Cape Peninsula in South Africa (~34°S) (Demarcq et al., 2003). It is unique in that it is bounded by warm currents at its northern and southern extremities, the Angolan Current at the former and the Agulhas

Current at the latter (Shillington, 1998). At the northern system boundary the warm Angola Current coincides with the cooler Benguela Current forming the Angola-Benguela Front (ABF), resulting in a sharp temperature gradient of 7.5°C (Holmes et al., 1996). To the west, the broad south Atlantic gyre forms an ill-defined outer boundary where Atlantic surface water, aged upwelled water and Agulhas 'leakage' mix into a myriad of complex eddies and filaments (Hutchings et al., 2009). Aside from the Benguela playing a vital role in the ocean carbon budget it is also involved in the mechanisms of heat and salt exchange between the Indian and Atlantic Oceans through eddies from the Agulhas Current (Gordon, 1985).

The ecosystem is made up of a cold, shallow (<80m) (Dowsett and Willard, 1996), equatorward flowing current and can be divided into two parts: the southern and northern Benguela. The division between the two is usually placed around Lüderitz (~26.5°S), a powerful upwelling cell subjected to perennially strong winds resulting in high offshore advection and strong turbulent mixing (Hutchings et al., 2009). The current is thought to be fed from three sources: the South Atlantic Current; the Agulhas Current and the sub-surface waters from the Antarctic Circumpolar Current (Garzoli and Gordon, 1996). Due to topographical variations in the Benguela, a further sub-division can be created according to discrete upwelling cells: the Namaqua, Cape Columbine and Cape Peninsula cells in the southern Benguela and the Lüderitz, Cunene, Walvis Bay and Cape Frio cells in the northern Benguela (Weeks et al., 2006).

1.4.2 Project Geographical Location

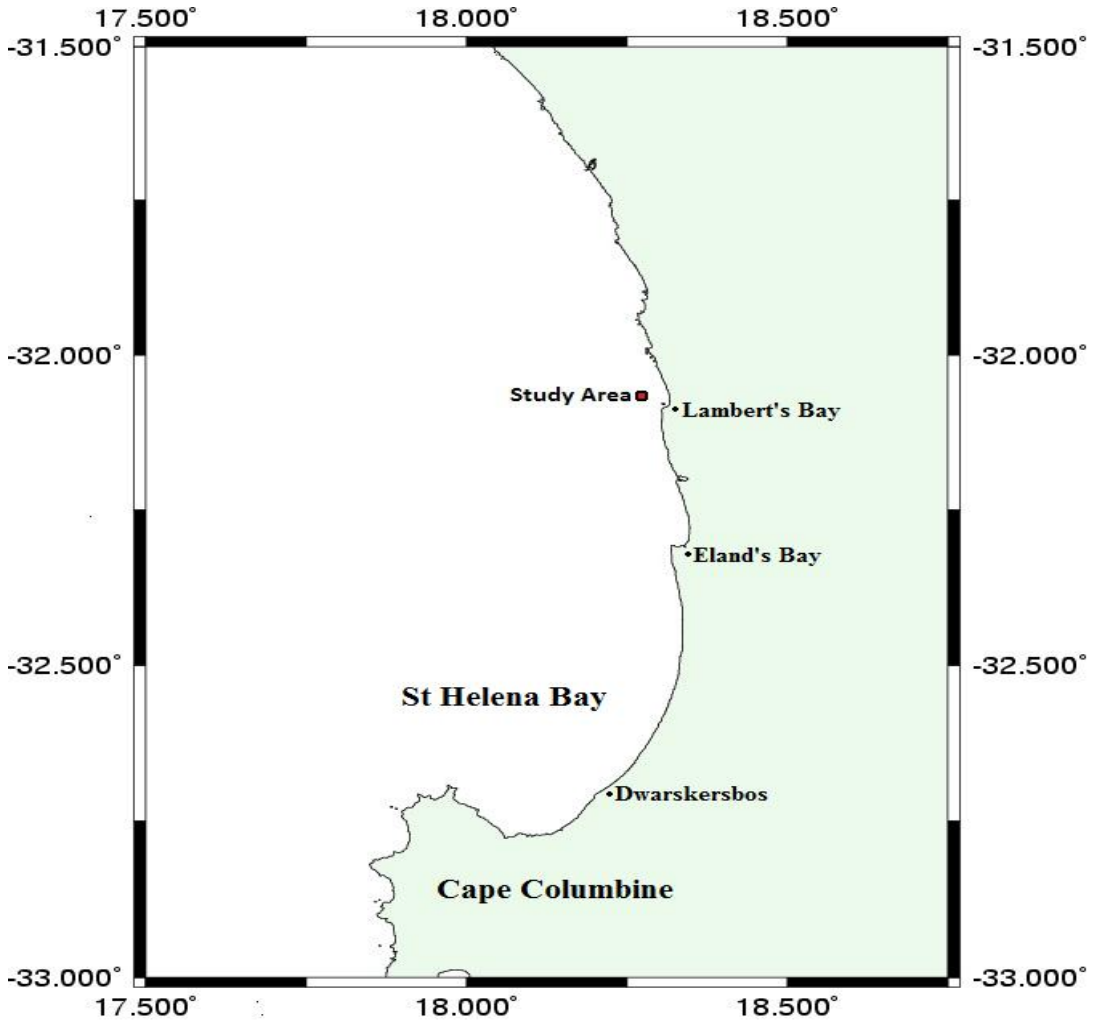

Figure 1.3 Map showing the study area off the south-western coast of South Africa near Lambert's Bay.

The study area for this project is located off the coast of Lambert's Bay ~32°S (Fig.1.3) which is approximately halfway between the Namaqua and Cape Columbine cells and is part of the greater St Helena Bay region in the southern Benguela. This region is of particular interest due to the retentive circulation that results in the formation of high biomass blooms that can impact upon the system through toxicity and/or hypoxia resulting from a bloom collapse (Pitcher et al., 1998). Due to its locality between 2 warm bodies of water and the varying nature of the upwelling in the ecosystem, the Benguela displays substantial short-term, seasonal and inter-annual variability that impacts significantly on its biological resources.

1.4.3 Atmospheric Circulation and Upwelling

Upwelling systems worldwide are dominated by a common set of physical forcing parameters and are likely to respond in the same way, with the primary driver being wind (Kudela et al., 2005). Along the southern Benguela there is a semi-permanent high pressure cell, the South Atlantic Anticyclone (SAA), which creates episodic, longshore, equatorward winds which result in Ekman transport away from the coast causing upwelling of cold nutrient-rich water along the coastal edge of the continental shelf into the euphotic zone. The seasonal peak for the upwelling phase is in the austral summer/autumn periods and there is a substantial weakening during the winter months due to the migration of the wind belt associated with the high pressure cell (Nelson and Hutchings, 1983). This differs from the northern Benguela where the perennial upwelling shows a peak in intensity during the late austral winter and early spring months (Lutjeharms and Meeuwis, 1987).

At the event scale, upwelling favourable south-easterly winds are punctured by coastal lows (west coast troughs) and other low pressure systems, which result in weak poleward winds that support water column stability and the possibility of bloom formation (Kudela et al., 2005). These episodic wind reversals correspond with quiescent and upwelling phases where poleward winds dominate in the former and equatorward winds in the latter (*ibid*). The cycle between the two lasts ~7-10 days with the relative balance between them being of utmost importance in bloom formation. In the southern Benguela with the predominantly strong wind stress being in the summer period, the winter months (April-mid July) have a lower intensity wind stress but these can at times reach gale force speeds during the easterly migration of mid-latitude depressions (Tyson and Whyte, 2000).

The upwelling in the southern Benguela occurs along two important frontal zones which help in the delineation of the western boundary of the ecosystem and between individual upwelling cells within the system. The first is the oceanic front which demarcates the border between the south Atlantic gyre surface water and aged southern Benguela upwelled water (Hart and Currie, 1960), and it is situated along the 300-400m bathymetric range on the continental shelf (Shannon and Nelson, 1996). The second are upwelling fronts which demarcate the boundaries between recently upwelled and aged upwelled water, with the surface temperatures used to differentiate between the two. These upwelling fronts are closely associated to individual upwelling centres (Lutjeharms and Meeuwis, 1987). The

general position of the upwelling front is usually around the continental shelf edge and the shelf width varies along the coast, and with it so does the upwelling front (Strub et al., 1998). Between the upwelling front and the coastline there is a further classification of the near shore waters in the southern Benguela based on their sequential development after upwelling (Barlow, 1982):

Classification	**Description**	**Temperature**	**Chlorophyll a, concentration**	**Nitrate concentration**
Type 1	Newly Upwelled	<10 °C	> 1 mg/m^3	High
Type 2	Maturing Upwelled	>10 °C	1-20 mg/m^3	2-15 mmol/m^3
Type 3	Aged Upwelled	12-16 °C	5-30 mg/m^3	<2 mmol/m^3

Table 1.1- Surface water classifications in the southern Benguela during the austral summer and autumn seasons

Upwelling strength and duration differ along the ecosystem due to the high wind variability at a local scale within the system, so it is important to understand the influence that local variability has on the coastal upwelling (Risien et al., 2004). In the St Helena Bay area southerly winds are deflected around Cape Columbine and blow with an on-shore component to the north of Cape Columbine (Fawcett et al., 2007) which is important for the retentive circulation of the region (Pitcher et al., 1992), thus fulfilling a requirement for the possibility of bloom formation. In this area phytoplankton accumulate during upwelling conditions and upon relaxation the communities advect southwards and concentrate inside St Helena Bay (Fig. 1.4).

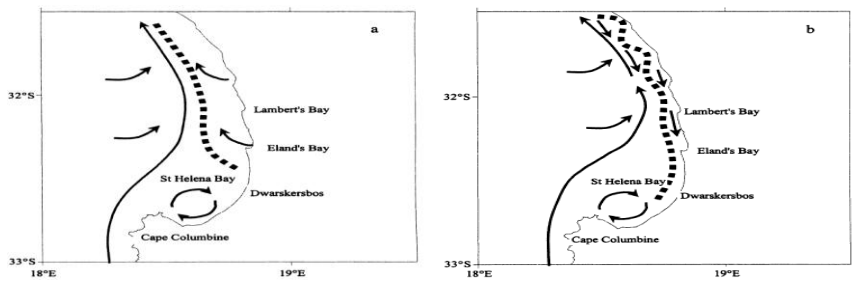

Figure 1.4 Conceptual advection of HABs in St Helena Bay during a)upwelling and b)quiescent phase. The broken line demarcates the area of highest dinoflagellate abundance. (Figure and description adapted from Pitcher and Nelson, (2006)).

1.4.4 St Helena Bay Circulation and Characteristics

Circulation

The varying local wind environment along with the topography, are the primary drivers of the circulation in the St Helena Bay (Fawcett et al., 2007). St Helena Bay is a shallow (depth<100m), bay that is characterized by sluggish currents (Touratier et al., 2003). According to Duncan and Nell, (1969) surface currents flow in a generally northerly and southerly direction in summer and winter respectively. The surface flow corresponds to the predominant wind direction in their respective seasons. In the summer/autumn months an inshore current at depth develops and persists (Fawcett et al., 2007). During upwelling an equatorward coastal jet forms in the bay where the shelf is narrow and deep leading to clockwise rotation and retention within the bay (Fawcett et al., 2007). The southward advection and the retention of blooms is thought to be associated with inshore barotropic flow generated by coastally trapped waves over the southern regions of the Namaqua shelf with periods of 3 to 4 days (Pitcher and Nelson, 2006, Lamberth and Nelson, 1987, Probyn et al., 2000; Weeks et al., 2006). At the southern border of the bay the Cape Columbine headland is critical in determining the response of the currents in the bay (Fawcett et al., 2007). The region to the north of Cape Columbine is particularly susceptible to bloom formation due to the retentive characteristics and the broadening shelf which both favour stratification and stability (Pitcher and Nelson, 2006).

Water Mass Characteristics

The SST in the bay exhibits a strong seasonal trend which is associated with diurnal warming and the frequency and strength of upwelling episodes. Remotely sensed SST values show an average summer temperature of 17°C and 15°C for the winter period but a larger pulsing range of SST values are experienced during the summer due to upwelling (Demarcq et al., 2003). The nature of upwelling results in a generally north-south band of cold water adjacent to the coast after equatorward winds (Taunton-Clark, 1985).

St Helena Bay is characterised by high biomass and the retention of blooms, as indentified by remotely sensed chlorophyll a (*chl a*) data (Weeks et al., 2006). These data show that there is an increase inshore and that the *chl a* variability is linked to SST (*ibid*). The seasonality of the

chl a is shown to be highest in St. Helena Bay from January to May (summer/spring) (*ibid*). This differs from the California and Iberian systems where the greatest *chl a* values are found in the spring/early summer season (Kudela et al., 2005). The seasonal range of the *chl a* values are of greater importance in the potential formation of blooms, than the seasonal averages.

1.5. THESIS

1.5.1 Rationale

In the southern Benguela there is a need to utilize real-time monitoring as a basis for improved HAB characterization and prediction (Bernard et al., 2006) accompanied with the need to simplify the many ecological components to 'streamline' the process of HAB forecasting. Earth observation allows for a high temporal and synoptic data collection regime, which better utilized could simplify an already convoluted process of HAB forecasting. Phytoplankton abundance is known to be highly variable within the system, with the highest values downstream of upwelling cells (Weeks et al., 2006) such as St Helena Bay. The use of earth observation allows for the extensive collection of offshore *chl a* data where maximum phytoplankton concentrations are known to occur in the southern Benguela (Brown et al., 1991). Given the dependence on real-time observations rather than ecophysiological modelling, effective HAB forecasting is likely to take 2 avenues: "Ecological Window" or "Fuzzy Logic Model" (Bernard et al., 2006).

This study takes the "ecological window" route in the probability of succession, determined from real time observations which could lead to HABs. The study aims to utilize earth observation techniques and our current understandings of phytoplankton theory in an attempt to articulate Margalef's mandala (Margalef, 1978) of: "*...different life-forms of phytoplankton are functionally interpreted as adaptations to survival in an unstable and turbulent environment*" in a robust manner which aides in bloom forecasting and prediction. The need to collocate, interpret and disseminate physical-chemical synoptic scale data which aides in prediction of HAB formation are important in building capacity in the region and is the essential target of this study

1.5.2 Objectives

The aim of this project is try and find an ideal ecological window where the survival of phytoplankton populations are the result of a temporary equilibrium between success in remaining afloat and inevitable sinking. By utilizing two different proxies derived from *in*

situ surface data and satellite derived wind, the goal is to try and establish an "optimum window" for the possibility of bloom formations. This project is based on the hypotheses of Margalef, (1978) and Silió-Calzada et al, (2008) and the principal goal of this assignment is to utilize locally derived robust algorithms along with remotely sensed SST, ocean colour and winds data to study the mesoscale upwelling events and the consequent phytoplankton response in the southern Benguela.

Two proxies used:

Nutrients

An analysis of the nutrients will be undertaken and their relative concentrations will be used as a proxy for the possibility of phytoplankton growth. In unison with *in situ* data, satellite derived SST, wind and ocean colour, the phytoplankton community structure and succession can be hypothesized using the "ecological window" model. The development of this proxy is based on the ability to create relatively accurate estimated NO_3 fields of the southern Benguela using algorithms developed via a technique hypothesized in Silió-Calzada et al, (2008). Silió-Calzada et al, (2008) utilized a "shift up" NO_3 utilization model (Zimmerman et al., 1987, Dugdale et al., 1989, Dugdale et al., 1990, Kudela and Dugdale, 1997, Kudela and Chavez, 2000) based on an idealized upwelling structure, which in part calculated estimations in upwelled dissolved inorganic N. The algorithms used in Silió-Calzada et al, (2008) were created on a system scale and may consequently not hold on a local scale. Newly developed algorithms will be used to create synoptic scale images of estimated surface NO_3 concentrations for the southern Benguela.

Due to the nature of this study being remotely sense based and the NO_3-temperature relationship in the ocean being a well established one, only NO_3 is used and termed as "nutrients". This however does not discount the large influence that other nutrients such as $Si(OH)_4$ have on the state of the system.

Turbulence/Stratification

Using an isotherm depth as a stratification proxy derived from *in situ* data, the primary objective is to predict the isotherm depth, which is indicative of the thermocline depth. As per the estimated NO_3, algorithms will be developed for the estimation of the isotherm depth which will be used to create synoptic scale data of the predicted isotherm depth. The relative intensity of the stratification is important in the formation of the community structure of the

phytoplankton, with smaller motile plankton being able to survive and remain afloat in increasingly stratified conditions due to their ability to utilize the nutrients at the thermocline and slightly beneath (Margalef, 1978). The increased stratification hinders the ability for the rapid growth of larger plankton due to the lack of input of nutrients into the euphotic zone (*ibid*).

Ecological Window

The overall objective of the thesis is to create reasonably accurate algorithms and produce remotely sensed data of estimated NO_3 and isotherm depths which can then be used with already available *chl a* data to determine phytoplankton functional types in the system using the ecological conceptual model. The estimated isotherm depths, estimated surface NO_3 concentrations and remotely sensed *chl a* will be compared in a time series format for the ecosystem with an aim at identifying periods when bloom formation was possible due to the physical-chemical characteristics of the surface waters.

Approach

The endeavour is to develop a simplistic method which can be used to define phytoplankton types according to the ecological niche indicators from the two proxies. The first proxy, nutrient availability, is based on the ability to accurately estimate local surface NO_3 concentrations using the method proposed in Silió-Calzada et al, (2008). The first method in the thesis is the estimation of the NO_3 concentrations as a function of the surface temperature and *chl a* concentrations. The second proxy, stratification, is based on the utilization of an isotherm as a proxy for the thermocline depth and thus a reliable representation of the stratification in the water column. For the stratification, the method is based on the estimated isotherm depth as a function of the temperature and the remotely sensed wind speed.

Important questions

The key questions that this thesis has tried to address are:

- Are the algorithms adapted from Silió-Calzada et al, (2008) valid on local scales in the southern Benguela?

  Are the newly locally derived algorithms able capture the event and seasonal scale coupling of the physics and biology of the system?

- Would the same principles with regards to phytoplankton life forms based on the optimum ecological niche apply to the entire southern Benguela and further more can the method be extrapolated to the system as a whole?
- Does a broad, simplistic approach in the analysis of the physical and biological interactions on the continental shelf capture the spatial and temporal variability of the system?

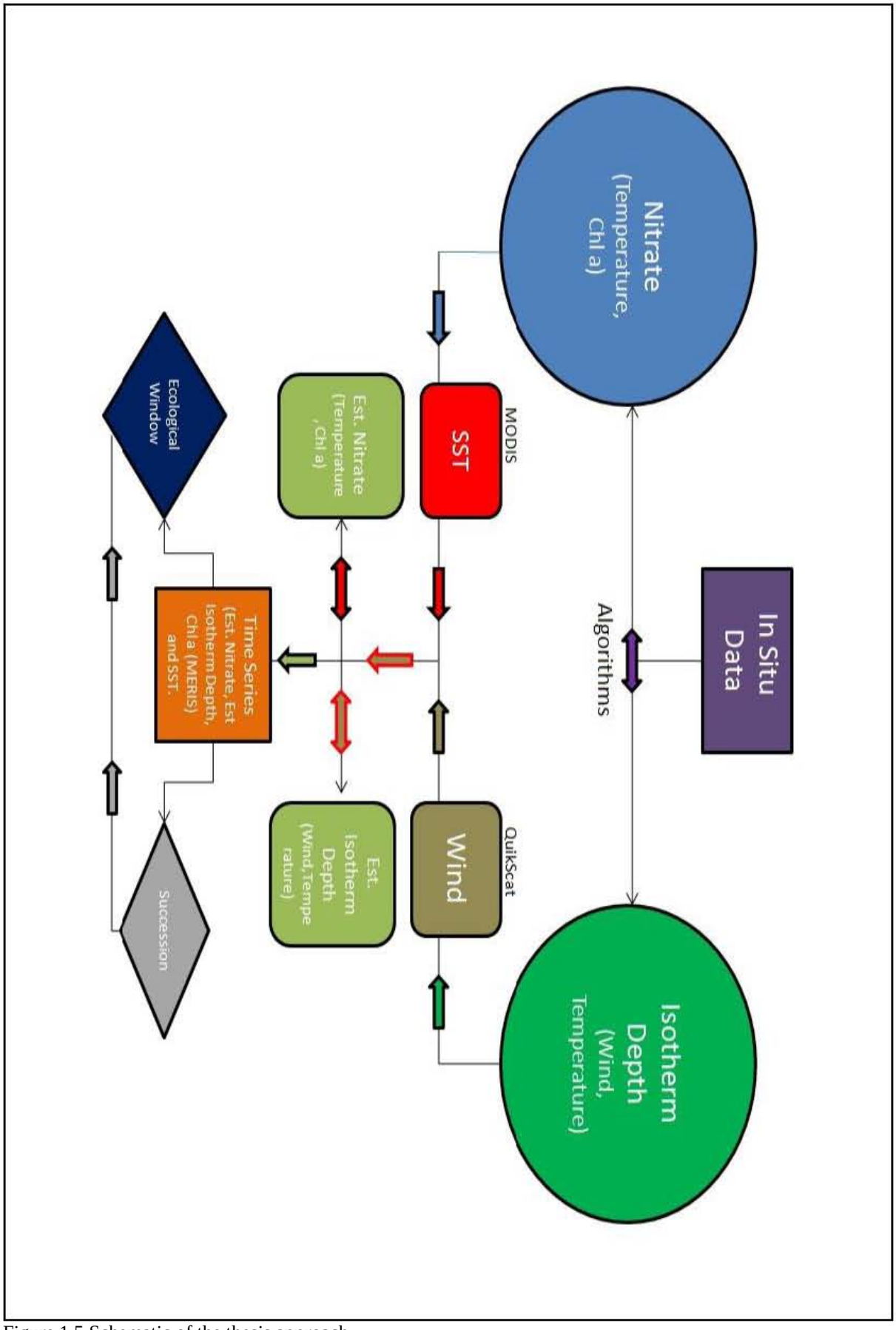

Figure 1.5 Schematic of the thesis approach.

1.5.3 Thesis Structure

Chapter (1) is a general introduction into the concepts of phytoplankton ecology and bloom dynamics, with a description of the ecosystem area under study.

Chapter (2) describes and discusses in detail the *in situ* data used in the derivation of the algorithms. The collection techniques and the environmental conditions during the late summer/autumn season at the study location over the 3 years are thoroughly described. Statistical analyses are described for the *in situ* NO_3, water temperatures and *chl a* concentrations. Chapter 2 concentrates on examining the event scale variability during the period of 2005, 2006 and 2007 and the response of the phytoplankton community to the change in the physical-chemical conditions.

Chapter (3) is dedicated to the description, merits or disadvantages of various NO_3 measurement techniques used in oceanography for *in situ* and remotely sensed studies past and present. The chapter continues with a detailed description of the new approach for the estimation of NO_3 developed in Silió-Calzada et al, (2008) for specific use in the Benguela which is utilized in this study. Furthermore the algorithms developed in Silió-Calzada et al, (2008) are tested to see if the estimated NO_3 displays similar characteristics to the *in situ* NO_3 concentrations and if the integrity of the algorithms is maintained on a local scale. The final product of the chapter is the derivation of robust algorithms for estimating surface NO_3 using *in situ* variables from the study site.

In Chapter (4) the thesis addresses the issue of the 2^{nd} proxy: turbulence/stratification which is a prerequisite of possible bloom formation. The initial part of the chapter is a description of the various stratification and turbulence quantifying techniques employed in oceanography. The main part of the chapter is the investigation of which isotherm best describes the thermocline depth in the southern Bengulea ecosystem. The chosen isotherm, *in situ* temperatures and remotely sensed winds data is then used to derive robust algorithms for the estimation of the isotherm depth.

Chapter (5) is dedicated to the validation of the both the estimated surface NO_3 concentration and isotherm depth algorithms across the southern Benguela. The algorithms are applied to daily 1km resolution SST data during the years of the *in situ* data collection. The chapter

primarily investigates whether the algorithms capture the event scale phenomena in the system and the offshelf-onshelf dynamics expected of the system.

Chapter (6) analyzes the role played by physical parameters such as SST, Ekman transport and wind stress in the biological variability of the southern Benguela. The specific focus is on the spatial and temporal variability in estimated surface NO_3 concentrations, estimated isotherm depths, upwelling and *chl a* concentrations on intra-seasonal time scales. The chapter deals with the seasonal and annual variability of 8 different years with a particular focus on 2005 and 2009. The final part of the chapter is a discussion on the event and seasonal scale performances of the algorithms. In examining the dynamic variations of the physical-chemical properties within the system, the phytoplankton abundance and succession are hypothesized using the mandala.

Finally, Chapter (7) addresses relevant questions on the future use of the proxies: Is it possible to extrapolate the methodology to a larger spatial area for instance the rest of the ecosystem? Is it possible to find discrete values which exhibit an ecological window with regards to the stratification, estimated NO_3 and *chl a*, where bloom prediction is possible? If not, why?

A further discussion on the shortcomings in the study are dealt with and if there are any improvements that could be made in future attempts to find an ecological window where bloom prediction is possible in the southern Benguela using earth observation.

This work attempts to simplify the already known knowledge of the key processes that lead to HABs which operate in the southern Benguela, and to extrapolate the known concepts on to a larger scale. In doing so the goal is to provide an input into the ecosystem management approach of HABs in the region.

IN SITU DATA SET

Chapter 2-In Situ Data Set

2.1 METHODS

2.1.1 Lamberts Bay Data Set

The collection of the *in situ* data set required for the derivation of both the nutrient and stratification proxies took place 3 km offshore of Lamberts Bay which is in the northern zone of St Helena Bay (Fig 1.3). The field data from the location has been collected annually during the late upwelling season since 2004, initially under the supervision of Marine and Coastal Management (MCM) and then later the Department of Agriculture, Forestry and Fisheries (DAFF). The collection of annual good quality field data is a joint effort by the University of Cape Town (UCT) and MCM for multi-disciplinary HAB research which adds an overall contribution to the Benguela Current Large Marine Ecosystem (BCLME) programme.

The data were collected over the following time periods:

	2005	**2006**	**2007**
Date	16 March- 5 April	7 March-23 March	22 March- 7 April

Table 2.1 Time periods of the *in situ* data collection.

During the collection periods there were data gaps within the time frames where data collection was not undertaken. After quality checks the data sets from the station (32, 1°S 18, 3°E) were pooled together, irrespective of the year of collection they were drawn from for the creation of the robust algorithms.

2.1.2 Instruments

CTD

A SeaBird Electronics' Seacat conductivity, temperature and density (CTD) profiler model 19, was used to measure conductivity (salinity), chlorophyll fluorescence and temperature profiles at a sampling interval of a ¼ of a second and a descending/ascending rate of 1m/s. The CTD was lowered once per day sometime between 10h00 and 11h00, local time, to a depth of ~50m at the site. The recorded data were saved to a 64MB FLASH memory and downloaded at the end of the each sampling period to a PC using the Seabird data processing software, Seasave, version 7.2 which is part of the manufacture created software suite Seasoft V2. The data were run through a low pass filter and aligned typically for conductivity, temperature and oxygen relative to pressure using the software. The software pre-filtered data collected using the CTD was then processed further using MathWorks' Matlab. The Matlab processing protocols were as follows:

1. Only the downcasts of the collected CTD data were considered for further processing, while the upcasts were not utilized due to the fact that on some sampling days the upcast data were unreliable.
2. The pressure values in the data were converted to meter values using the Seawater Toolbox for Matlab distributed by the Commonwealth Scientific and Industrial Research Organisation (CSIRO) which is readily available for download from their website (http://www.cmar.csiro.au/datacentre/ext_docs/seawater.htm).
3. All the data were passed through a median filter with a bin size of 10 in order to remove the data spikes not eradicated during the initial processing by the CTD software and the data were then resampled.
4. The data were binned into 1m depths using one dimensional 'linear' interpolation on Matlab, which was simply the linear interpolation between the two closest data points.

It is important to note that due to the lack of data values at depths <1m, Matlab was unable to interpolate data values at the surface (i.e. 0m). For this reason only data >=1m were available for further analysis and use in this thesis. The 1m depth was then taken to represent the surface for all relevant analyses with the exception of the discrete water samples.

Chlorophyll a

The *chl a* concentration was extracted in 90% acetone from 5 discrete depths using 100 ml water samples which were filtered on to 25mm Whatman GF/F filters and extracted for 24 hours. The filters were treated prior to acidification with 2 drops 10% HCI to correct for phaeopigments as per the protocols described in Parsons et al., (1984). The fluorescence profiles were measured with the CTD profiler.

2.1.3 Chemical Analysis of the Water Samples

The seawater samples were collected at the same time as the daily CTD casts from discrete depths in the water column. The samples were taken for depths 0, 5, 10, 15 and 20 metres. All the nutrient analysis was undertaken within 30 minutes of collection on a land-based laboratory and the samples were analyzed for NO_3 concentrations.

Nitrites/Nitrates

The determination of NO_3 in seawater requires its reduction to NO_2. The NO_2 and NO_3 concentrations were determined following the cadmium reduction procedure described in Nydahl, (1976). The method involved running the water samples through a prepared cadmium column that quantitatively reduced NO_3 to NO_2. The reduced samples were further processed with the addition of a diazotising agent, in acidic media, forming a temporary diazonium salt. The addition of a coupling agent formed a stable azo-compound resulting in a purple solution. The absorbance of the solution is measured colourimetrically and it is proportional to the concentration of NO_2 in the sample (Parsons et al., 1984). This cadmium reduction method is easier and less tedious than using expensive and analytical instruments like a spectrophotometer to measure UV wavelengths at an array of wavelengths to estimate NO_3 concentrations.

2.1.4 *Analysis of In Situ Characteristics*

The primary variables used in the characterisation of the *in situ* data were temperature, conductivity, *chl a* and NO_3. The temperature and conductivity values both had error margins of +/- 0.005℃ and +/-0.005 per salinity unit (psu) respectively as mentioned in the CTD

operating manual. The fluorometer consistently exhibited sub-surface *chl a* maximum values which could have been caused by the photo-inhibition of fluorescence (McCarthy and Strickland, 1969). The photo-inhibition is caused by the inhibition of photosynthesis created by excessive radiance at the sea surface. The process may damage the photosynthetic apparatus of a biomass, causing the photo-destruction of the photosynthesizing pigments (Powles, 1984) which are measured by the fluorometer. The resultant outcome is a lower fluorescence at the surface due to photo-inhibition and a non-inhibited higher concentration just beneath the surface.

2.2 RESULTS

2.2.1 2005

Temperature Profiles

In 2005 the water column temperature structure (Fig.2.1) was categorized by persistent surface water warming for the first half of the period and a cooling interval in the second half due to upwelling. From 16th March to 28th March the surface warming was confined to the upper 15m. However from 29th March the consistent warming was interrupted by a slight intrusion of cooler 14°C water at the surface. There was upwelling from ~ 2nd April until 4th April, with a peak on the 3rd which was characterized by the complete cooling of the water column (Demarcq et al., 2003). The surface temperatures exhibited diurnal warming and cooling during the early days of 2005.

Surface temperatures for the period ranged from 11.5°C to 17.8°C (Table 2.2), while temperatures at 30m exhibited a much smaller range of between 9.9°C and 10.9°C. The mean difference between the surface and 30m temperatures was 4.3°C, with a maximum difference of 7.5°C on the 24th of March, which was indicative of increased stratification within the water column. The minimum difference was 1.6°C on the 3rd of April which was consistent with moderate to strong upwelling.

Surface Chlorophyll and Nitrates

In 2005 there was one period of very high surface biomass from 29th March to 1st April, with a peak on 1st April of ~200mg/m^3 (Fig.2.2). In the days preceding the high surface biomass the *chl a* levels were primarily < 25mg/m^3. Immediately after the increased surface *chl a* period the concentrations dropped back to levels preceding the bloom. The surface NO_3 values were undetectable 95% of the occasion during the quiescent phase of the time period (Pitcher et al., 1989) as to be expected with the exception of a 2-day interval on 2nd April and 3rd April where the concentrations were >20µmol/l.

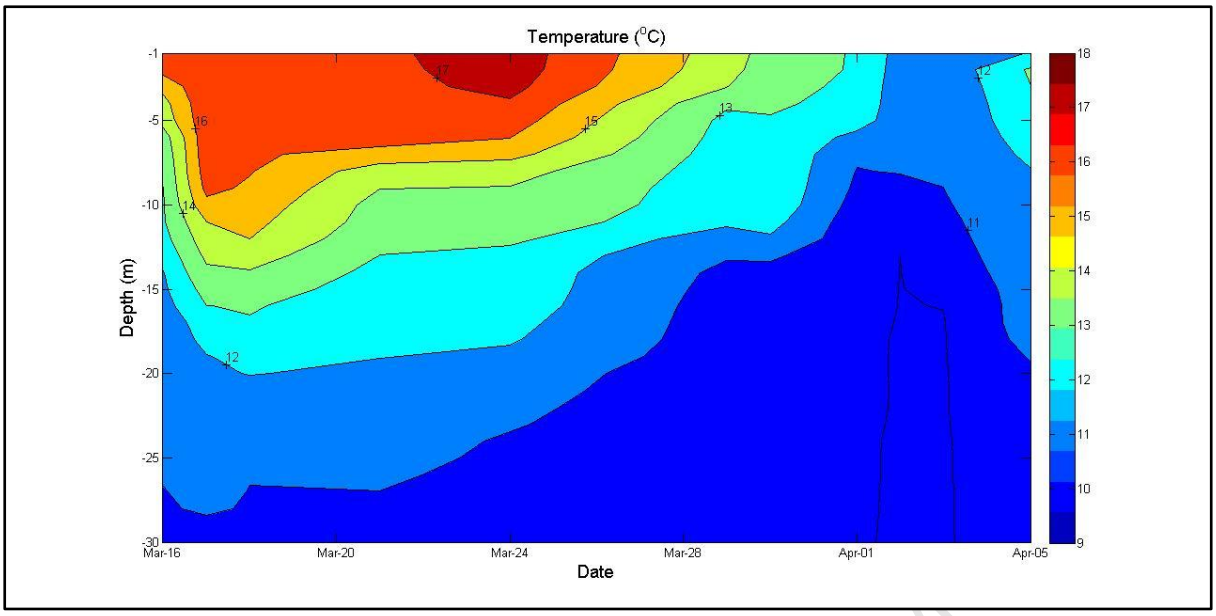

Figure 2.1-Temperature profile data between 1 and 30m depth. Note data gaps from missing days were interpolated.

	1m Temperature	30m Temperature	Period Range in 1m Temperature	Difference between 1m and 30m temperature
Mean	14.8 °C	10.4 °C	1 °C	4.3 °C
Standard Deviation	2.2 °C	0.4 °C	0.6 °C	2.1 °C
Maximum	17.8 °C	10.9 °C	2.3 °C (24th Mar)	7.5 °C (24th Mar)
Minimum	11.5 °C	9.9 °C	0.1 °C (3rd Apr)	1.6 °C (3rd Apr)

Table 2.2-Characteristics of the temperature data gathered from the CTD profiles.

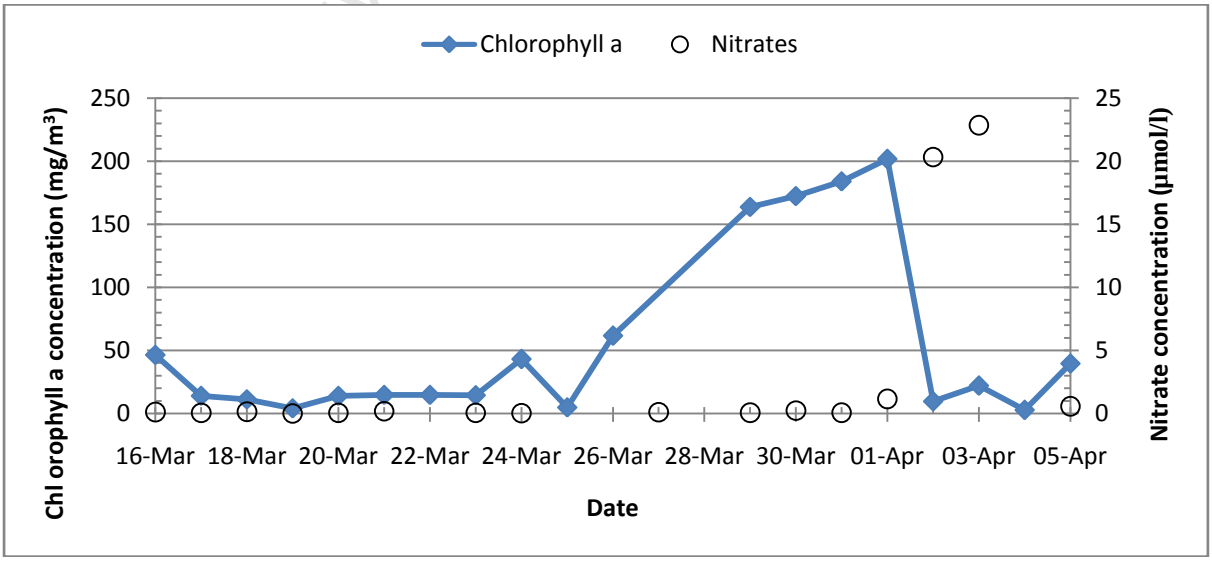

Figure 2.2-Daily surface NO_3 concentrations (µmol/l) and extracted surface chlorophyll a concentrations (mg/m^3) for 2005.

2006

Temperature Profiles

2006 was different from 2005 and exhibited water column instability throughout the period (Fig. 2.3). The entire time period had consistently cool temperatures throughout the water column with surface temperatures not reaching above 15.7°C. The constant upwelling throughout the period was punctured by a very slight increase in surface temperatures over a 2 day period, increasing from ~11°C to 13°C. The surface temperatures for 2006 ranged from 10.4°C to 15.7°C (Table 2.3), while temperatures at 30m exhibited a much smaller range of between 9.8°C and 10.6°C. The mean difference between the surface and 30m temperatures was markedly lower than the same period in 2005 at 2.4°C, with a maximum difference of 5.1°C on the 8th of March. The minimum difference was 0.6°C on the 23rd of March which was consistent with strong upwelling. In 2006 there was no form of significant temperature stratification.

Surface Chlorophyll and Nitrates

The *chl a* levels in 2006 differed from the same period in 2005 with 3 distinct period peaks which were much shorter (~1day) and lower at values between 30 and 60 mg/m^3. The periods between the peaks had consistent concentrations of ~10mg/m^3. The corresponding surface NO_3 levels were highly variable with an initial phase of between 10 and 20µmol/l, and with a middle period of undetectable concentrations (Fig. 2.4). The concentrations did increase for the final 3 days of the study period indicative of upwelling conditions.

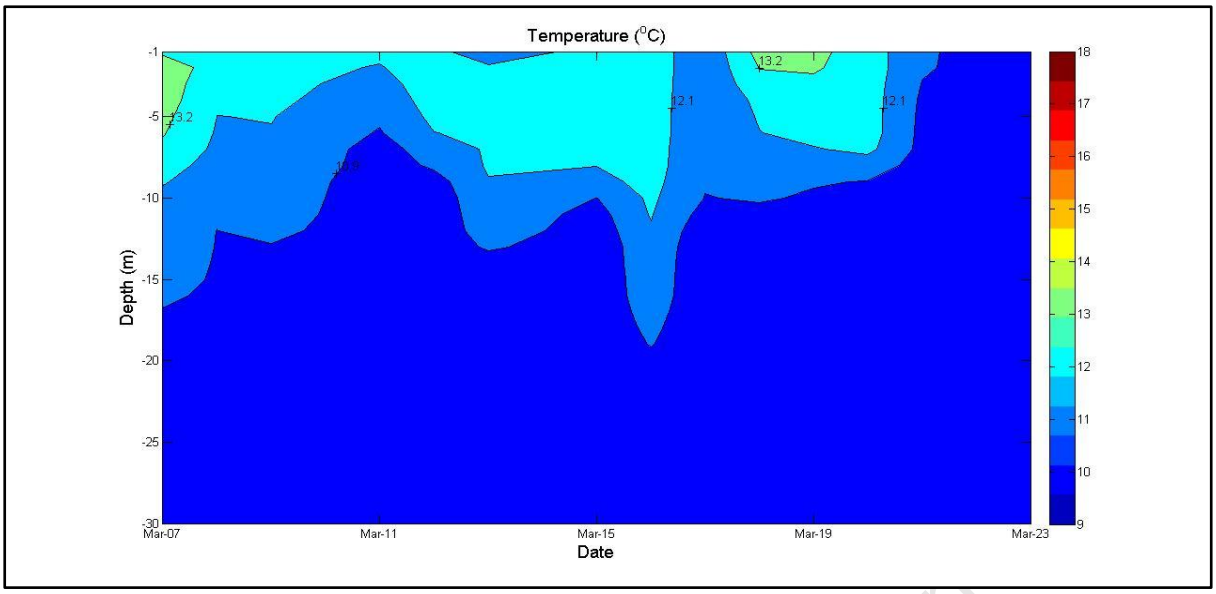

Figure 2.3 Temperature profile data between 1 and 30m depth. Note data gaps from missing days were interpolated.

	1m Temperature	30m Temperature	Period Range in 1m Temperature	Difference between 1m and 30m temperature
Mean	12.4 °C	10 °C	0.8 °C	2.4 °C
Standard Deviation	1.3 °C	0.2 °C	1 °C	1.2 °C
Maximum	15.7 °C	10.6 °C	3.4 °C (8th Mar)	5.1 °C (8th Mar)
Minimum	10.4 °C	9.8 °C	0 °C (23rd Mar)	0.6 °C (23rd Mar)

Table 2.3-Characteristics of the temperature data gathered from the CTD profiles.

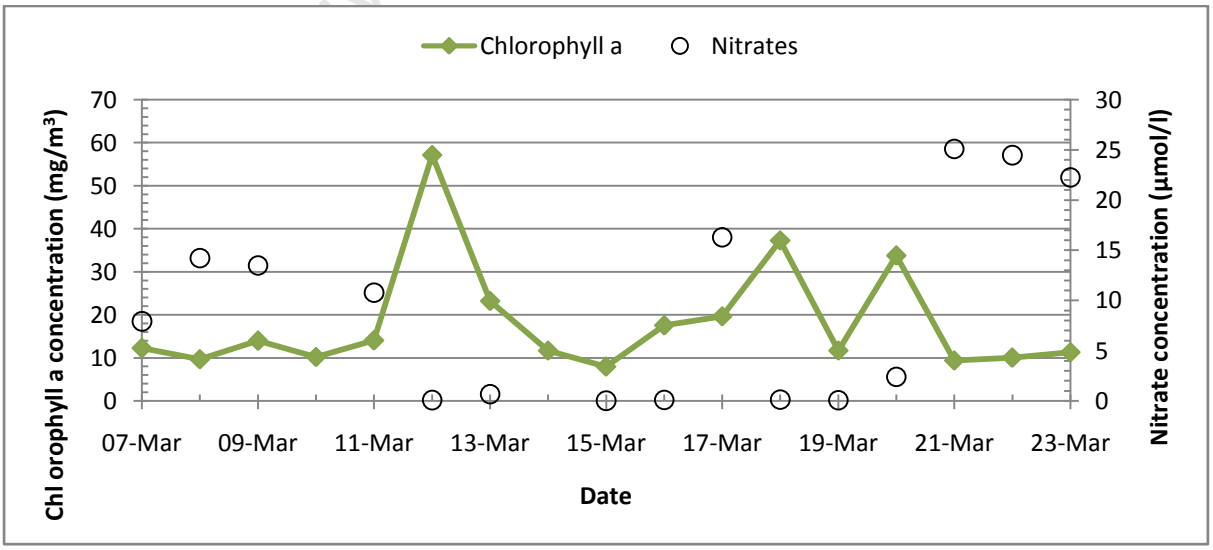

Figure 2.4 Daily surface nitrate concentrations (µmol/l) and extracted surface chlorophyll a concentrations (mg/m^3) for 2006.

2007

Temperature Profiles

In 2007, the water column structure (Fig. 2.5) was categorized by an initial intrusion of cool water at the surface which progressed into full intensity upwelling between 26th and 28th March. Following the upwelling episode there was a period of consistent surface water warming from 31st March until the conclusion of the study period. As with 2005, the surface warming was confined to the upper 15m, with a greater increase as the period continued.

The surface temperatures for the period ranged from 11.1°C to 17.1°C (Table. 2.4), similar to 2005, while temperatures at 30m exhibited a much smaller range of between 9.8°C and 10.8°C. The mean difference between surface and 30m temperatures was 3.9°C, with a maximum difference of 6.5°C on 7th April which was indicative of increased stratification of the water column. The minimum difference was 1.3°C on 27th March which was consistent with moderate upwelling.

Surface Chlorophyll and Nitrate

The *chl a* signal in 2007 was characterized by peaks on 24th and 30th March with concentrations ~ 30mg/m^3 which were significantly less than in 2005 and 2006 (Fig. 2.6). In between the surface peaks the values dropped drastically to levels < 5mg/m^3 and rose again on 30th March. Post the 2nd period peak the *chl a* signal had a decreasing trend for the rest of the period to values of between 0 and 5mg/m^3. At the start of the data set in 2007 the surface NO_3 concentrations were between 0-5µmol/l, followed by a rapid increase from 24th March until 28th March, with a period peak of 33µmol/l on 27th March. From 29th March until the end of the study there was no appreciable NO_3 at the surface as to be expected during the quiescent phase of an upwelling cycle.

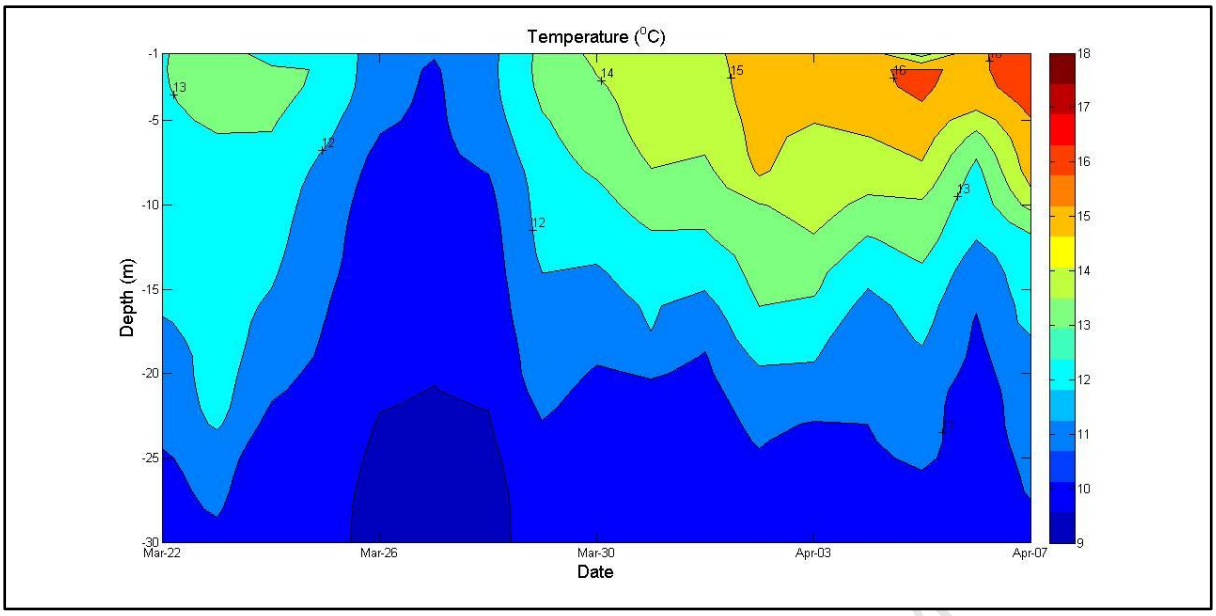

Figure 2.5 Temperature profile data for 2007 between 1 and 30m depth. Note data gaps from missing days were interpolated.

	1m Temperature	**30m Temperature**	**Period Range in 1m Temperature**	**Difference between 1m and 30m temperature**
Mean	14.2 °C	10.3 °C	0.7 °C	3.9 °C
Standard Deviation	1.7 °C	0.3 °C	0.6 °C	1.5 °C
Maximum	17.1 °C	10.8 °C	2.1 °C (28th Mar)	6.5 °C (7th Apr)
Minimum	11.1 °C	9.8 °C	0 °C (23rd Mar)	1.3 °C (27th Mar)

Table 2.4 Characteristics of the temperature data gathered from the CTD profiles.

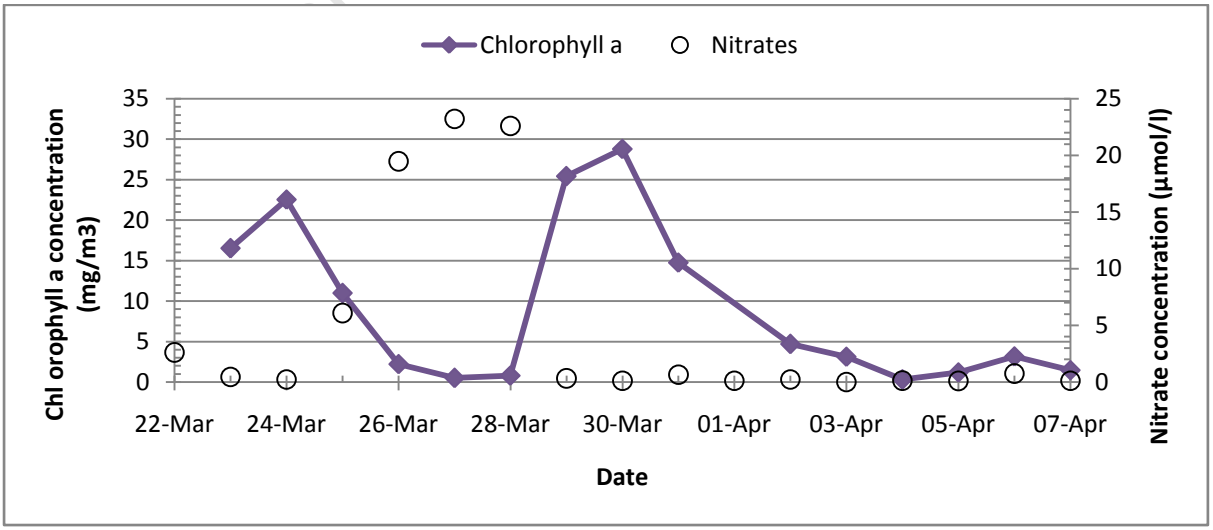

Figure 2.6 Daily surface nitrate concentrations (µmol/l) and extracted surface chlorophyll a concentrations (mg/m^3) for 2007.

2.2.2 Water Column Profiles on Select Days

A few select days in each year were chosen for closer analysis and these days corresponded to those that had either the greatest or the lowest 1-30m temperature range, and those which were susceptible to excessive phytoplankton growth within the collection periods due to their mid level mixing in the water column. The days chosen corresponded to 3 distinct physical water conditions: highly stratified (24/03/05; 08/03/06; 07/04/07); weakly stratified (30/03/05; 19/03/06 and 02/04/07) and well mixed (03/04/05; 23/03/06 and 27/03/07).

On 24th and 30th March 2005; 2nd and 7th April 2007, the water column had a 2-layered physical structure. There was little change in the water column salinities on those days with surface and bottom values averaging 35 and 34.8 per salinity unit respectively, so the layered structure was controlled by the temperature gradient. The temperature gradient showed a 2-layered structure which is typical of moderately to strongly stratified seas with a weak thermocline separating the euphotic zone from the central water. The temperature variability in the bottom layers (Fig. 2.7) ~depth>10m was very low with a standard deviation of +/- 0.9°C and the average temperature gradient throughout the water columns was ~0.180°C/m. On 3rd April, 2005, 23rd March, 2006 and 27th March, 2007 due to upwelling the water column was well mixed (Fig. 2.7) with a relatively constant temperature throughout the columns.

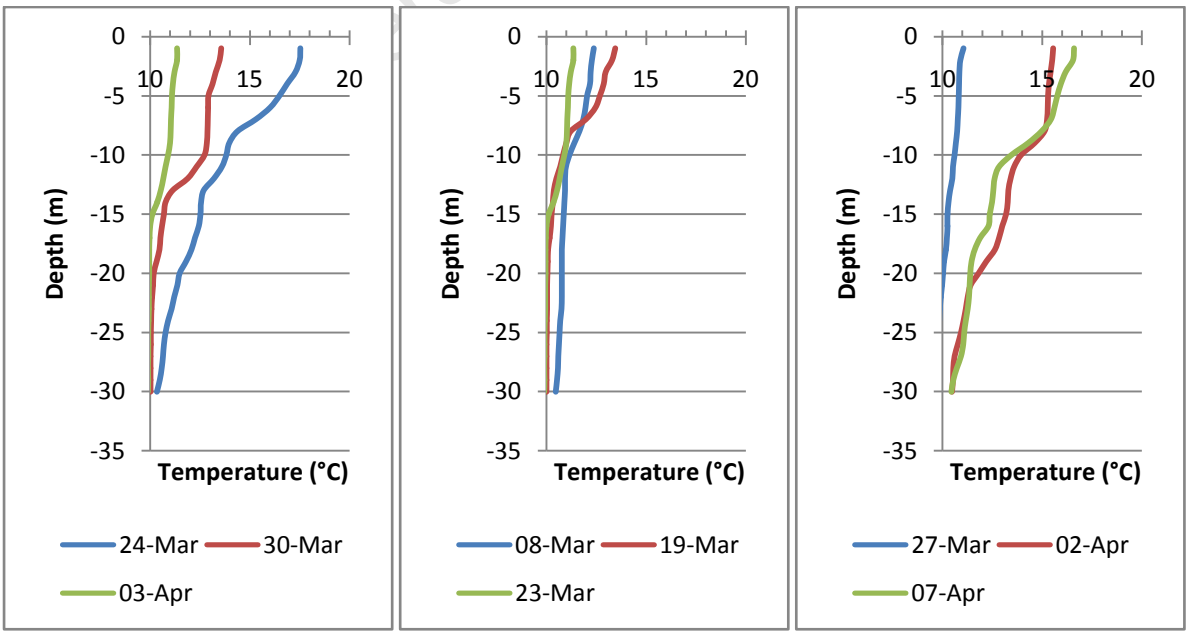

Figure 2.7 Temperature (°C) profiles for 3 different days over the 3 years, 2005 (left panel), 2006 (centre panel) and 2007 (right panel).

A comparison between the extracted *chl a* and fluorometer derived *chl a* is shown on the days in each year that had a weakly stratified water column (Fig. 2.8). There were two periods of significantly high biomass observed throughout the 3 years on 30th March, 2005 and 19 March, 2006. High biomass levels would be harmful if the bloom decays following nutrient exhaustion leading to marine vertebrates and invertebrate deaths due to anoxic conditions. On 30th March, 2005 the fluorometer showed a narrow subsurface *chl a* maximum due to photo-inhibition, which was situated in the upper 5m, with a vertical thickness of at least ~1.5m. Both the extracted and flourometer derived *chl a* displayed similar concentrations with high values (>100mg/m^3) at and close to the surface and a steep decline below 5m. On 19th March, 2006 however the subsurface peak was at a greater depth than the similar day in 2005 and illustrated a larger vertical thickness.

The extracted peak values at the surface reached as high as ~200 mg/m^3 in 2005, 40 mg/m^3 in 2006 and 20 mg/m^3 in 2007. The average maximum concentration for the selected days was 105 mg/m^3 in 2005, 16 mg/m^3 in 2006 and 5 mg/m^3 in 2007 when analyzing the flourometer derived *chl a*. In the surface mixed-layer the *chl a* concentrations were high on 24th and 30th March, 2005 (~60 and ~175 mg/m^3 respectively) and low (~17 mg/m^3) on 3rd April 2005 during active upwelling. In the bottom mixed-layer there was a depth-uniform concentration of ~5-10 mg/m^3 throughout the 3 years. A medium to high surface layer of *chl a*; a declining and increasing *chl a* concentration with depth; and a low but significant concentration below 15m was a constant feature illustrated by all of the *chl a* profiles and extracted values on the weakly stratified days (Fig. 2.8).

The NO_3 data demonstrated the classic pattern of a well-stratified, temperate shelf sea (Sharples et al., 2001), with undetectable NO_3 levels in the surface layer and high NO_3 (< 10µmol/l) in the bottom mixed layer (Fig. 2.9). However upwelling days were characterized by surface concentrations > 15µmol/l and increased concentrations at depth too (Fig.2.9). The nitracline was situated at a depth of between 10 and 15m, just beneath the thermocline on weakly and highly stratified days, and the upwelling days were characterized by moderate to high NO_3 concentrations within the subsurface *chl a* maximum.

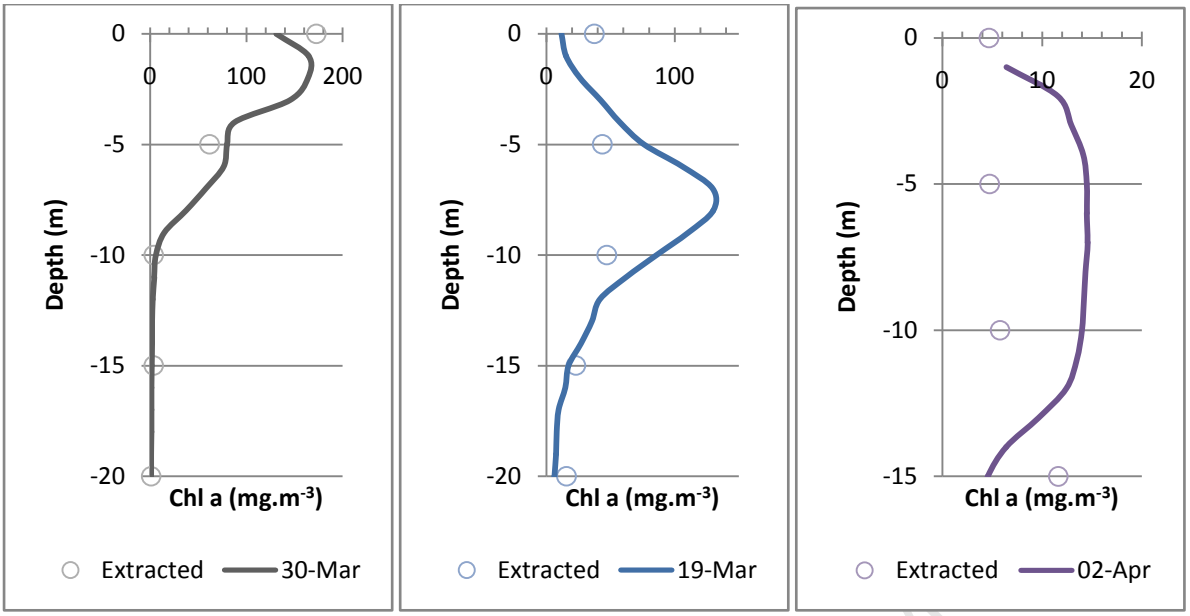

Figure 2.8 Chlorophyll a concentration (mg.m^{-3}) profiles taken from the CTD and the extracted *chl a* concentrations at discrete depths for the weakly stratified days in 2005 (left panel), 2006 (centre panel) and 2007 (right panel).

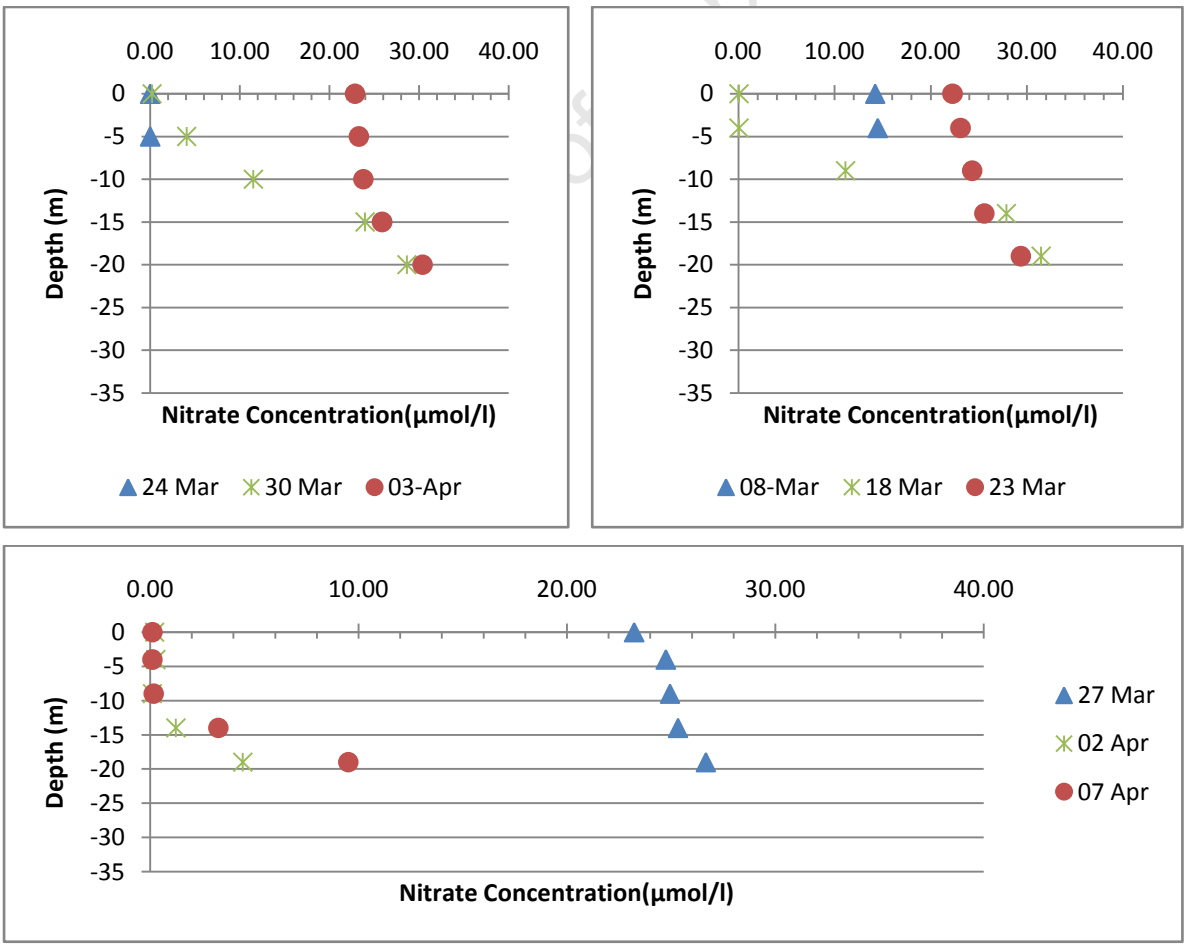

Figure 2.9 Nitrate concentrations (µmol/l) at discrete depths from the water sample analysis for 3 different days over the 3 years, 2005 (left panel, top), 2006 (right panel, top) and 2007 (bottom panel).

2.3 DISCUSSION AND CONCLUSIONS

There are 4 pre-requisites required for successful phytoplankton bloom development (Kudela et al., 2005): Sufficient nutrients in the euphotic layer; sufficient light in the euphotic layer; fast growth rates of the phytoplankton to take advantage of high nutrients and weak or trapped circulation so the bloom is not dispersed.

Sufficient Nutrients

The initial 14 days in 2005 and final 7 days in 2007 were in a quiescent phase of the upwelling cycle and this can be inferred from the relatively low surface NO_3 concentrations, weak to strongly stratified conditions and medium to high surface *chl a* concentrations.

One would expect that the predominant wind direction for the above mentioned time period would be equator-ward due to the periodic weakening of the SAH leading to the persistence of the quiescent phase (Nelson and Hutchings, 1983). The water during both the quiescent phases exhibited characteristics of mature to aged upwelled water (i.e. T: 12°-16°C; low NO_3 accompanied by medium to high surface *chl a* concentrations) (Kudela et al., 2005). Due to the lack of vertical movement within in the water column the thermocline strengthened as the periods wore on, which culminated with the largest water column temperature range on the 24th March, 2005 and 7th April, 2007. The stratification created would lead to a scenario where the input of nutrients from the below the euphotic zone into the euphotic zone would not be likely, thereby creating a situation where the nutrients would have become limiting over time (Johnson et al., 2006). The southern Benguela is dominated by diatoms (Tyrrell and Lucas, 2002), so it is to be expected that the overwhelming phytoplankton concentrations would be of the diatom class in higher turbulence newly upwelled waters on 3rd-4th April, 2005, 23rd March 2006 and 27th March 2007. Diatoms which have fast growth rates and require highly lit environments would have sufficient NO_3 to be sustained (Dugdale et al., 1994). The "shift down" utilization in the NO_3 during the following days would lead to a community succession in the phytoplankton, from diatoms to flagellates (Johnson et al., 2006). Due to the low surface NO_3 concentrations, the diatoms cannot grow, so smaller phytoplankton (i.e. flagellates) are able to out compete diatoms for the scare nutrients (*ibid*). The euphotic layer NO_3 concentrations on: 30th March 2005; 19th March 2006 and 2nd April 2007 were low and would not be able to sustain a diatom bloom. They would however have

been able to sustain a dinoflagellate bloom as they can survive in low light conditions and so move to greater depths to get the nutrients they require for growth at a depth ~10m.

Even though the $Si(OH)_4$ concentrations were not considered in this thesis it is worthwhile noting the role that $Si(OH)_4$ plays in the community and development of blooms (Dugdale et al., 1994). According to Redfield, (1934) the $Si(OH)_4$: N ratio in sea water is ~ 1:1, meaning that the silicate and nitrogen uptake during phytoplankton growth is the same, and it is well understood that the $Si(OH)_4$ utilization is high in diatom cell function thus affecting the proliferation of the phytoplankton type.

Sufficient light and growth rates

Phytoplankton growth is highly proportional to the amount of available light in the mixed layer for photosynthetic purposes (Kudela et al., 2005). The stratification of the water column is important and it is driven by the wind and sun-warming of the mixed layer. The balance of the wind is an integral part of the process, as too much wind will lead to the thermocline deepening and too little wind would lead to a strong stratification where convective motion in the water column would not exist (Bode et al., 1997). The gradual warming that preceded the upwelling on 3rd April, 2005 created a thermocline which was responsible for creating a two-layered system in the ocean, where there was very little mixing at the thermocline boundary at ~ 10m. On 30th March, 2005 however the thermocline was eroded slightly allowing a slight influx of NO_3 into the euphotic layer resulting in increased biological activity at the site shown by the high surface and sub-surface *chl a*. The sudden increase in high fluorescence during this period showing high biomass was mostly likely due to the utilization of the nutrients from below the mixed layer and the advection of high biomass blooms into the region at the surface within the convergence zone inshore of the coastal jet (Pitcher and Boyd, 1996; Pitcher et al., 1998).

The phytoplankton community composition on 30th March 2005 was most likely flagellate dominated due to the low surface nutrients and warmer surface waters, and 19th March 2006 was most likely diatom dominated due to the increased turbulence in the water column.

2.3.1 *Conclusions*

The characteristics of 2006 were of a consistently well mixed water column with an appreciable amount of surface NO_3 throughout the year. The *chl a* values were predominantly

lower during the period due to the well mixed nature of the water column which increased mixing to depth (Carr, 2002). 2005 and 2007 illustrated the classic late summer/early autumn event scale physical and biological coupling for the southern Benguela of a highly variable surface: NO_3 and *chl a* concentrations and temperatures (Nelson and Hutchings, 1983, Armstrong et al,, 1987, Bode et al., 1997, Pitcher and Nelson,. 2006). The intermittent changes in the water column and levels of stratification influenced and determined the phytoplankton life forms illustrated by the high surface biomass values namely in 2005. There was a bloom analysis limitation with a cell count data set not considered which would have been useful in determining the different stages of succession. The data set was intentionally omitted from the *in situ* dataset analysis as this is an earth observation based study and the empirical phytoplankton taxonomy determination is beyond the scope of this study. In this study one should only infer the species type due to the water mass characteristics and our understanding of phytoplankton biology. In 2007 there was no bloom of any significance but rather patches of high biomass which were in all likelihood advected to the sampling location. The impact of the currents and inertial oscillations which influence the bloom favouring retention characteristics of this location were unresolved and prevented the investigator from establishing the role of physical transport in the local development and composition of the blooms.

ALGORITHM DEVELOPMENT AND VALIDATION

Chapter 3-Estimated Surface NO_3 Concentrations

3.1 INTRODUCTION

3.1.1 Nitrate: Estimation and Measurement Using Modelling Approaches

A variety of methods have been developed over the past four decades by researchers in estimating NO_3 concentrations and new production using earth observation based methods in an effort to yield increased spatial and temporal scales. The base model from which a variety of estimation techniques have been created was first proposed by Strickland et al., (1970). Strickland et al., (1970) conducted a six month study in the California Upwelling System off the coast of La Jolla. The authors proposed using NO_3-temperature relationships based on matching vertical water profiles of the two to estimate phytoplankton crop size, growth rates and primary production. The attempt at using proxies to estimate NO_3 concentrations involving the strong inverse relationship between temperature and NO_3 discussed in Strickland et al., (1970) has spawned a multitude of further of studies (Zentara and Kamykowski, 1977, Kamykowski and Zentara, 1986, Waldron and Probyn, 1992, Waldron et al., 1997) and even the future extrapolation of remotely sensed estimations have always been based on the fore-mentioned relationship.

The advent of satellite technology at the end of the 1970s allowed for alternative approaches in estimating surface NO_3. "Remote-Sensing is, broadly but logically speaking, the collection of information about an object without making physical contact...."-Rees, (2001). With the arrival of satellite technology, data collection in the ocean has undergone substantially greater improvements in the last four decades, thus eliminating one of the fundamental problems experienced by oceanographers-the sheer size of the ocean. Over the ocean surface a multitude of variables can be measured directly or through derivations. From satellite remote sensing we can measure the temperature, topography (which can be used to infer other variables such as tides and currents), wind velocity, wave energy spectra and ocean colour (Rees, 2001). But despite the importance of nutrients in ocean productivity remotely sensed measurements are still not a realized ability. It is at this juncture that the known and

extensively researched NO_3-temperature relationship becomes paramount in deriving meso- and synoptic scale productivity.

The result is that with earth observation, NO_3 can now be estimated from remotely-sensed properties such as SST and *chl a*. Early approaches in the remotely sensed estimation of new production involved applying the Eppley-Peterson algorithm and multiplying the estimated primary production by averaged f-ratios of the region of interest (Eppley and Peterson, 1979, Platt and Harrison, 1985, Chavez and Barber, 1987). This technique allowed for the calculation of carbon export rates and was a means to define the efficiency of the BCP. However even though estimations of NO_3 have improved greatly with earth observation the NO_3-temperature relationship has been limited by large temporal and spatial zones and the time and space varying nature of this relationship (Chavez et al., 1996).

Traganza et al., (1983) used satellite data and applied the techniques discussed in Strickland et al., (1970) and derived inverse relationships between NO_3 concentrations and SST. The initial processing and estimation of surface NO_3 using the relationship was confined to local scales where satellite-retrieved SST was processed using algorithms based on the regressions between *in situ* surface temperatures and NO_3 to estimate local nutrient concentrations (Traganza et al., 1983, Dugdale et al., 1989, Kudela and Chavez, 1996, Morin et al., 1993). An example of such a study in which the model was successfully reproduced resulted in a locally derived seasonal pattern of NO_3 concentrations reported in Kudela and Chavez, (1996) where correlations between estimated and *in situ* NO_3 were $r^2 = 0.7$.

More recently however, approaches involving the estimation of new production using satellite data have been complex (SC). Oschlies and Garçon, (1998) used a dynamic-biological model assimilating sea surface height linked with eddy migration. This approach utilized nutrient input derived from eddy migration, which differed from others who commonly had nutrient input in the euphotic zone from upwelling to estimate NO_3. Another attempt not using SST was derived by Stoens et al., (1999) by using weekly winds coupled with a NO_3 transport model in an attempt to estimate new production. Platt et al., (1995) used another variable, *chl a*, in an attempt to estimate productivity. This technique required the construction of a local algorithm and the development of a protocol for the extrapolation of the parameters specified in the local algorithm which influence NO_3 concentrations. One notable parameter involved was based on the partition of the ocean into domains and provinces within which the physical forcing and the algal response to it were distinct.

Further methods have involved the simultaneous use of multiple variables which contribute and affect NO_3 concentrations. Goes et al., (1999, 2000) proposed adding a *chl a* term to the already established algorithms using SST, as variations in the phytoplankton content can account for a large part of the variability in estimated NO_3. By adding the *chl a* term it helped in the NO_3 prediction by reducing local and regional differences in the character of the NO_3-temperature relationship. In the study, Goes et al., (1999, 2000) divided the north Pacific Ocean into 2 separate domains as per Platt et al., (1985), and developed separate empirical algorithms for each of the 2 regions. Goes et al., (1999, 2000) showed that if biologically enforced changes in the character of the NO_3-temperature relationships are taken into account, it is possible to generate high resolution estimated surface NO_3 maps. SC proposed an alternative approach based on NO_3-temperature relationships and Goes et al., (1999, 2000) for dynamic upwelling areas such as the Benguela. The estimated surface NO_3 concentrations in this study are based on the approach proposed by SC.

3.1.2 Silió-Calzada et al., 2008 Method

In this thesis the estimated surface NO_3 concentrations were calculated using the approach proposed in SC for utilization in the Benguela. The foundation of the proposal was built on the known NO_3-temperature relationships but also took into account the works done by Goes et al., (1999, 2000) which included the effect of *chl a* concentrations on NO_3 concentrations. In work done by SC, NO_3-SST relationships were developed using best-fit functions parameterized from discrete *in situ* measurements from the World Ocean Database (WOD) collected between 1989 and 2005 in the Benguela to estimate NO_3 concentrations. The SC approach was structured to explicitly incorporate seasonal and latitudinal variability of the NO_3–SST relationship affecting the ecosystem. For this reason, different algorithms were developed for seasonal groupings of: autumn/winter and spring/summer. The results from such tests showed that segregating areas within the ecosystem resulted in strong discontinuities which implied the need for a unique algorithm for the whole Benguela (SC).

In the approach, SC used the *in situ* surface temperatures, referred to as SST_{depth} from here onwards, as a predictor in the estimation of surface NO_3 concentrations. The regression of the *in situ* NO_3 and SST_{depth} in SC yielded the following algorithms:

$$NO_3\,(SST_{depth}) = 615.84 - 121.96*(SST_{depth}) + 8.815*(SST_{depth})^2 - 0.184*(SST_{depth})^3$$

(N= 149, r^2= 0.296, RMSE= 6.87)

- autumn/winter period (April-September) (3.1a)

$$NO_3\,(SST_{depth}) = 192.20 - 29.21*(SST_{depth}) + 1.488*(SST_{depth})^2 - 0.025*(SST_{depth})^3$$

(N= 246, r^2= 0.742, RMSE= 2.82)

- spring/summer period (October-March) (3.1b)

When considering processes affecting the surface layer, the progressive heating after an upwelling event constitutes one of the many factors responsible in the time and space variability found in the NO_3-SST_{depth} relationship. The following excerpt from *Silió-Calzada, PHD Thesis, 2008* explains the need for a new approach in the methodology of the estimation of NO_3 concentrations in dynamic upwelling areas:

"*The temperature of the upwelled water increases by the effect of the solar radiation at a variable rate depending on the geographic location and time of the year. Moreover, such a heating rate responsible for this thermal deviation from the source water is not necessarily coupled with the phytoplankton uptake rate. Phytoplankton nitrate consumption and water heating do not necessarily happen at the same rate, which leads to deviations from the initial conditions of temperature and nitrate in the source water (Traganza et al., 1983). The time and space variability in the NO_3-SST relationships are also due to the differences in the source of the upwelled water. Even though it is generally assumed that upwelled waters usually come from depths of 200m or less (Barber et al., 1971, Dugdale, 1985), the intensity of the upwelling, the local bathymetry and the coastal orientation play a relevant role in the variability of the depth of the water source. These differences in depth may imply physical-chemical differences, in temperature and nutrient concentration as a result of oceanic circulation patterns. It is on these differences in the temperature of the upwelled water that we have focused our attention for the development of an alternative approach to estimate nitrate surface concentrations. Retaking the tests performed in the Benguela upwelling system, we found that the seasonal and geographical dispersion affecting the NO_3-SST*

relationships may be reduced by taking into account the variability in the upwelled water temperature, $T_{up.}$"

The term, $T_{up,}$, taking into consideration the temperature of upwelled water was used in SC in an attempt to reduce the scatter between the NO_3 concentrations and the SST_{depth}. The proposal used the following assumptions when estimating the temperature of upwelled water: *"1) source water upwells within the 0-200m deep fringe of the continental shelf, 2) the upwelled water presents a characteristic potential density of 26.5 (Carr and Kearns, 2003), and 3) within a given latitudinal band, T_{up} is considered to be the minimum water temperature within the 26.5 isopycnal."* The fore-mentioned assumptions were primarily based on Carr and Kearns, (2003), where according to the authors, between 20°S and 35°S, upwelled water comes almost uniformly from the 26.5 potential density surface. Therefore SC used the simultaneous *in situ* profiles of temperature and salinity extracted from the WOD05 data set of the NOAA-NEDIS-National Oceanographic Data Center to determine T_{up} as a function of latitude and season. The profiles in the WOD05 data set were grouped into twenty 1° latitude intervals from 15°S to 35°S, and the density profiles were derived from the salinity and temperature profiles. In order to delineate the on-shelf upwelling area, only the profiles which corresponded to bottom depths of less than 200m were considered. According to SC *"for each couple of temperature/density profiles, the temperature corresponding to the potential density 26.5 ($T_{26.5}$) was recorded; then the T_{up} temperature was taken as the minimal $T_{26.5}$ value obtained within each 1° box"* (Fig. 3.1). The discrete T_{up} estimates, which reflected the latitudinal dependency were then fitted to a continuous function (linear interpolation) for each season (Fig. 3.2)

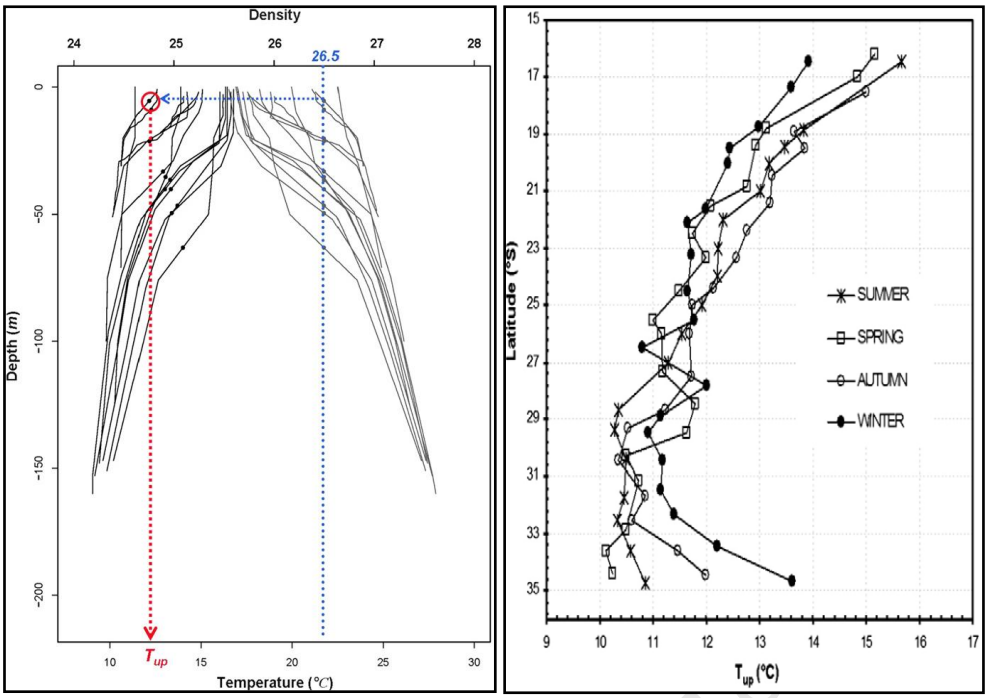

Figure 3.1 (left panel) Scheme for the estimation of the temperature of source water, T_{up}, based on *in situ* profiles of temperature and density, as extracted from WOD05 data set of the NOAA-NESDIS-National Oceanographic Data Center (Boyer et al., 2006). The profiles represented here correspond to a 1° latitude box (only stations with a bottom depth lower than 200m were included). Grey lines correspond to density profiles, whereas the black ones represent tem -perature. The dots on the temperature profiles correspond to a density of 26.5.

Figure 3.2 (right panel) Variations with the estimated temperature of upwelled water, T_{up}, for the seasons in the Benguela System (15°S-35°S). (Both figures and descriptions adapted from Silió-Calzada et al., 2008)

NO_3 concentrations can then be predicted for a given latitude and season, as a function of the temperature difference (δT) between SST_{depth} and that of upwelled water:

$$\delta T = SST_{depth} - T_{up}\,(\text{latitude, season}) \qquad (3.2)$$

When this was taken into account the T_{up} term was found to produce higher determination coefficients when δT was substituted in place of SST_{depth} and regressed against the NO_3 concentrations. The regression analysis in SC yielded the following algorithms:

$$NO_3(\delta T) = 25.700 - 13.863*(\delta T) - 2.585*(\delta T)^2 + 0.155*(\delta T)^3$$

(N= 149, r^2= 0.672, RMSE= 4.69)

-autumn/winter period (April-September) (3.3a)

$$NO_3(\delta T) = 21.355 - 7.008*(\delta T) + 0.804*(\delta T)^2 - 0.0313*(\delta T)^3$$

(N= 246, r^2= 0.749, RMSE= 2.93)

-spring/summer period (October-March) (3.3b)

The tight correlation between δT and the surface NO_3 concentrations was due to the latitudinal and seasonal variability being taken into account when estimating T_{up} (SC). The utilization of the term ($SST_{depth} - T_{up}$) was not a new proposal as it was already used by Dugdale et al., (1989) and Kudela and Chavez, (2000) in their new production models to estimate the "age" of upwelled water (assuming a constant heating rate). Dugdale et al., (1989) considered T_{up} as constant whatever the season and location which differed from Kudela and Chavez, (2000) who considered the seasonal variations of T_{up}, but assumed that its spatial variations were negligible. Due to such an approximation's likely validity only applicable for a restricted area such as Monterey Bay analyzed in Kudela and Chavez, (2000) and not a large marine system, SC proposed the derivation of T_{up} as a function of latitudinal and seasonal variations. The substitution of SST_{depth} by δT constituted an attempt at tracing the water heating from the upwelling moment up to the actual observation. The proposed idea is based on the underlying assumption that upwelled water moves from the upwelling cell westwards, which the authors acknowledged was a rough approximation.

SC found that the temperature of source water varies little with season and that the maximum values are found north of 20°S and south of 32°S. The authors also noted that the temperature range of the source water they derived was consistent with that of "upwelled Benguela Current Water" described in O'Toole, (1980), but higher than those described by Calvert and Price, (1971) and Andrews and Hutchings, (1980) for the northern and southern regions of the ecosystem respectively. According to SC the southern subsystem of the Benguela (26°S-35°S) presented a less defined trend than the northern ecosystem with oscillating values up to

32°-33°S, and (except in spring) increasing temperatures from 33 to 35°S. This might be due to the influence of the Agulhas Current which induces a warming of the waters, therefore the results in this latitudinal band must be considered with caution (SC).

The addition of a *chl a* concentration term was first proposed in Goes et al., (1999, 2000) and it was used in SC to evaluate the influence of phytoplankton on the accuracy of the estimated NO_3 concentrations. The multiple regression of: δT, NO_3 and *chl a* in SC yielded the following algorithms:

$$NO_3\,(\delta T, chl\ a) = 24.992 - 9.463*(\delta T) + 0.947*(\delta T)^2 - 0.435*(chl\ a)$$

(N= 145, r^2= 0.782, RMSE= 4.01)

-autumn/winter period (April-September) (3.4a)

$$NO_3\,(\delta T, Chl\ a) = 21.747 - 4.840*(\delta T) + 0.273*(\delta T)^2 - 0.342*(chl\ a)$$

(N= 214, r^2= 0.823, RMSE= 2.90)

-spring/summer period (October-March) (3.4b)

The estimated NO_3 concentrations were calculated for the project location as per the method described above from SC using the *in situ* dataset collected in: 2005, 2006 and 2007. The performance of the derived algorithms was then compared to that of: Eqn. 3.1b, Eqn. 3.3b and Eqn. 3.4b at the sampling location.

3.2 METHODS

3.2.1 Algorithms

The nutrient proxy was created using the *in situ* dataset, and an attempt was made to model the surface NO_3 for the southern Benguela. The estimated surface NO_3 concentration fields were calculated first as a function of the *in situ* surface temperature (SST_{depth}) followed by temperature with extracted surface *chl a* concentrations.

In view of the fact that this study is earth observation based, the analysis was restricted to variables at the sea surface only. However *in situ* data from the subsurface was included in the final analysis in Chapter (6) of the algorithm performances. In the derivation of the estimated NO_3 algorithm, *chl a* was chosen as the predictor biological variable as per Goes et al, (1999, 2000). The variable was preferred largely because of its known relationship with NO_3 in the euphotic zone and its accessibility from remote sensing along with SST (Goes et al., 1999, 2000).

Statistics

The derivation of the both the estimated NO_3 algorithms were based on 44 data points of the surface *in situ* temperature and extracted *chl a* which were Lillifors tested for bivariate normal distribution. In all the cases outliers were analyzed and removed if they were outside the range of 2 standard deviations. The relationship between NO_3 and its predictor variables were examined using: non-linear regression for SST_{depth} and δT with Microsoft Excel 2007; multivariate regression with Statistica 10 and the Pearson product-moment correlation used to describe the coefficient, *r*. The standard deviation was used as a measure for variation between the estimated NO_3 and *in situ* NO_3 and calculated as follows:

$$\text{Standard Deviation} = \sqrt{\frac{\sum (x-\bar{x})^2}{(n-1)}} \qquad (3.5)$$

- where x-bar is the mean of the distribution.

The root mean squared error which summarizes the overall errors was calculated using Statistica with the following equation:

$$RMSE = \sqrt{a^2 + b^2 + c^2 \ldots} \quad (3.6)$$

3.2.2 In situ data set alterations

In this chapter only a single T_{up} value from autumn at ~32°S was utilized for 2005-2007 according to the time period of the *in situ* data collection and the nearest latitude to the location. The T_{up} derived in S.C for 32°S was ~10.8°C. A minor adjustment was done to the *in situ* surface values of the variables used in the derivation of the estimated NO_3 concentrations. The adjustment done was the removal of NO_3 concentrations at temperatures >15.2ºC because values were usually below detection as was the case in Lucas et al., (2013) where the NO_3-temprature relationship above 16ºC was negligible for the same region. For this reason the algorithm is only valid and applicable at a water temperature interval of between 10°C and 15.2°C and any estimated NO_3 concentrations above that interval were assumed to be 0µmol/l.

3.3 RESULTS

3.3.1 Estimated Surface NO_3

New algorithms were developed for St Helena Bay using the method described in SC. The locally derived algorithm performances were then compared to those developed in SC for the estimation of surface NO_3 concentrations in the Benguela.

NO_3- SST_{depth} relationship

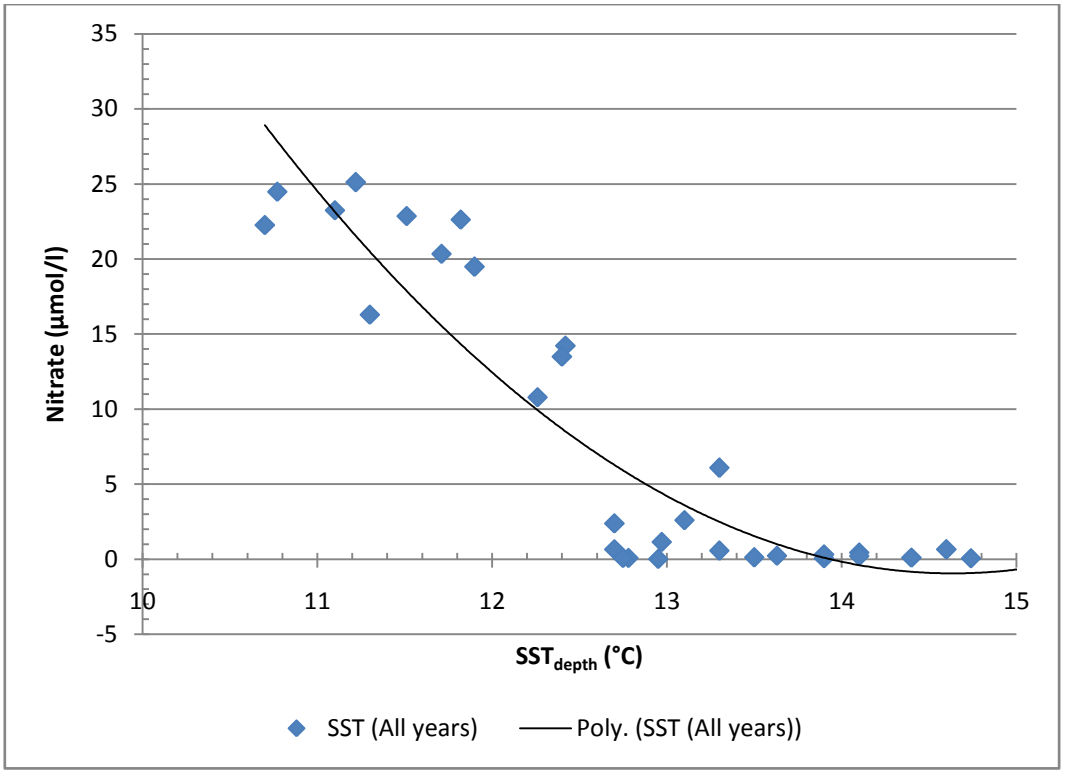

Figure 3.3-Relationship between NO_3 concentrations (µmol/l) and SST_{depth} (ºC) at the study site, for the periods in 2005, 2006 and 2007. Data has been extracted and calculated from the daily CTD casts and water samples, and have been fitted to a best-fit function (Eqn. 3.5).

The NO_3-SST_{depth} relationship at the site illustrated increased dispersion at moderate to low surface temperatures and high surface NO_3 (i.e. upwelling phase), and less scatter at moderate to high temperatures and low surface NO_3 (i.e. quiescent phase) (Fig. 3.3). The event scale variability at the site was suitably revealed in which the different phases of an upwelling cycle can clearly be identified with temperatures from 13-15°C being associated with the

quiescent period and temperatures < 13°C being during the early to late upwelling period. The regression analysis of the local surface NO_3 concentrations and the SST_{depth} was done and the analyses yielded the following algorithm:

$$NO_3 = 411.8 - 56.40*(SST_{depth}) + 1.926*(SST_{depth})^2$$
$$(N = 34,\ r^2 = 0.838,\ adj\ r^2 = 0.818,\ RMSE = 5.66) \qquad (3.7)$$

The regrouping of the data into two main seasons according to distributions and trend similarity as conducted in SC was unnecessary due to the consistent time period of this study. The NO_3-SST_{depth} relationship was characterized both by a small high dispersion period and a larger tightly fitted trend which resulted in a strong correlation between the two of *adj* r^2 = 0.818. A further analysis of the dispersion observed in the NO_3- SST_{depth} relationship showed that most of the outliers corresponded to 2006. This suggested that while the NO_3-SST_{depth} relationships were similar between the different years, consistent upwelling without a substantial quiescent period resulted in the maintenance of surface NO_3 even with slightly increased water temperatures. It is to be noted that Eqn. 3.7 may sometimes yield negative NO_3 values for SST_{depth} values ranging from 14-15°C (Fig. 3.3). However in this temperature range the measured NO_3 concentrations were generally approaching undetectable values and hence, these negative values can be considered as 0µmol/l.

Figure 3.4 showed the comparison between utilizing the locally derived algorithms based on the current project data and the SC derived algorithms for the ecosystem in predicting surface NO_3 concentrations. From the results presented in figure 3.4, right panel, it is evident that when the area under investigation is small, the predictions of NO_3 using large-scale derived algorithms from SC are insufficient. Algorithm 3.1b performed poorly on a localized scale shown by the inappropriate coefficient of determination. However algorithm 3.7 from the current study showed a good correlation between the NO_3-SST_{depth}, with an increased determination coefficient and a decreasing RMSE value (Fig. 3.4, top panel). The performance evaluation between the thesis derived and the SC derived algorithms isn't wholly surprising considering that the derivation of one is based on the current *in situ* data. What is of greater significance is the comparison between how each of the algorithms performed with their respective *in situ* datasets from which they were derived. On a larger

ecosystem scale the SC algorithm showed a lower but significant determination coefficient with its own particular dataset during the summer/autumn window. The locally derived algorithm performed slightly better than Eqn. 3.1b from SC with respect to its own *in situ* data set.

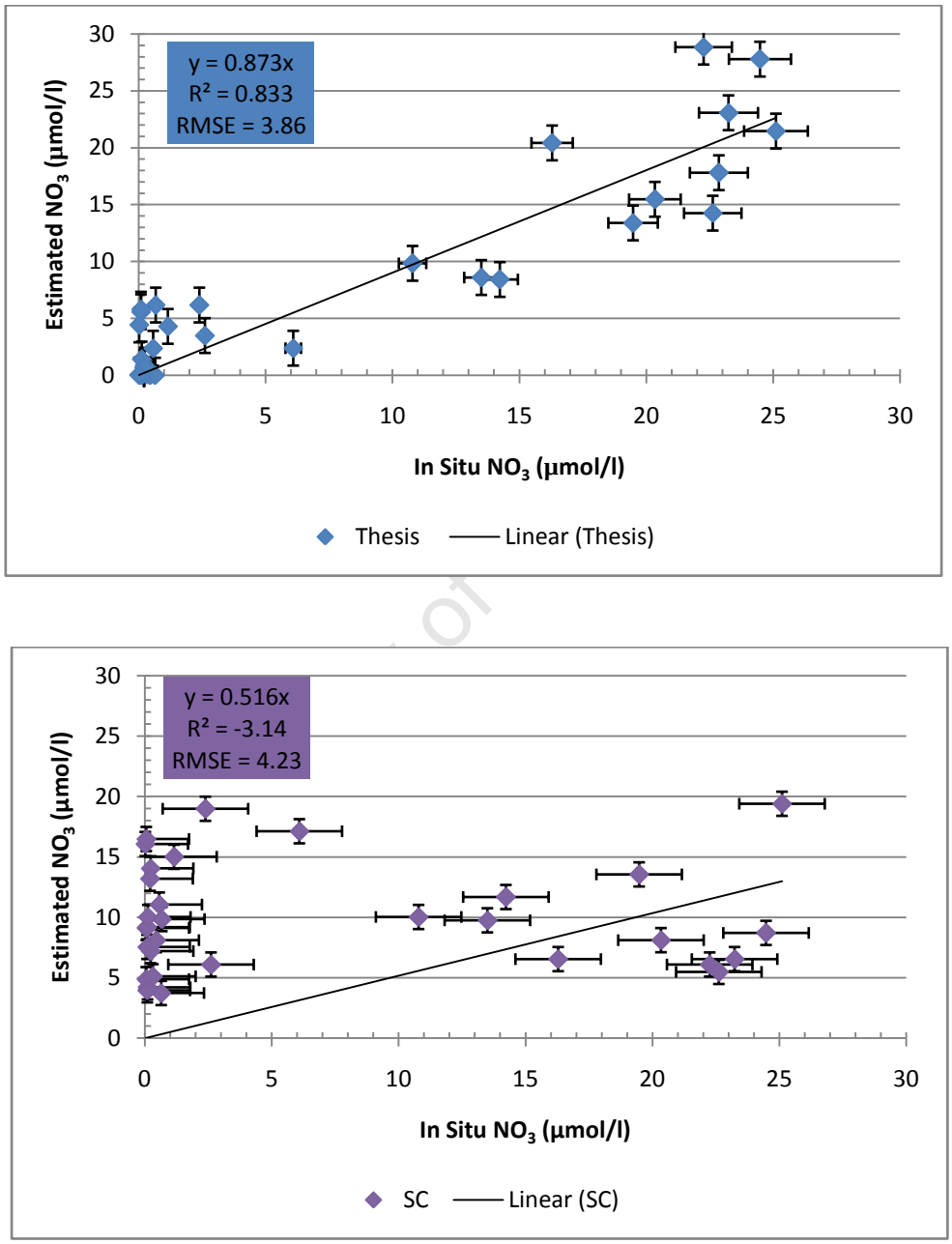

Figure 3.4 Estimated vs. measured NO_3 (µmol/l), using Eqn. 3.7 (top panel), and Silió-Calzada et al., 2008, Eqn. 3.1b (bottom panel). Vertical error bars indicate the standard deviation of the data mean and horizontal error bars indicate the total calculated uncertainty associated with the estimated NO_3 values.

NO_3- δT relationship

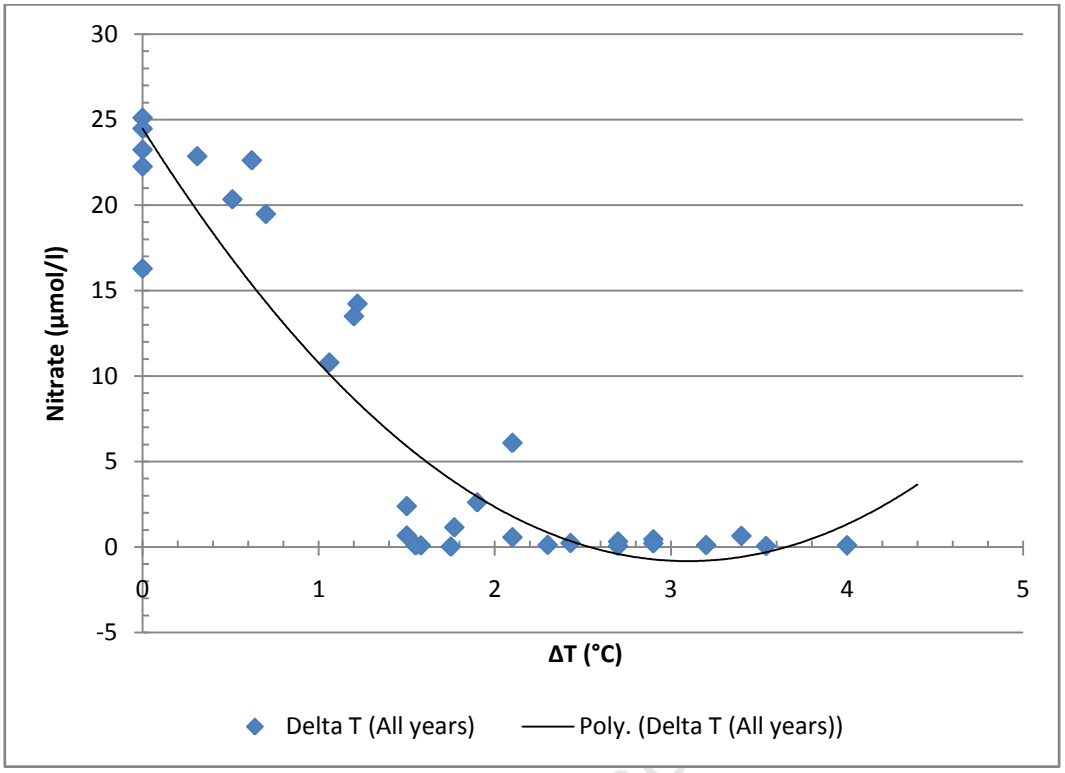

Figure 3.5 Relationship between NO_3 concentrations (µmol/l) and the temperature difference from upwelled water, using T_{up} (ºC) from autumn-winter. The dataset is identical to that in Figure 3.3, and the polynomial fit corresponds to Eqn. 3.8.

On a synoptic scale it is thought that the introduction of the δT term in place of the SST_{depth} term would improve the prediction capability in the algorithms (SC). On a local scale when the δT term is substituted in place of the SST_{depth}, the regression analyses yielded the following algorithm:

$$NO_3 = 24.26 - 15.68*(\delta T) + 2.405*(\delta T)^2$$
$$(N = 34,\ r^2 = 0.871,\ adj\ r^2 = 0.864,\ \text{RMSE} = 2.4)$$
$$\text{-using } T_{up} \text{ from the autumn-winter period} \qquad (3.8)$$

A comparison between figures 3.3 and 3.5 showed that substituting the δT term for the SST_{depth} term led to a slight statistical improvement shown in the slightly greater determination coefficient. The scatter in the NO_3-temperature relationship between figure 3.3

and figure 3.5 showed much less dispersion in the region of high NO_3 and low temperature. This suggested that introducing the δT term from the autumn-winter period showed that the NO_3 concentration is more tightly correlated to the temperature increase of upwelled water when spreading off shore, than to the direct temperature of the surface water (SC).

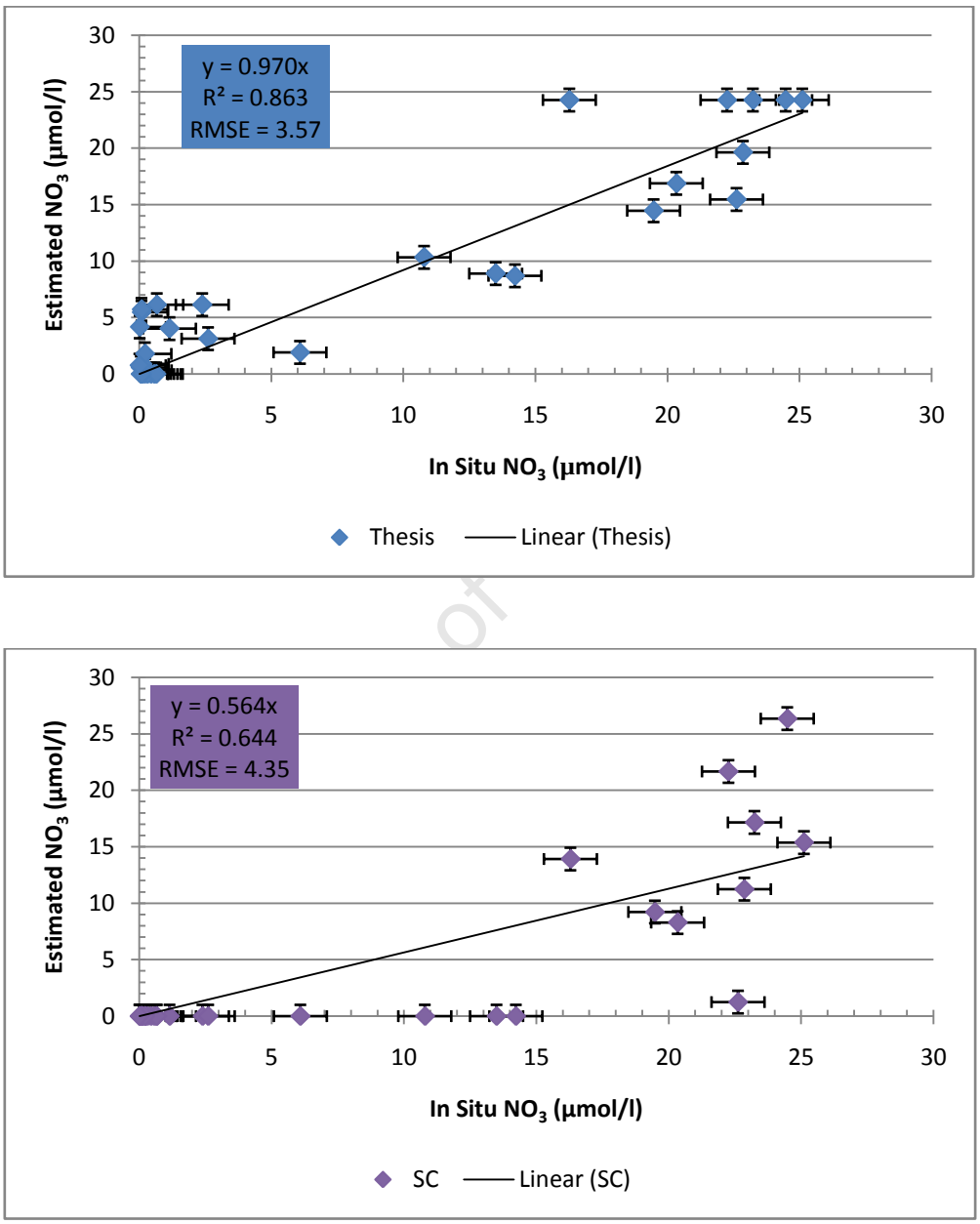

Figure 3.6 Estimated vs. measured NO_3(µmol/l), using Eqn. 3.8 (top panel), and Silió-Calzada et al., 2008, Eqn. 3.3b (bottom panel). Vertical error bars indicate the standard deviation from the data mean and horizontal error bars indicate the total calculated uncertainty associated with the estimated NO_3 values.

There was a slight increase in the determination coefficients from figure 3.4 (top panel) to figure 3.6 (top panel). Substituting in the δT term into the algorithm did make an improvement in the prediction of the surface NO_3. There was significant variability between the observed and the estimated surface NO_3 concentrations < 20µmol/l where the predicted NO_3 underestimated values. Eqn. 3.3b from SC showed a marked improvement from figure 3.4 (bottom panel) to figure 3.6 (bottom panel). However the reasonable $r^2 = 0.64$ still shows considerable scatter between the estimated and observed NO_3 concentrations at low estimated NO_3 concentrations.

Inclusion of chlorophyll a in the NO_3- δT relationship

Based on the work initially done by Goes et al., (1999, 2000) and used in the Benguela by SC, the *chl a* concentration was included in the NO_3- δT regression analysis. For the location the following empirical algorithm was obtained:

$$NO_3 = 18.50 - 0.76*(\delta T) - 0.21*(chl\ a)$$
$$(N = 34,\ r^2 = 0.67,\ adj\ r^2 = 0.64,\ \text{RMSE} = 1.7)$$
$$\text{-using } T_{up} \text{ from the autumn-winter period} \qquad (3.9)$$

The scatter in the relationship is increased with respect to the NO_3- δT when the *chl a* concentration is included in the algorithm. This goes against the predicted suggestion that the variations in biomass abundance explain part of the variations in NO_3 concentrations and therefore a fraction of the scatter in the NO_3-SST_{depth} relationship. Eqn. 3.9 implied that the surface *chl a* concentration at local levels is not beneficial in the prediction of surface NO_3 concentrations due to the possibility of the advective movement of high biomass patches through a fixed location and a particular time, and that there is a distinct decoupling between the biology and the physics in the system on a instantaneous temporal scale. The surface advection of high *chl a* patches on a local scale would not be indicative of NO_3 utilization at the same location thus the inclusion of *chl a* was detrimental in the process of predicting surface NO_3 at a given location and time. This is shown in figure 3.7 (top panel) where the determination coefficient decreased from figures.3.4 and 3.6 (both top panel) and the RMSE increased. This however differs from the utilization of the *chl a* concentrations on a synoptic

scale (Fig. 3.7, bottom panel) where they yielded a very good correlation between the predicted and observed NO_3.

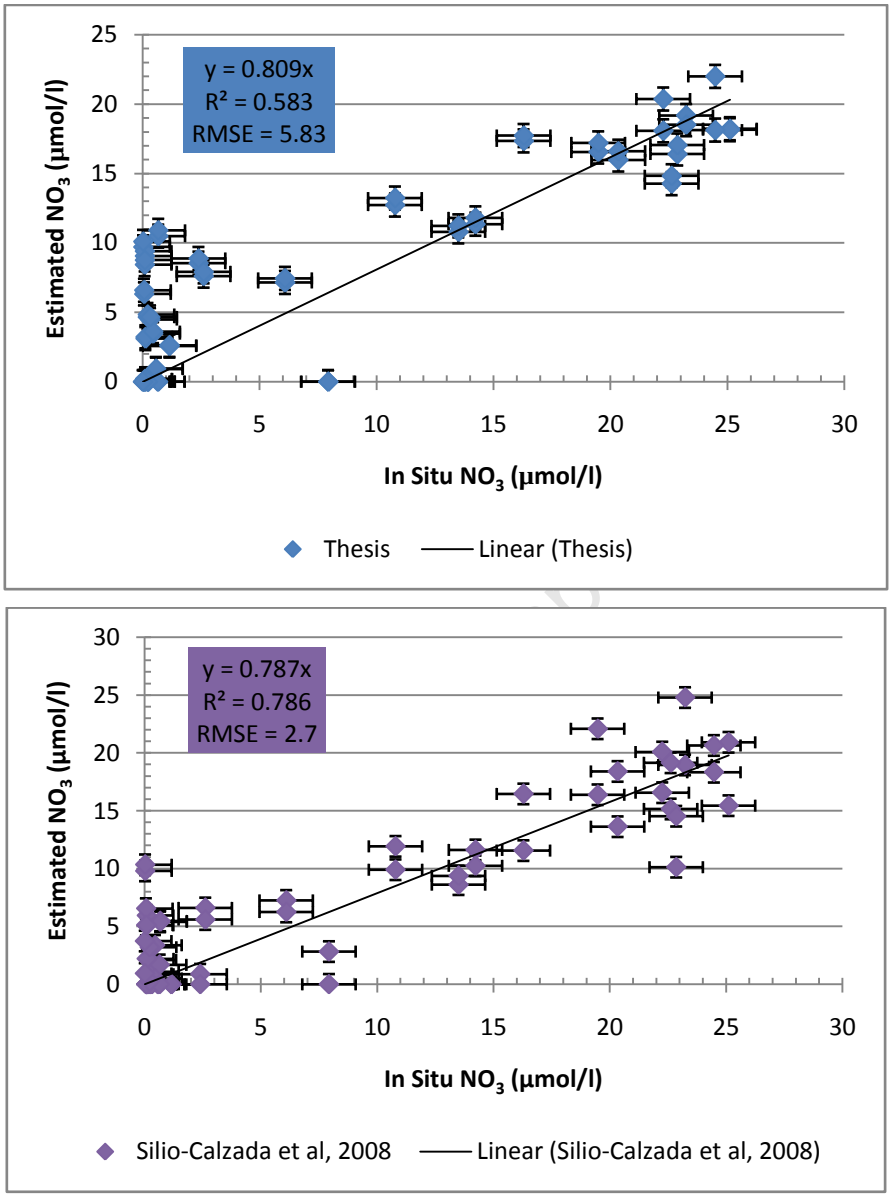

Figure 3.7 Estimated vs. measured NO_3 (µmol/l), using Eqn. 3.9 (top panel), and Silió-Calzada et al., 2008, Eqn. 3.4b (bottom panel). Vertical error bars indicate the standard deviation from the data mean and horizontal error bars indicate the total calculated uncertainty associated with the estimated NO_3 values.

Overall the introduction of the δT term in the NO_3-SST_{depth} relationship, as an indicator of the time elapsed since upwelling slightly improves the performance of the initial algorithm based solely on temperature. The addition of a *chl a* term into the algorithm decreased the

performance of the estimation of surface NO_3. The supplementation of the *chl a* concentrations did however show a good correlation when utilizing Eqn. 3.4b from SC. It was evident that on a local scale, the substitution of the δT term improves the algorithm performance but the introduction of a *chl a* term does not. The regressions between the *in situ* NO_3 and temperature showed a very narrow range where there was appreciable NO_3 and for this the reason the margin of validity for the algorithms is very small.

Chapter 4-The Derivation of the Estimated Isotherm Depth

4.1 INTRODUCTION

4.1.1 Turbulence/Stratification

In past and current literature the estimation and measurement of turbulence in sea water has either been measured directly, modelled directly, or inferred by the estimation of the thermocline, the mixed layer depth or the isotherm depth.

The important feature in understanding or predicting an ecological niche whereby bloom formation is possible is an appreciation that turbulence and stratification are different physical processes. Turbulence is the biophysical stressor which is capable of impairing individual phytoplankton cells and stratification influences phytoplankton population dynamics through interactions with vertical irradiance and nutrient gradients (Smayda, 2002). Smayda, (2002) discussed the need for the re-evaluation of the classic stratification-HAB paradigm, where watermass stratification has been considered the essential physical condition that dinoflagellates require to bloom. In the publication the interlinked relationship between turbulence and stratification was examined and further evidence was shown that turbulence has a greater influence on the possibility of bloom formation over stratification. Experimental studies suggest that flagellates are more sensitive than diatoms to turbulence and associated shear-stress, resulting in the physiological impairment and loss of cellular integrity (Estrada and Berdalet, 1997), but dinoflagellates have evolved to deal with biophysical tolerance in water-column disturbance rather than wait for stratification that would not provide nutrients and would limit growth (Smayda, 2002). According to Smayda, (2002) watermass stratification that often accompanies flagellate blooms is probably a secondary, less essential and parallel event to the other factor(s) in triggering a bloom. In addition, Smayda, (2002) highlighted the coping and adaptive strategies dinoflagellate species have acquired to increase their tolerance to greater turbulence. These adaptive strategies result in dinoflagellate species being able to develop in slightly higher turbulence areas such as offshore and in upwelling frontal zones, resulting in "pelagic seed banks" from which HABs could form (Smayda, 2002). In the southern Benguela it is at these frontal zones where dinoflagellate blooms could potentially occur and under particular wind and current conditions these frontal

blooms are transported and accumulated inshore and red tides are formed (Pitcher and Boyd, 1996).

4.1.2 Turbulence

Basis of Turbulent Studies

Turbulence studies in the ocean take a multitude of methodologies which are all inherently linked to the equations of motion with viscosity, which are used to calculate vertical mixing. Munk, (1966) used a very simple observation to calculate average vertical mixing in the ocean based on that: "the ocean has a thermocline almost everywhere and that the deeper part of the thermocline doesn't change seasonally". This observation changed the thinking at the time, where downward mixing was thought to continuously deepen the thermocline, but this was not the case. Therefore, a steady-state thermocline required that the downward mixing of heat by turbulence must be balanced by an upward transport of heat by a mean vertical current, which would be necessary in calculating the average vertical flux in the ocean.

Dynamic Stability

In the process of understanding vertical stability in the ocean, turbulence studies are best quantified by the Brunt-Väisälä frequency (Eqn. 4.1) which can be interpreted as the angular frequency at which a vertical displaced parcel will oscillate within a stratified environment (Stewart, 2007).

$$N \equiv \sqrt{-\frac{g}{\rho}\frac{d\rho}{dz}} \quad \text{where } \rho \text{ is the potential density.} \qquad (4.1)$$

According to the frequency if $N^2>0$ then the parcel would remain in the new vertically displaced position, illustrating water column stability. If however $N^2<0$ the newly displaced parcel would accelerate back towards its initial position, and then the water column is said to be unstable, and generally overturning or convection happens. A number of studies have used the Brunt-Väisälä frequency in an attempt to explain water stratification. Houry et al., (1987) calculated Brunt-Väisälä frequency profiles for the south Atlantic to depict gradients in the upper ocean and infer the thermocline depth. This was a continuation of works done initially

by Emery et al., (1984) who calculated the seasonal profiles of the Brunt-Väisälä frequency and the Rossby Radii for the north Pacific and Atlantic Oceans.

Estimating the Mixed Layer Depth

The calculation of the mixed layer depth (MLD) is another perspective from which turbulence can be inferred, not quantitatively but in a qualitative manner. Cury and Roy, (1989), Robinson et al., (1994), Wijesekera and Gregg, (1996) emphasized the importance of MLD estimation to the upper-ocean and productivity. Many different characterizations of the MLD exist in scientific literature but the commonly used characterization is that "the base of the MLD is the depth at which the potential density in the upper layer changes by 0.01 kg/m^3 relative to the ocean surface density" (Peters et al., 1988, Schneider and Muller, 1990, Wijffels et al., 1994, Smyth et al., 1996a, b, Skyllingstad et al., 1999). Current literature methods in MLD estimation can be split into three broad categories:

1. Threshold methods which find a predefined step in the surface profile by specifying a threshold slope for the vertical density gradient or a threshold for the density offset relative to the ocean surface (Price et al., 1986, Peters et al., 1988).
2. Least squares regression methods, which fit two or more line segments to near-surface density profile data (Papadakis, 1981, 1985).
3. Integral methods which calculate a depth scale for the upper layer utilizing the Brunt-Väisälä frequency (Freeland et al., 1997).

Calculating Turbulence

Methods in the quantitative calculation of turbulence in the ocean can be separated into techniques: observational methods and numerical modelling methods. Burchard et al., (2008) released a review paper detailing the most commonly used methods for calculating small scale turbulence and mixing with applications to coastal oceans. Observational methods involve: the estimations of Reynolds stresses utilizing the comparison of the velocity variances of opposing beams of an Acoustic Doppler Current Profiler (ADCP) (Lu and Lueck, 1999, Stacey et al., 1999, Simpson et al., 2005, Rippeth et al., 2002, 2003) and calculating turbulence through resolving particle image velocimetry in the bottom boundary layer (Adrian, 1991, Nimmo-Smith et al., 2002, 2004). Modelling techniques involve the application of a: Large Eddy Simulation to simulate surface-layer mixing due to ocean surface forcing or heat fluxes via convection (Ferziger and Perić, 2001, Wang et al., 1998; Large and Gent, 1999) and empirical turbulence models based on energy conservation

considerations in the mixed layer which traditionally depict the MLD, mixed layer temperature and salinity (Kraus and Turner, 1967; Denman, 1973).

4.1.3 Stratification

Estimating Thermal Stratification

In the fore-mentioned studies the thermal stratification was inferred from the turbulence values, MLD and/or Brunt-Väisälä frequencies. Palacios et al., (2004) quantified the thermal stratification and its changes in the California Upwelling System using a state-space model decomposition of subsurface temperatures. The state space model first proposed in Schwing and Mendelssohn, (1997) decomposes a mean-level "trend term" which is the maximum $\frac{dt}{dz}$, to extract stratification. In combination with the Kalman filter and the "maximum likelihood estimation" explained in Durand and Mendelssohn, (1998) the method produces statistically consistent estimates of the monthly and seasonal component of the stratification in the system. In the Benguela Upwelling System, Pitcher and Nelson, (2006) derived a stratification index to measure the vertical stability of the water column, where the temperature gradient at the base of the mixed layer was chosen as a proxy for stability, which was then multiplied by the depth of the mixed layer and divided by the surface temperature. The method differed from conventional studies which used Brunt-Väisälä frequency methods as a proxy for stratification because it intrinsically took into account the development time associated with upwelling events and associated changes in the phytoplankton community structure.

Estimating the depth of the thermocline

The use of earth observation as a means of measuring or inferring stratification is primarily split into two approaches. The first approach involves using Synthetic Aperture Radar (SAR) images to estimate the depth of the thermocline (New and Da Silva, 2002, Porter and Thompson, 1996, Gerkema, 2001, New, 1988). The methodology is based on the proven assumption that internal waves in the ocean measured by SAR travel within the thermocline. The thermocline depth can then be computed from the wave speed which is derived from a simple 2-layer fluid-model.

The second method in the utilization of earth observation in turbulence/stratification studies employs an isotherm depth as a proxy for the thermocline depth. Ocean altimetry derived from satellites is used to infer changes in the depth of the thermocline due to sea-level being a robust indicator of thermocline movement in the equatorial Pacific Ocean (Turk et al., 2004). Turk et al., (2004) used altimetry in the equatorial Pacific to infer the thermocline depth in the investigation of the net-effects of El Niño and La Niña on biogeochemical cycles in the region. In the study the 20°C isotherm was used as a proxy for the thermocline because of the high correlation between it and new production. The isotherm anomalies were tightly correlated with the altimetry ergo the isotherm was the thermocline. This method was first proposed in Chaen and Wyrtki, (1981) where the high correlation that existed between the 20°C isotherm depth and dynamic topographs of sea surface height were first discovered. In this study however the thermocline wasn't inferred from the isotherm but rather the isotherm served as an indicator in monitoring geostrophic flow in the equatorial currents by using a 2-layer approximation of the density structure.

Stratification using earth observation in the southern Benguela

The multitude of methods used in previous studies were primarily in tropical oceans where the 2-layer density is perennial and complete mixing of the water column due to wind is low to non-existent. In this study the following hypothesis is proposed:

The 11° or 12° isotherm depth serves as a proxy for the thermocline in the southern Benguela. This enables the utilization of earth observation techniques in the prediction of the thermocline depth which is important in bloom dynamics and formation.

Chapter (4) in this thesis provides a clear description of the derivation of the isotherm chosen as a proxy for the thermocline for 2005-2007. Further more in the section the creation of the robust algorithms in estimating the chosen isotherm's depth is explained. The results section measures the performance of the estimated isotherm depth algorithms first as: a function of temperature and secondly as a function of both the remotely sensed wind and temperature over the 3 years.

4.2 METHODS

4.2. 1. Estimated Isotherm Depth

The establishment of the stratification/turbulence proxy involved tracing the 11th and 12th degree isotherm (Iso_{temp}) depth through the water column using the *in situ* data. The daily isotherm depths were calculated by using the 'interp1' function in Matlab, which estimates the depth of the required isotherm according to the temperature profile.

Statistics

The dataset as was with the estimated NO_3, were tested for bivariate normal distribution. The 11th and 12th degree isotherm depths were then regressed against the estimated thermocline depths using a linear regression fitting routine with Microsoft Excel with the following equation:

$$m = \frac{\sum (x - \bar{x})(y - \bar{y})}{\sum (x - \bar{x})^2}$$

$$b = \bar{y} - m\bar{x} \qquad (4.2)$$

Pearson's product moment correlation was used to find the isotherm with the larger determination coefficient and it was chosen as the isotherm that would be utilized as a proxy for the thermocline depth. The estimated depth of the thermocline was calculated using the 'gradient' function in Matlab and the depth at which the gradient of the temperature profile was the largest was taken as the thermocline depth. During upwelling episodes there was a lack of a definitive temperature gradient in the water column, on such days the thermocline was assumed to be at the surface (i.e. 1m). The standard deviation and RMSE were calculated in this chapter in the same way as in Chapter (3).

Choosing the isotherm to be used as a proxy for the thermocline

The Iso_{11} depth in 2005 did not go deeper than 30m and it did not reach a depth shallower than 5m. There was large scatter (Fig. 4.1, left panel) between the Iso_{11} depth and the thermocline depth throughout the time period at both shallow and deep depths. The resultant

$r^2=0.601$ showed the moderate relationship between the Iso_{11} depth and the thermocline depth, and for this reason it was insufficient to use the Iso_{11} as a proxy for the thermocline depth. The Iso_{12} depth however was tightly correlated to the thermocline depth (Fig. 4.1, right panel) for the same period with an $r^2=0.890$. The relationship between the two showed no scatter but a single outlier was evident. The Iso_{12} depth was markedly shallower than the Iso_{11} depth throughout the period and captured the upwelling of cooler water with the isotherm reaching the surface on these occasions.

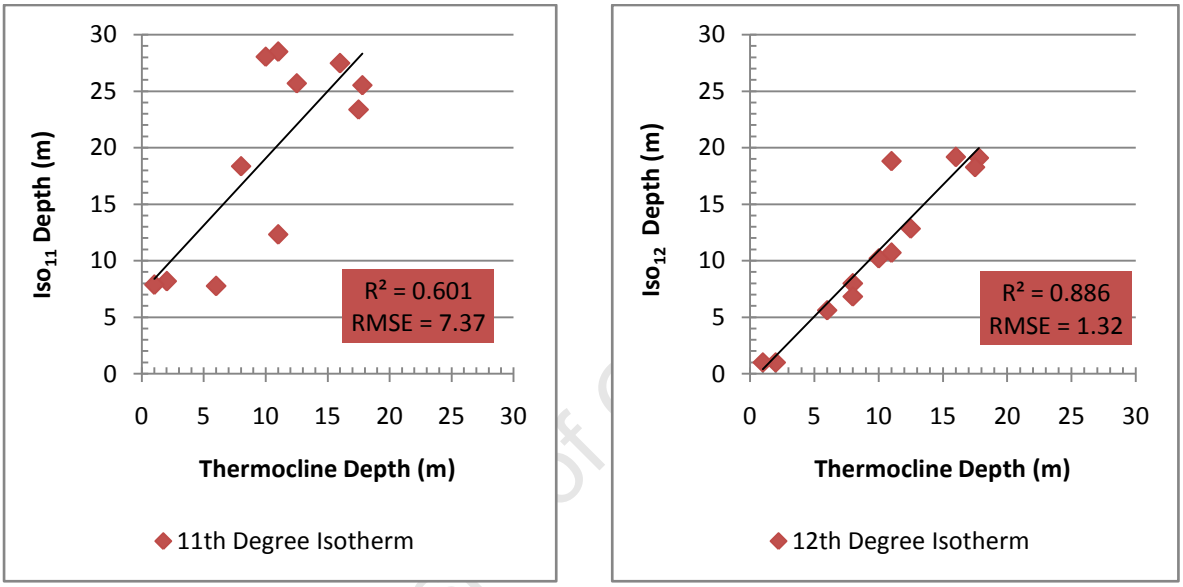

Figure 4.1 Relationship between the 11ºC isotherm depth and the thermocline depth (left panel), and the relationship between the 12 ºC isotherm depth and the thermocline depth (right panel) both for 2005.

In 2006 the relationship between the Iso_{11} and the thermocline depths was significantly less scattered (Fig. 4.2, left panel) than in 2005. Throughout the period the thermocline depth showed appreciable shoaling due to the constant upwelling experienced at the site and the Iso_{11} depth on occasions did correlate with the thermocline at the surface. However significant scatter still persisted at depths greater than 10m. The Iso_{12} depth during the same period only went above 10m once exhibiting the same shoaling effect evident in the thermocline depth (Fig. 4.2, right panel), for this reason the good correlation of ~ $r^2=0.8$ is still maintained between 2005 and 2006. At depths between 5 and 10m the relationship however showed slightly increased scatter yielding one significant outlier (i.e. > 2 standard deviations).

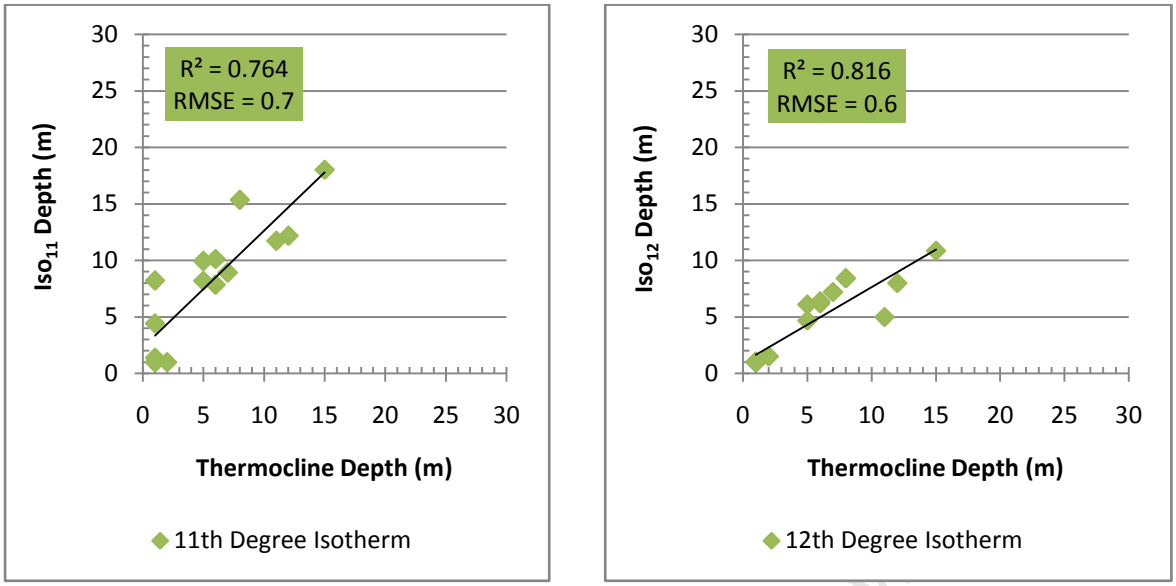

Figure 4.2 Relationship between the 11 ºC isotherm depth and the thermocline depth (left panel), and the relationship between the 12 ºC isotherm depth and the thermocline depth (right panel) both for 2006.

In 2007 the relationship between the Iso_{11} depth and thermocline was the strongest throughout the 3 years (Fig. 4.3, left panel). There was significantly less scatter at the depths >15m between the two, but increased scatter still persisted at the depths <15m. The initial strength of the correlation between the Iso_{12} depth and the thermocline shown in 2005 was retained in 2007 (Fig. 4.4, right panel). This is as to be expected due to the similar nature of the water column temperatures between the two years.

When all the Iso_{11} depths were considered for all of the periods it was evident there was lack of a strong correlation between it and the thermocline depths (Fig. 4.4, left panel). At depths between 0 and 10m the Iso_{11} was too deep when compared to the thermocline thus not picking up the signal of newly upwelled water. Comparatively at depths >10m the scatter was markedly less and the relationship showed greater parallels, helping improve the overall correlation to $r^2=0.742$. The Iso_{12} depth- thermocline relationship over the entire time periods was similar in 2005 and 2007 with an overall r^2 *of 0.878* (Fig. 4.4, right panel). The data in figure 4.4 (right panel) show that Iso_{12} is a good robust indicator of the thermocline depth.

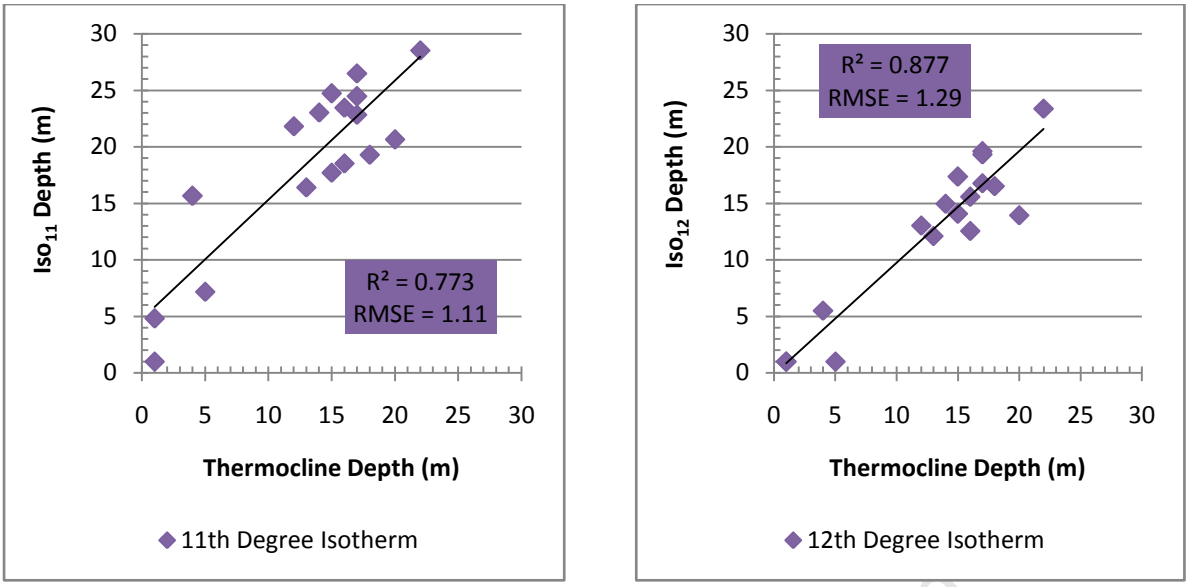

Figure 4.3 Relationship between the 11 ºC isotherm depth and the thermocline depth (left panel), and the relationship between the 12 ºC isotherm depth and the thermocline depth (right panel) both for 2007.

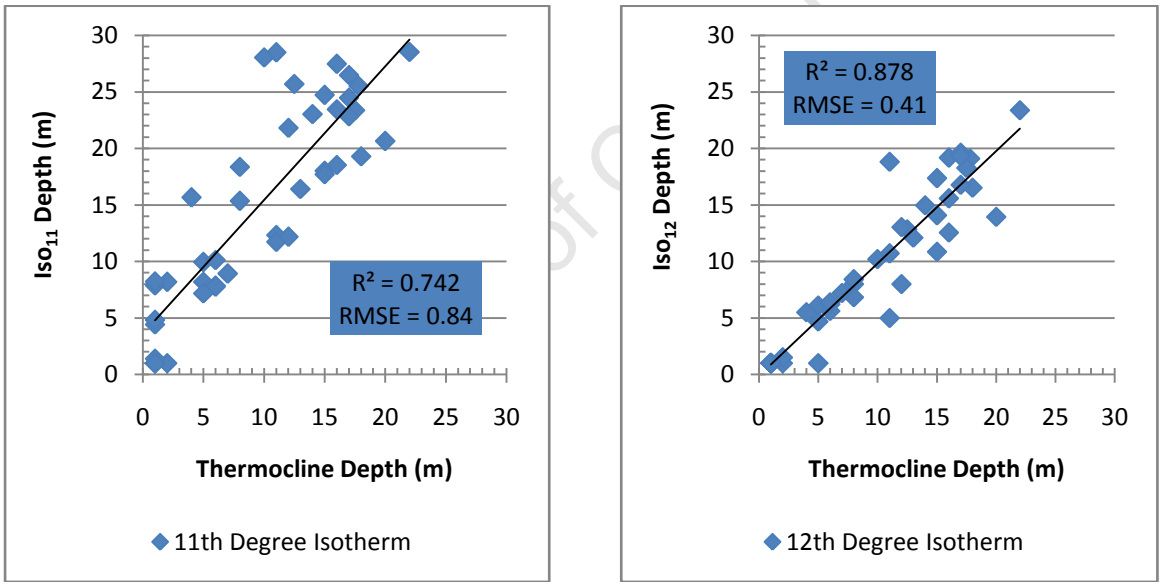

Figure 4.4 Relationship between the 11 ºC isotherm depth and the thermocline depth (left panel), and the relationship between the 12 ºC isotherm depth and the thermocline depth (right panel) both for 2005, 2006 and 2007.

4.2.2 Wind Dataset

In the Benguela various remote sensing instruments are used. NASA's now non-operational sun-synchronous (QuikSCAT mission launched in June 1999) Seawinds scatterometter which uses a specifically designed microwave 1800-km-wide swath radar to measure near ocean surface vector winds of between 3 and 20m/s . The ability to provide broad synoptic coverage by satellite cannot be over-estimated. But as useful and relatively accurate as the low resolution satellite data provided by the scatterometer is, as with other variables the ability to resolve the temporal and spatial variability of the upwelling along the system has serious limitations (Weeks et al., 2006). The wind vector measurements used in the derivation of the robust isotherm depth algorithm were level 2B, 25 km resolution fields consisting of time averaged 6-hourly daily gridded data files with an accuracy of +/- 0.75 m/s in the along wind component and +/- 1.5 m/s in the crosswind component (Chelton et al., 2006) and directional accuracy of +/- 20°. The winds are referenced to 10m height. The wind vectors acquired were already processed using the QSCAT -1 geophysical model function from the SeaWinds processing and Analysis Center. In the ecosystem the along-shore winds are responsible for the water displacement and for this reason only the meridional wind vector components were utilized in this chapter. The initial wind vector data extracted for use was in a 2x3 matrix which included the *in situ* site at the border between pixel 3 and 6 (Fig. 4.5). The 6 pixels considered for use were chosen due to the upwelling favourable southerly winds in St Helena Bay area being deflected around Cape Columbine and blowing with an on-shore component to the north of Cape Columbine (Fawcett et al., 2007). The 6 pixels each represent the north/south wind vector component at a 25km resolution. The pixels throughout the years showed minimal variability, even though a large percentage of pixels 3 and 6 overlapped onto land (Table 4.1).

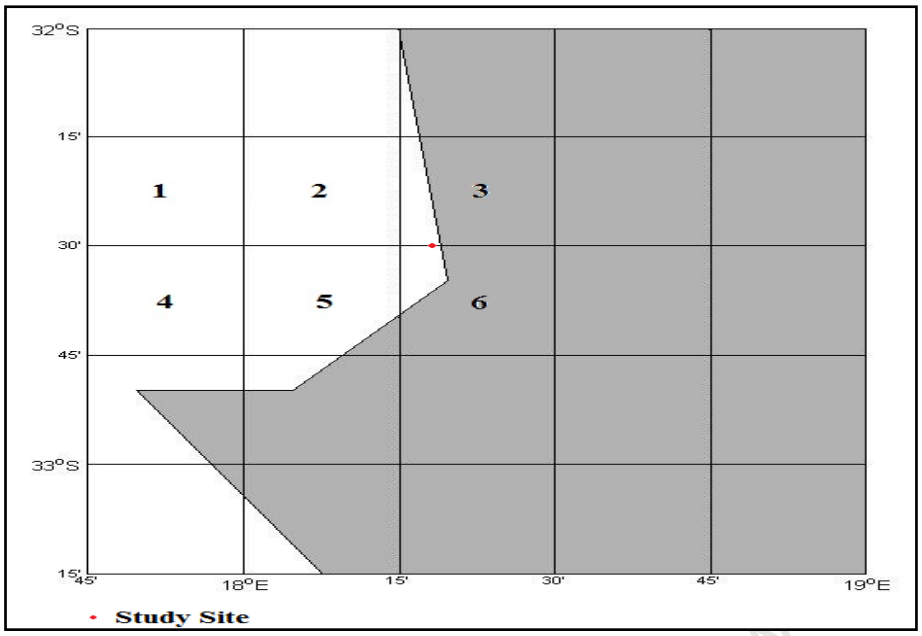

Figure 4.5 QuickScat wind data grid representation for St Helena Bay. The numbered blocks correspond to the data grid compared and later used in the algorithm derivation.

Grid	Pixels Used (#)	Average Wind Speed (m/s)	Standard Deviation (m/s)
2x3	1-6	3.80	2.94
2x2	1,2,4 & 5	3.81	2.96
1x2	3 & 6	3.73	2.89

Table 4.1- Characteristics of the gridded wind data gathered from the daily QuickScat Seawinds overpasses.

Due to the minimal change between the various grids, the choice of which combination to use was arbitrary. The 2x2 matrix compromising of pixels 1, 2, 4 & 5 was eventually chosen for use in the derivation of the estimated Iso_{12} depth due to the lack of land overlap onto the pixels. The rain contamination which is a well documented problem affecting scatterometers and tends to result in erroneous cross track vectors and/or unrealistically high wind speeds didn't not seem to affect the region. The QuickScat data had 12% missing data overall, with an average of 2 days per year during the study period where wind fields in the region were unavailable.

4.3 RESULTS

4.3.1 Estimated Iso_{12} depth

The relationship between the Iso_{12} depths and *in situ* surface temperatures was analyzed during the periods for 2005, 2006 and 2007. The Iso_{12} depths were linearly regressed against the *in situ* surface temperatures (SST_{depth}) and the resultant equation was used as the robust algorithm in the prediction of the estimated Iso_{12} depth as a function of temperature:

$$Iso_{12}\,\text{depth} = -31.52 - 2.940*(SST_{depth})$$
$$(N = 44;\ r^2 = 0.68;\ adj\ r^2 = 0.67;\ RMSE = 4.24) \qquad (4.3)$$

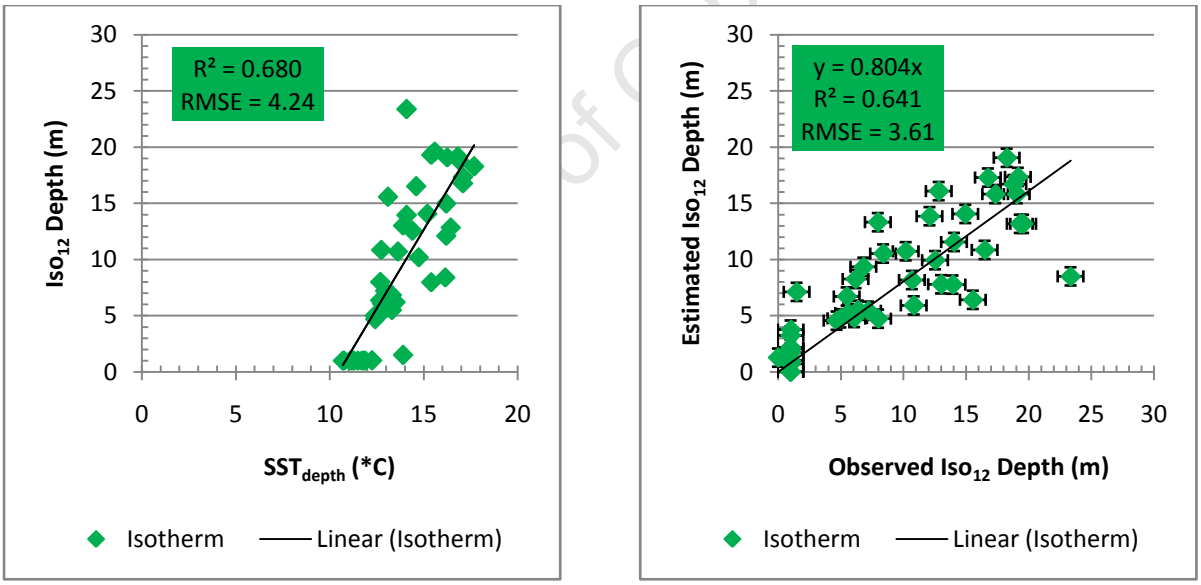

Figure 4.6 Relationship between the Iso_{12} depth (m) and surface temperature at the study location (left panel), and estimated vs. measured Iso_{12} (m) using Eqn. 4.3 (right panel) for the periods in 2005, 2006 and 2007. The vertical error bars indicate the standard deviation from the data mean and horizontal error bars indicate the total calculated uncertainty associated with the estimated Iso_{12} values.

The Iso_{12} depth and the *in situ* temperature were moderately correlated with one another. The coefficient of determination, r^2, was 0.68 and the *adj* r^2 was 0.67. The relationship showed slightly increased scatter at depths > 10m. The relationship between the observed and

predicted Iso_{12} depth showed large dispersion at depths > 5m, with a moderate determination of coefficient of r^2 = 0.631 and an *RMSE* of 3.61. It is worth noting that Eqn. 4.3 yielded negative estimated Iso_{12} values for temperatures < 11°C. However below this temperature the measured negative Iso_{12} depth values were considered as zero as it is impossible for the Iso_{12} depth to break the surface. Negative values indicated that there was no discernable thermocline in the water column.

Iso_{12}- wind, temperature relationship

In wind driven upwelling systems the water temperature in the mixed layer is a function of the wind speed. In most occurrences the influence of the wind on the physical characteristics of the water has a lagged effect. In the calculation of the second algorithm for the prediction of the Iso_{12} depth, a multivariate regression using Statistica was done between the interpolated Iso_{12} depths, SST_{depth} and the remotely sensed wind speeds from the preceding day ($Wind_{rs}$). In the derivation of the estimated Iso_{12} depth only the upwelling favourable/non favourable (i.e. north/south component) wind was included and the following empirical algorithm was derived:

$$Iso_{12}\,Depth = -25.10 + 2.57*(SST_{depth}) - 0.39*(Wind_{t-1})$$

(t = present day)(N = 34; r^2 = 0.75; *adj* r^2 = 0.73.3; *RMSE* = 5.09) (4.4)

The determination of coefficient improved with 75% of the daily variability in the Iso_{12} depth accounted for by Eqn. 4.4 when the wind speed from the preceding day was taken into account. The RMSE does however become larger than in Eqn. 4.3. The algorithm improvement was further translated into the accuracy of the estimated Iso_{12} depths when regressed against the observed values (Fig. 4.7). The marked dispersion was still evident at depths > 5m and the estimated Iso_{12} depth showed greater variability than the observed during upwelling. The relatively larger dispersion at cooler temperatures was due to the fact that temperatures which constituted as upwelling had a ~1°C range throughout the 3 years. This affected the estimated Iso_{12} values as the algorithm is very sensitive to temperature changes thus yielding a slightly larger variance in estimated Iso_{12} depths at low temperatures.

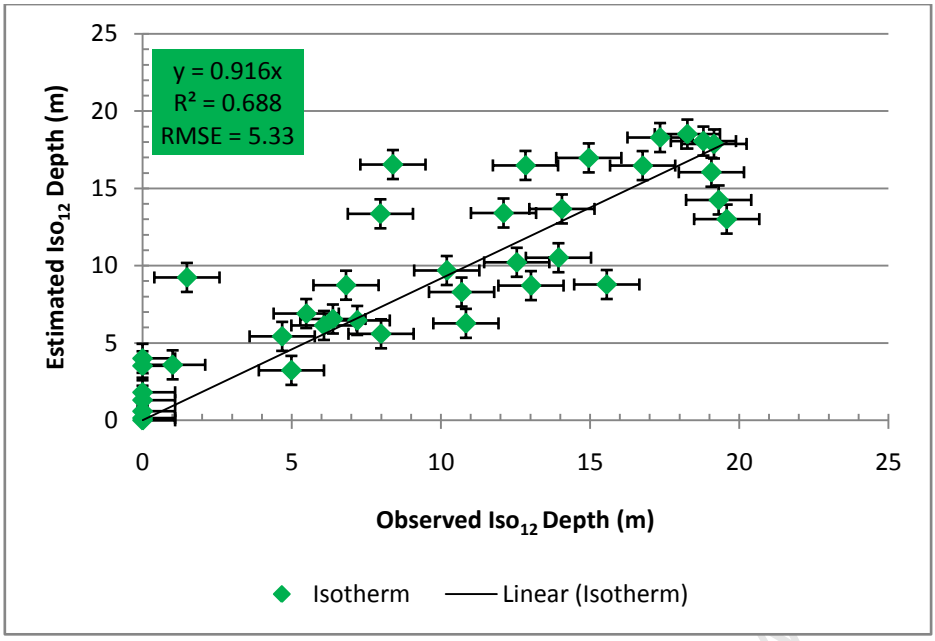

Figure 4.7 Estimated vs. measured Iso_{12} (m) using Eqn. 4.4 for the periods in 2005, 2006 and 2007. The vertical error bars indicate the standard deviation from the data mean and horizontal error bars indicate the total calculated uncertainty associated with the estimated Iso_{12} values. .

Chapter 5-Algorithm Validation (Event Scale Variability)

5.1 INTRODUCTION

The efficacy of the derived robust algorithms is dependent on the ability to demonstrate the change in the estimated surface NO_3 fields and the Iso_{12} depths from dynamic variations in upwelling and phytoplankton biomass within the system. To build consistent NO_3 and Iso_{12} maps from satellite data over synoptic scales in the ecosystem requires a consistent time series of SST and wind data from the Moderate Resolution Imaging Spectoradiometer (MODIS) and the QuickScat.

Many projects and sensors "serviced" or still currently "service" the Benguela such as the European Space Agency satellite Environmental Satellite (*Envisat-1*), which houses the now unavailable Medium Resolution Imaging Spectrometer (MERIS) sensor. The National Oceanic and Atmospheric Administration (*NOAA*) and the National Aeronautics and Space Administration (*NASA*) products are primarily: the Advanced Very High Resolution Radiometer (*AVHRR*) onboard the POES satellite; the Sea-viewing Wide Field-of-view Sensor (SeaWiFS) on NASA's OrbView-2 satellite; the Quick Scatterometer (QuikScat) and the Moderate Resolution Imaging Spectoradiometer (*MODIS*) on the Terra and Aqua satellites.

In the Benguela the primary fields of interest in remote sensing science are ocean colour and SST and their subsequent ability to derive other variables such as new production. The use of remote sensing in the ecosystem as with other upwelling systems requires a detailed knowledge of the primary forcing mechanisms which drive the system. Using a simplified template to describe the temporal changes in an upwelling system, it is well documented that the primary or initial forcing mechanism is wind. The wind leads to a physical response in the system in the form of water displacement. The resultant physical (SST) and chemical (NO_3, $Si(OH)_4$, urea, NH_4 etc) change of the water garners an immediate or delayed biological response from the system. In the Benguela, remote sensing is engaged in the data collection of the: system driver; physical response and the eventual biological response.

This chapter provides the methods and the processing procedures for the remotely sensed data used in the application of the robust algorithms on southern Benguela regional waters, to investigate event scale processes. Equations 3.8 and 4.4 were applied to daily MODIS images to examine the synoptic event and seasonal scale (discussed in Chapter 6) variability of the ecosystem. The daily estimated NO_3 and Iso_{12} depth maps derived from the MODIS data correspond to the specific days chosen in Chapter (2) for further analysis in 2005-2007.

5.2 METHODS

5.2.1 Event Scale Analysis

Ecosystem Physical Response

The physical response of the system is exhibited primarily in the change of SST during the upwelling and quiescent phase. In this thesis, data sets pertaining to SST were collected using MODIS which is a part of a collection of sensors that measure a multitude of variables associated with earth observation. SST is the central tenet in the process of ocean dynamics and in order to describe the dynamic variations in upwelling, a consistent, high resolution dataset of SST is required.

To demonstrate the utility of the algorithms in obtaining both the NO_3 and Iso_{12} fields, the equations were applied to local area coverage daily SST data for the event scale analysis. The data obtained were from MODIS onboard NASA's Terra and Aqua satellites which measure SST_{skin} radiances in the infrared part of the wave spectrum. The satellites are 705 km from the earth's surface and a +/- 55° scanning angle covers a 2330 km swath (Hosoda et al., 2007), with a 1:30 PM ascending equator crossing time for Aqua and a 10:30 AM descending equator crossing time for Terra (Savtchenko et al., 2004). Although MODIS is a 36-band sensor that spans the spectral range from 0.4 to 14.4 µm, the bands used in the collection of SST_{skin} radiances are in the atmospheric 'windows' at wavelengths of 3.5 to 4.2 µm and 10 to 12µm (Minnett et al., 2002). On MODIS the SST product contains one thermal and one mid-infrared SST parameter. The thermal product is retrieved from MODIS bands 31-32 (10.8-12.3µm) and the one mid-infrared parameter from bands 22-23 (3.9-4.1µm) (Savtchenko et al., 2004).

The Level 2 daytime MODIS (1 km resolution) SST_{skin} data used in this project were collected in the thermal infrared between 11 and 12µm and generated using the base MODIS Infrared Sea Surface Temperature Algorithm (Brown and Minnet, 1999). The atmospheric correction algorithm used was the same one used for the Pathfinder SST product (Minnet et al., 2002) which is based on the non-linear SST algorithm (Walton et al., 1988). Consistent parameters were applied to all the data where the standard products used were: the sea

surface temperature which measured values using the 11 and 12µm channels and the sea surface temperature quality level for 11µm, where the sea surface temperature values were determined based on the algorithm flagging criteria. The already processed SST data were downloaded from the Ocean Colour website (http://seadas.gsfc.nasa.gov/seadas) and extracted using the SeaWiFS Data Analysis System (SeaDas). The processing done prior to the download was prepared according to the algorithm changes associated with MODIS-Aqua R2009.1 (refer to http://seadas.gsfc.nasa.gov/seadas for more information).

The local overpass times for Aqua and Terra were between 2:00 PM - 2:45 PM and 10:00 AM-11:00 AM respectively. The local overpass times varied from day to day and only "matched-up" directly with the *in situ* data collection on a few occasions. The intervals between the *in situ* data collection and the satellite recorded values varied throughout the 3 years from a few minutes up to five hours. Due to the large temporal gap between the Aqua data and the collection of the *in situ* samples the Terra data was used for the SST values due to its closer temporal range with the *in situ* data collection. The temporal variations however did still persist in the collection of the *in situ* and remotely sensed data resulting in a significant disparity between the 1m bulk SST (SST_{depth}) from the *in situ* dataset and remotely sensed SST_{skin} values and largely eclipsed the common error quoted in validation studies between the two.

The common validation technique of remotely sensed data is done by comparing the radiometer values to *in situ* bulk temperatures from buoys (Minnett, 2003,Donlon et al., 2002). The error associated with SST_{skin} and SST_{bulk} (i.e SST_{depth}) values commonly found is between 0.3°C to 0.5°C (Reynolds et al., 2002, Minnett et al., 2002, Esaias et al., 1998, Hosada et al., 2007). In the present data set there was a large warm bias between the Terra SST_{skin} pixel at the site and the *in situ* SST_{depth}. Only a single Terra pixel was utilized for comparison purposes due to the pixel being representative of the local area. The region showed a lack of variability between various pixel configurations, and it was decided to keep the closest resolution possible between the remotely sensed and *in situ* values (Fig.5.1) (Table 5.1).

	2005	2006	2007
5x5	0.19	0.06	0.54
4x4	0.16	0.08	0.24

Table 5.1 The standard deviations (°C) of the 5x5 and 4x4 pixel configurations for the local area during the study periods.

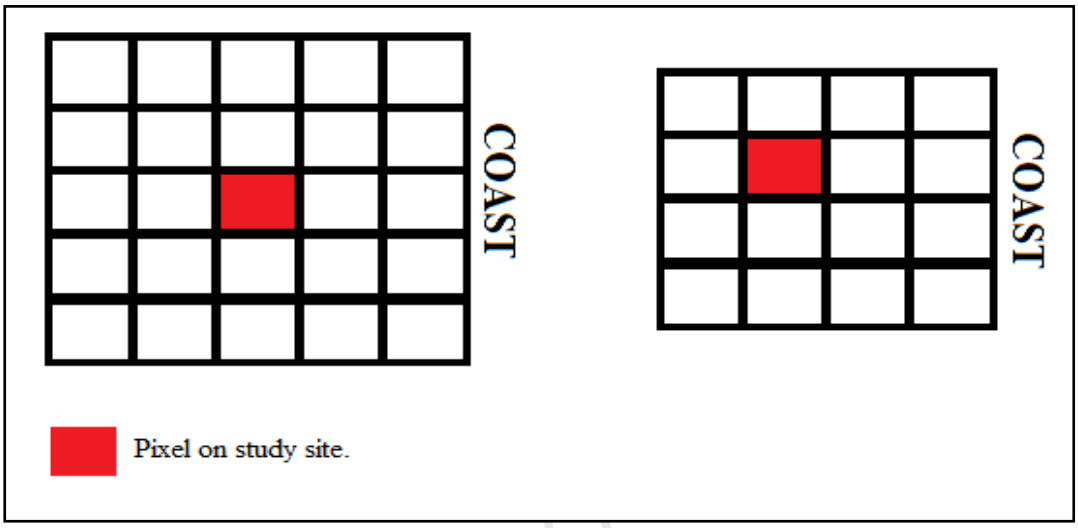

Figure 5.1 The pixel layout for both the 5x5 (left side) and 4x4 (right side) configurations. The red box in the grid denotes the pixel representative of the *in situ* site.

The diurnal warming of the upper surface of the ocean is a common in oceanography with considerable observational evidence confirming this relationship amongst others of the noticeable temperature differences between various depths in the upper 5m of the ocean (Saunders 1967, Hasse, 1971, Donlon and Robinson, 1997, Ward and Minnett, 2001). The concern is due to the inherent difficulty in measuring the vertical temperature structure of the upper 10m of the ocean due to shear-driven ocean turbulence and air-sea fluxes of heat, moisture and momentum (Donlon et al., 2002). An idealistic relationship between the SST_{skin} and the SST_{depth} amongst others is shown in figure 5.2 in the late morning-early afternoon following a period of light or absent wind and high insolation. The figure clearly shows the possibility of a marked difference between the SST_{skin} and the SST_{depth} illustrating the decoupling of the two due to diurnal skin layer heating (*ibid*).

The warm bias in this study was not consistent, with a greater bias (+/- 2°C) at cool temperatures (10-12°C) and a significantly lower bias (+/- 0.3°C) at warmer temperatures.

Pivotal to establishing the bias is the understanding the influence the wind speed together with the high insolation have on the extent of the bias. The relationship between the 3 variables (i.e. temperature, wind and insolation) is well characterized for both day and night, where approximately above a wind speed of 6 m/s the relationship between the SST_{skin} and SST_{depth} is well defined and the cool or warm bias is well understood (Donlon et al., 2002, Gentemann et al., 2003, Gentemann et al., 2008, Stuart-Menteth and Robinson, 2003). At lower wind speeds with excessive insolation the relationship is however complicated during the day due to diurnal warming leading to the stratification of the upper ocean layers. In this thesis the low-wind speed and the high late summer/autumn insolation are thought to be the main contributing factors to the extensive warming of the skin layer. There is considerable observational evidence confirming the relationship between the SST_{skin} and SST_{depth} (Donlon et al., 2002), where a large number of studies have been undertaken in an attempt at quantifying the diurnal warming signal exhibited over large areas (Gentemann et al., 2008,Minnet, 2003, Gentemann et al., 2003). Gentemann et al., (2008) illustrated in a multi-sensor study investigating diurnal warming showed that 2km resolution, MODIS Aqua fields off the coast of southern Africa, during low wind speeds resulted in a large 6.4K diurnal heating event when wind speed was <1m/s. What was important to note in this study is that it was shown that the amplitude of warming decreases with a decrease in spatial resolution and that the maximum warming measured was dependant on the spatial resolution of the sensor. This adds to the possible reasons for the bias in this study and that the resolution of the Terra grid could be a contributing factor too.

The lack of consistency between the SST_{skin} and the SST_{depth} has overarching consequences on the two proxies where there would be an inaccurate representation of both the estimated NO_3 concentrations and the estimated Iso_{12} depths. Due to the extreme sensitivity and small temperature window where the algorithms could detect change within the NO_3 concentrations and/or the Iso_{12} depths, even a minor difference between the SST_{skin} and SST_{depth} would have a profound effect on the algorithm performances.

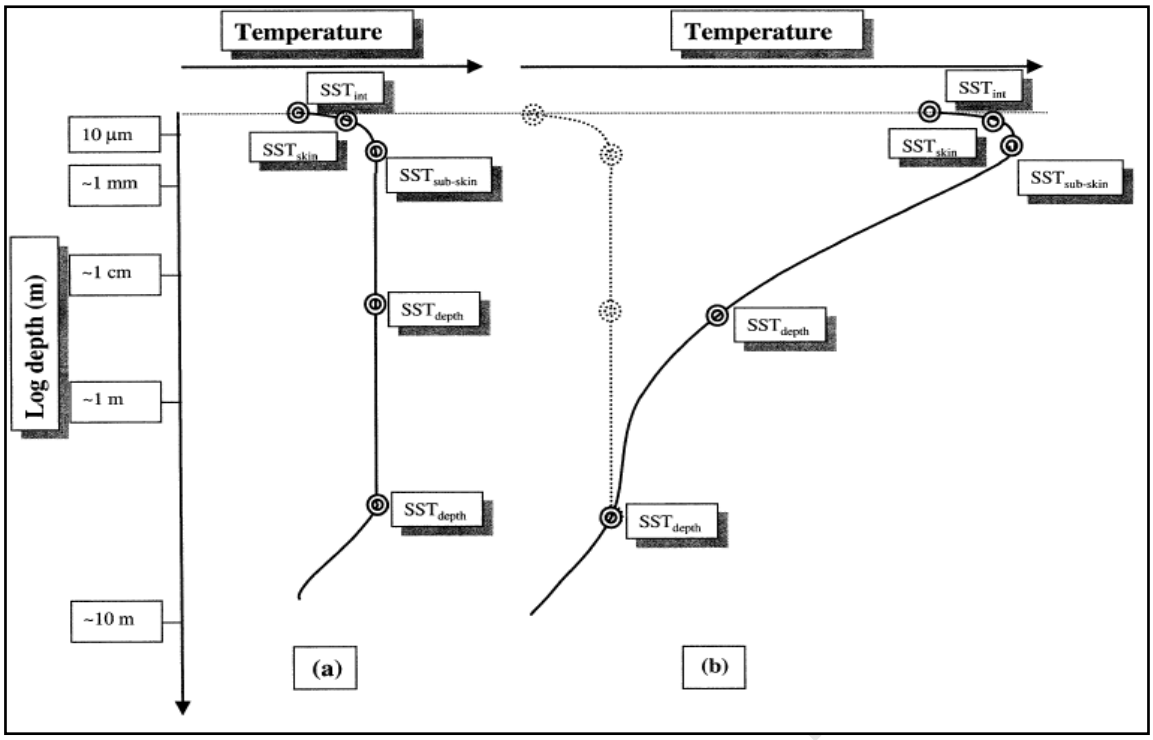

Figure 5.2 Idealized temperature profiles of the near-surface layer (~10m depth) of the ocean during (a) nightime (light grey) and daytime during strong wind conditions and (b) daytime low-wind speed conditions and high insolation resulting in thermal stratification of the surface layers (Figure and descriptions adapted from Donlon et al.,2002).

The inability to quantify the diurnal warming bias as a single value resulted in the use of the off-set of a linear function when SST_{skin} and the SST_{depth} were plotted against each other (Fig. 5.3). This was the most simplistic method in characterising the warming signal throughout the time periods. Whether or not a single quantified warming signal is endemic to the entire southern Benguela at high spatial resolutions, it is unknown and there would need to be extensive validation studies which are beyond the scope of this project. The attempt at creating a single bias is a quick technique in "matching up" the SST_{skin} and SST_{depth} values. The off-set chosen was 0.749°C and it was deducted from each pixel value in the Terra SST data. The robust algorithms were then applied to the resultant SST_{skin} value and tested for their efficiency.

The MODIS Terra SST dataset had 11% of the data missing, with a consistent spread throughout the 3 years of the data collection. The largest hindrance associated with radiometers in the collection of SSTs is cloud cover (Hosoda et al., 2007) but during the

periods, within the upwelling zone the issue was inconsequential with only the south Atlantic gyre significantly affected by extensive cloud cover.

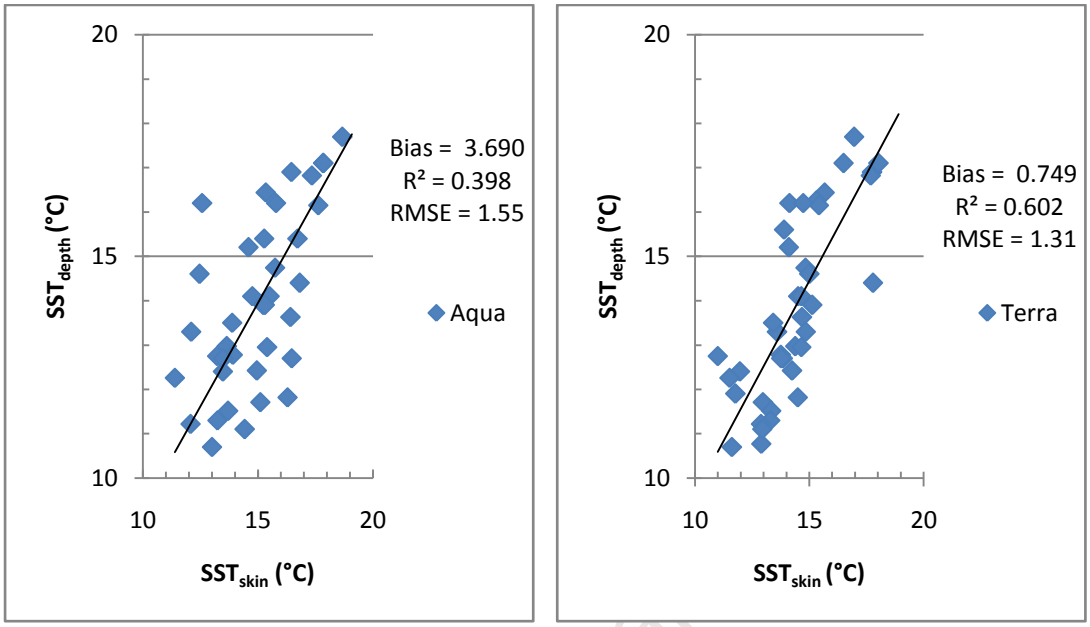

Figure 5.3 Comparison between MODIS Aqua (left panel) and Terra (right panel) with *in situ* surface temperatures for 2005, 2006 and 2007.

5.3 RESULTS

5.3.1 Event Scale Variability

In the following section, sequences of images from 2005, 2006 and 2007 illustrate the estimated surface NO_3 concentrations, Iso_{12} depths and SST values for the southern Benguela. These images that were selected correspond to the days which were closer analyzed in Chapter (2). The examples of the performance of the algorithms on a synoptic scale illustrate the range of the water characteristics endemic to the system in the late summer/early autumn seasons.

2005

On 24th March there was extensive warming (>14°C) throughout the southern Benguela with a slight intrusion of cooler waters at the Cape Columbine and the Namaqua upwelling cells, yielding very low NO_3 local patches (Fig. 5.4, left panel). The band of cool water running parallel to the coast from 33-35°S can be ignored due to the unnatural line of cool temperature pixels (Fig. 5.4, left panel). A possible reason for the observed unnatural pixel striation of low SSTs in the area could be due to the incomplete flagging of scattered cloud or fog banks. There were no estimated Iso_{12} depths in the important St Helena Bay area which could match up with the very low NO_3 on the same day.

The distribution of the surface NO_3 on 30th March showed a large off-shelf region with concentrations ~30µmol/l and shallow Iso_{12} depths < 5m. The high concentrations and the shallow depths in the area were due to the uncharacteristically low temperatures in this region. The low temperatures can be ignored and in most likelihood suffer the same incomplete flagging of cloud contamination seen on 24th March. In the St Helena Bay area, Cape Columbine and Namaqua cells there were concentration patches of nutrient poor waters of between 1-5µmol/l, which were engulfed by NO_3 depleted waters evident in the broad on-shelf region north of Cape Columbine (Fig 5.4, centre panel). On the same day there were weak to moderately stratified conditions along the coast of the ecosystem. The estimated Iso_{12} depth image on this day displayed moderately stratified conditions adjacent to the coast. The continuous Iso_{12} depth homogeny along the coast was interrupted at ~31.5°S by a slight

intrusion of warmer water which yielded Iso_{12} depths >12m. The Iso_{12} depths in the St Helena Bay region are consistent with depths of 5-12m (Fig. 5.5, centre panel).

The images clearly showed the already established major role of SST in the estimation of NO_3 concentrations and the Iso_{12} depth. It is possible to identify the major thermal structures from both the NO_3 fields and Iso_{12} depths. The thermal structures were indicative of the main upwelling cells in the southern Benguela especially during intensive coastal upwelling (Fig. 5.6, right panel). There were 2 noticeable features on 3rd April: 1) the ability to discern the Cape Peninsula (~34°S), Cape Columbine (~33°S) and the Namaqua (~30°S) upwelling cells according to NO_3 concentrations > 20µmol/l and Iso_{12} depths of < 5m, and 2) the NO_3 concentrations are well within the range to be expected for on-shelf values and are decreasing towards the upwelling front. The extent of NO_3 rich water (>10µmol/l) was adjacent to the length of the coast and was only punctured by an intrusion of a slightly warmer plume at ~33, 5°S resulting in a patch of low to non-existent NO_3 (Fig. 5.4, right panel).

The evolution of the coastal SST patterns in 2005 were as to be expected for wind-driven upwelling systems in the late summer/early autumn seasons, as is the increased variability of the surface NO_3 concentrations and Iso_{12} depths.

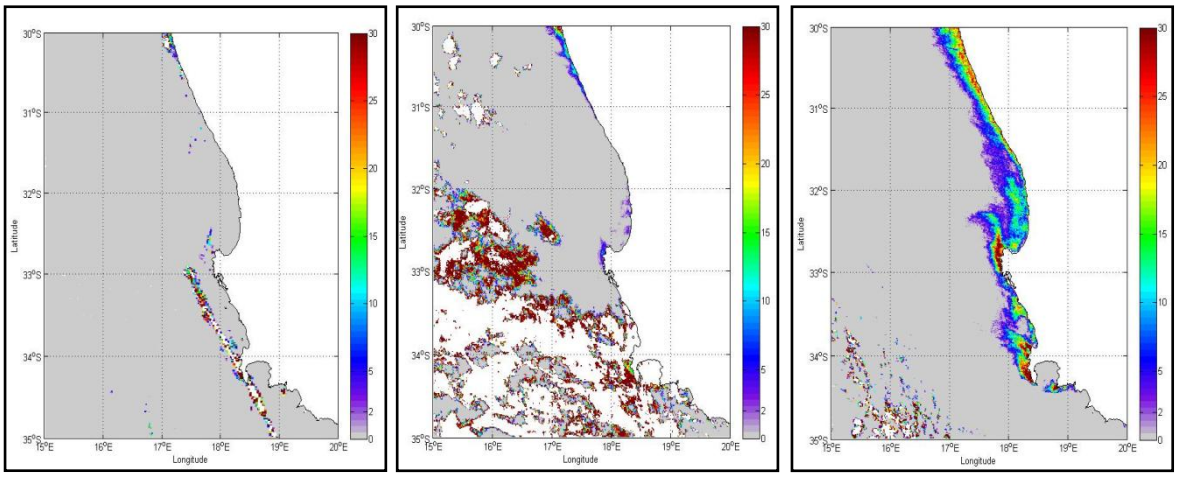

Figure 5.4 Examples of estimated NO_3 concentrations (µmol/l), derived from MODIS Terra sea surface temperatures using Eqn. 3.8 on 24 March (left panel), 30 March (middle panel) and 3 April (right panel), 2005. The white areas correspond to cloud cover or invalid satellite data.

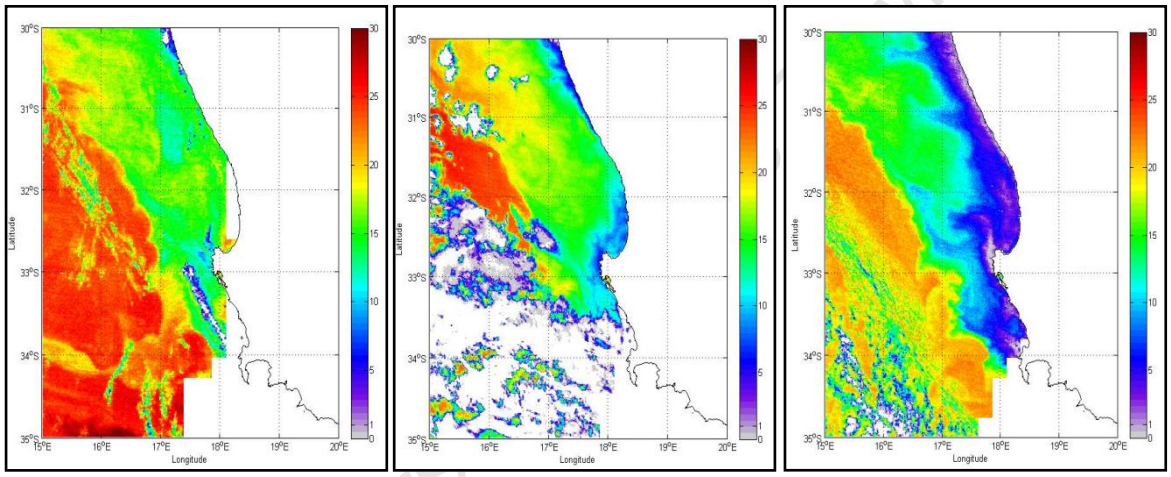

Figure 5.5 Examples of estimated Iso_{12} depths (m), derived from MODIS Terra sea surface temperatures and QuickScat seawinds using Eqn. 4.4 on 24 March (left panel), 30 March (middle panel) and 3 April (right panel), 2005. The white areas correspond to cloud cover or invalid satellite data.

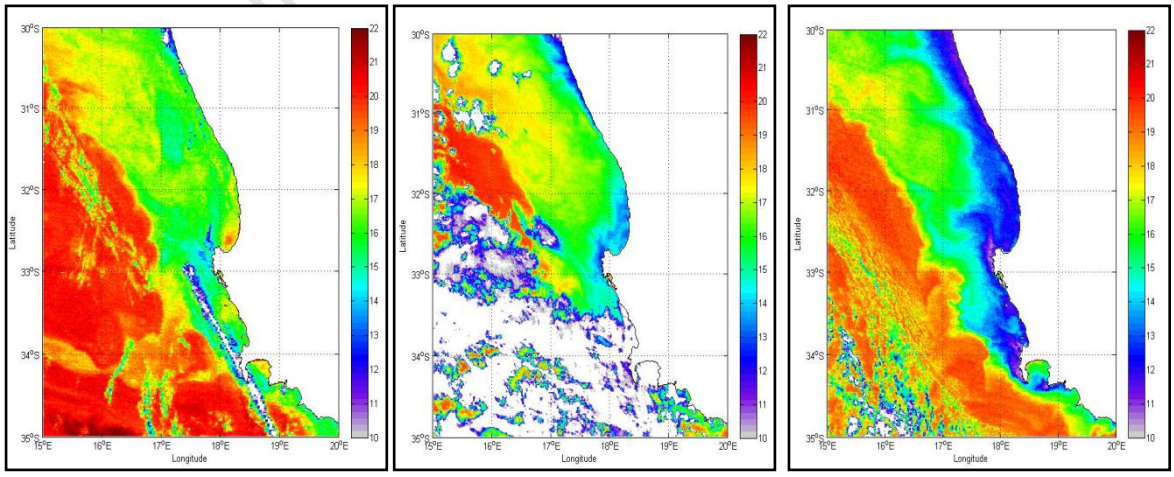

Figure 5.6 MODIS Terra sea surface temperatures (°C), on 24 March (left panel), 30 March (middle panel) and 3 April (right panel), 2005. The white areas correspond to cloud cover or invalid satellite data.

2006

While the examples discussed for 2005 clearly showed the event scale variation of the system with an upwelling phase typical of upwelling-conditioned surface waters and a classic quiescent phase of eastern ocean coastal upwelling systems, 2006 was very different. On the SST image for 8th March, 2006 (Fig. 5.9, left panel), i.e. during the warmest period of the year, there was a cool tongue of water adjacent to the coast extending from the Cape Peninsula to the north of Cape Columbine. At the same time there was cold water at the south-western coast of the continent. A patch of warm water in the inner regions of St Helena Bay with temperatures between 14-16°C was evident. This patch of water resulted in an on-shelf nutrient poor region between the Cape Columbine and Namaqua cells, with NO_3 concentrations of between 2-10µmol/l in the 2 upwelling cells (Fig. 5.7, left panel). The resultant Iso_{12} depths in the same area showed a greater degree of variability with depths of ~5-13m. It was unfortunate that on March 19, the MODIS Terra coverage was insufficient for the estimation of both the surface NO_3 concentrations and Iso_{12} depths in the system (Fig 5.7, 5.8, 5.9, centre panel).

In the days that followed in 2006, the coastal upwelling intensified with a large spread of vigorously upwelled waters on the shelf (10-12.5°C) extending from the Cape Peninsula to the Namaqua Cell on 23rd March (Fig 5.9, right panel). In the north, cold shelf-waters there was a further drop in the SST values with an extensive area of temperatures ~11°C. This produced a large area adjacent to the coast at 30-31°S of high NO_3 concentrations and consistently shallow Iso_{12} depths. There were however inconsistent on-shelf NO_3 concentrations and Iso_{12} depths from 31-34°S (Fig 5.7, right panel). The estimated NO_3 concentrations and Iso_{12} depth images of the most intense upwelling of 2006 on 23rd March resembled the off-shelf and on-shelf identities exhibited on 3rd April, 2005. The extent however of the on-shelf moderate to high NO_3 concentrations covered a larger spatial area on 23rd March, 2006. The markedly colder upwelling temperatures on 23rd March, contributed to the intense estimated NO_3 concentrations and shallow Iso_{12} depths at the upwelling cells (>25µmol/l & =<1m respectively) and increased concentrations and depths in St Helena Bay, comparative to the similar day in 2005. The images in 2006 clearly show that remotely sensed data can be utilized effectively within a constantly upwelling environment to extend the resolution of *in situ* data, and, therefore provide a clearer instantaneous synoptic representation of NO_3 distribution not possible with *in situ* data alone.

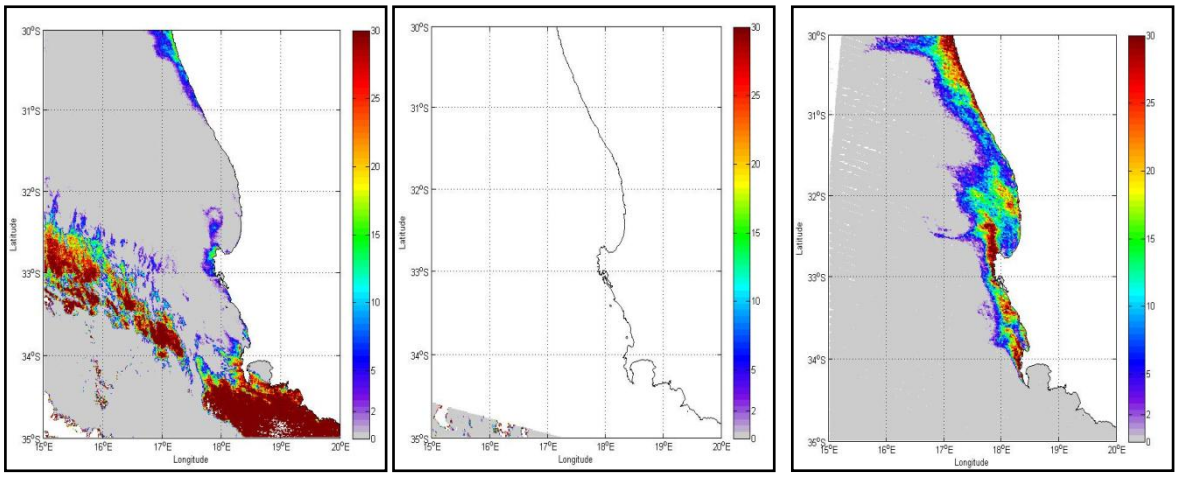

Figure 5.7 Examples of estimated NO_3 concentrations (µmol/l), derived from MODIS Terra sea surface temperatures using Eqn.3.8 on 8 March (left panel), 19 March (middle panel) and 23 March (right panel), 2006. The white areas correspond to cloud cover or invalid satellite data.

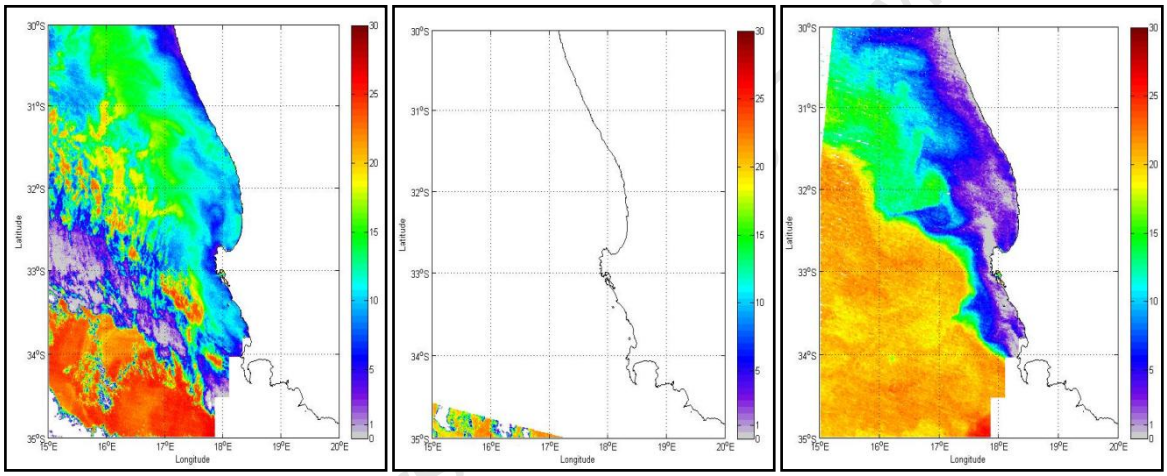

Figure 5.8 Examples of estimated Iso_{12} depths (m), derived from MODIS Terra sea surface temperatures and QuickScat seawinds using Eqn. 4.4 on 8 March (left panel), 19 March (middle panel) and 23 March (right panel), 2006. The white areas correspond to cloud cover or invalid satellite data.

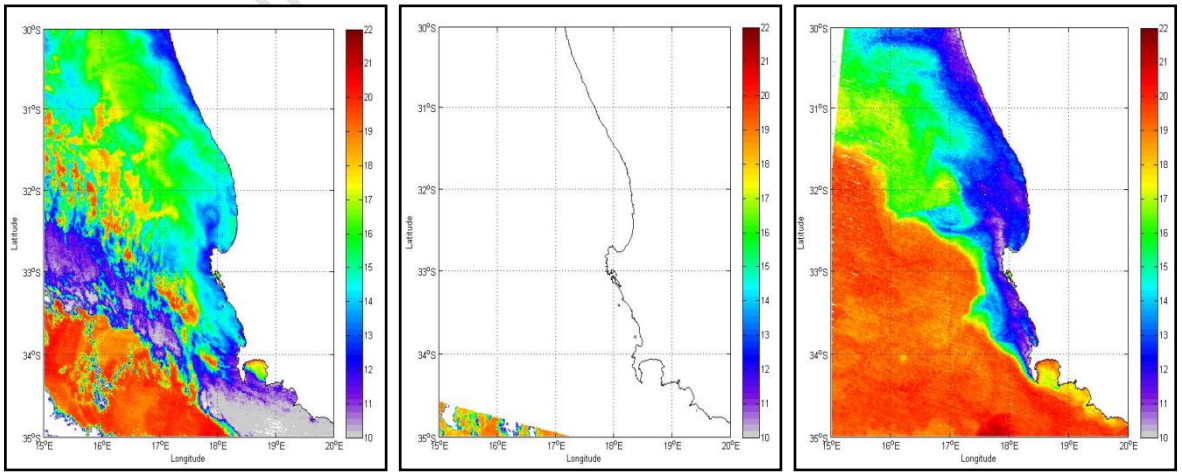

Figure 5.9 MODIS Terra sea surface temperatures (°C), on 08 March (left panel), 19 March (middle panel) and 23 March (right panel), 2006. The white areas correspond to cloud cover or invalid satellite data.

2007

While the examples of 2005 and 2006 clearly coincide with upwelling pulses and quiescent phases typical of the southern Benguela, and the event scale resolution from the robust algorithms is satisfactory, the examples examined in 2007 were different. The particular days in question were 27th March, 2nd and 7th April. On 27th March the *in situ* data collection area was in a small patch of cold (~12°C) water on the shelf, which was indicative of the rest of upwelling along the coast, where there were very patchy cold temperatures too (Fig. 5.12, left panel). Due to the robust nature of the estimated NO_3 algorithm and the small temperature window where appreciable NO_3 concentrations can be predicted, the resultant on-shelf along-shore NO_3 concentrations were very sparse. The only zones where there were noticeable NO_3 concentrations was in the upwelling cells and midway between the Cape Columbine and Namaqua cells (Fig. 5.10, left panel). This is a marked difference from the other days in 2005 and 2006 where when there was upwelling the entire shelf had appreciable NO_3 concentrations. The SST images from 2nd and 7th April document a warming trend in the St Helena Bay area with temperatures increasing from between 12 and 14°C on the 2nd to between 16 and 20°C on the 7th (Fig. 5.12, centre & right panel). This is mirrored by the low NO_3 concentrations at the centre of the bay and an increasing trend as you move northwards towards the Namaqua upwelling cell (Fig. 5.10, centre & right panel). The estimated Iso_{12} depths in St Helena Bay were characterised by significant deepening along the coast and towards the southern parts of the bay, just north of the Cape Columbine headland (Fig. 5.11, centre panel). On 7th April, the high NO_3 concentration patches were confined to the south-western and southern coasts of the continent. The area to the north of Cape Columbine had no detectable concentrations but the area was bordered to north by low concentrations which increased from 31° to 30°S to concentrations > 10µmol/l.

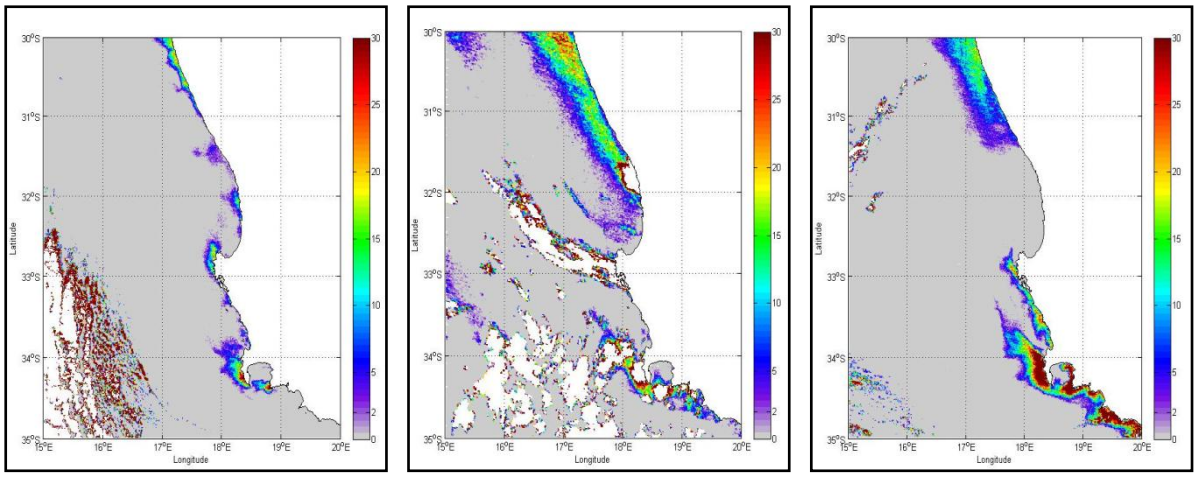

Figure 5.10 Examples of estimated NO_3 concentrations (µmol/l), derived from MODIS Terra sea surface temperatures using Eqn. 3.8 on 27 March (left panel), 2 April (middle panel) and 7 April (right panel), 2007. The white areas correspond to cloud cover or invalid satellite data.

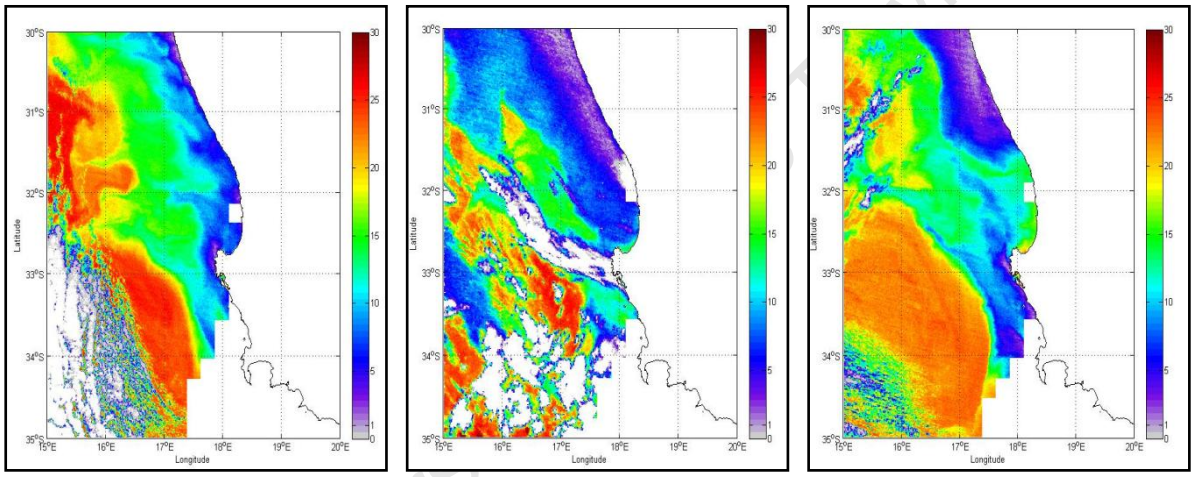

Figure 5.11 Examples of estimated Iso_{12} depths (m), derived from MODIS Terra sea surface temperatures and QuickScat seawinds using Eqn. 4.4 on 27 March (left panel), 2 April (middle panel) and 7 April (right panel), 2007. The white areas correspond to cloud cover or invalid satellite data.

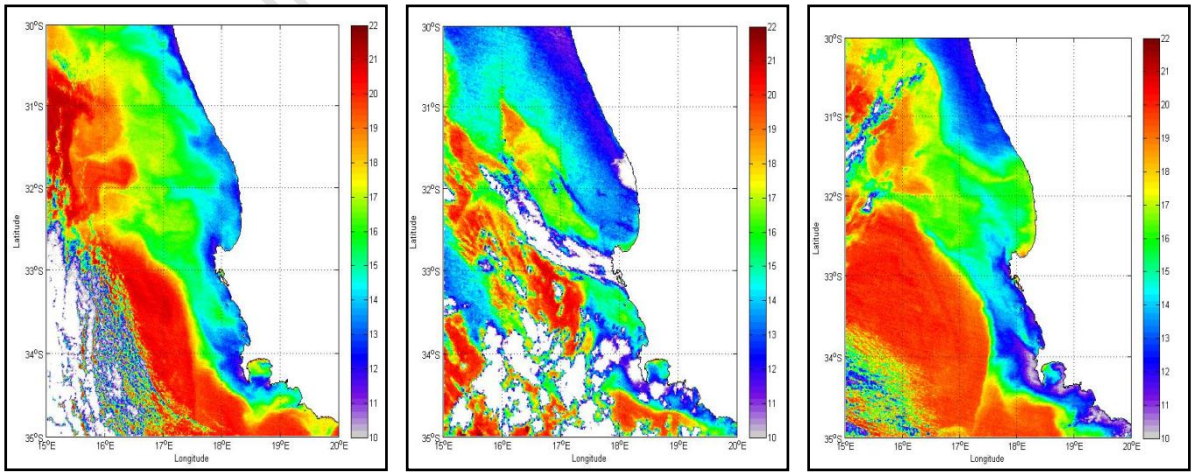

Figure 5.12 MODIS Terra sea surface temperatures (°C), on 27 March (left panel), 2 April (middle panel) and 7 April (right panel), 2007. The white areas correspond to cloud cover or invalid satellite data.

5.3.2 Overall Algorithm Performance

The robust algorithms Eqn. 3.8 and 4.4 were satisfactory when applied across the southern Benguela. The algorithms were able to successfully categorize the temporal and spatial variability within the system with regards to the NO_3 concentrations and Iso_{12} depths. The proposed influence of the *chl a* was not tested due to a suitable temporal resolution which mirrored the MODIS Terra maps being unavailable. During the 3 years on the upwelling days, strong temperature gradients were visible from the coast to the offshore regions. Cool temperatures (11-13°C) were confined along a narrow margin between the coastline and the continental shelf in 2005 and 2007, generating a strong front between high and low estimated NO_3 concentrations. What was clearly evident was that the upwelling domain in 2006 was larger and colder than the other 2 years and thus yielded a larger and higher NO_3 concentration field. The seaward extension of the upwelling domain in 2006 is reminiscent of the northern Benguela system where due to different wind regimes and shelf morphology the upwelling tends to cover a broader area off the coast (Bakun and Nelson, 1991). The upwelling domains in 2005 and 2007 covered a narrower area with a sharper front closer in-shore which is typical of the southern Benguela (Shannon, 1985; Holmes et al., 1997). The NO_3 fields displayed the features expected of the system but there was still an inherent under sampling of the surface concentrations by the algorithm in the upwelling cells, with only a very few regions displaying concentrations >15µmol/l during strong upwelling.

The estimated Iso_{12} depth spatial-temporal variations as expected were comparable to those of the SSTs with some nuances from the input of the wind-field. The overall depth of interest with regards to the possibility of bloom formation was the 5-10m Iso_2 depth range where the 2-layered system in on-shelf temperature seas would be clearly evident on 30th March, 2005 and 2nd April, 2007. The estimated Iso_{12} algorithm was able to capture the suitable depth range and displayed encouraging estimates but there was the persistent issue of under sampling the depth during moderate upwelling, where the Iso_{12} (i.e. thermocline) is expected to collapse and shoal to the surface. This was not immediately evident in 2005 and 2007, where the estimated Iso_{12} depths oscillated in the 2-5m depth range within the water column.

Chapter 6-Algorithm Validation (Seasonal Variability)

6.1 INTRODUCTION

The past chapters were focused on the derivation and validity of the algorithms over synoptic spatial and local temporal scales. In this chapter, the algorithms' validities are analyzed in key areas within the southern Benguela where the potential formation of HABs is feasible, and the algorithms' abilities in assessing high frequency signals over the summer/autumn upwelling season for several years can be tested. The *in situ* physical, biological and chemical variables with the estimated NO_3 and Iso_{12} values and remotely sensed biological values were combined, for a better understanding and evaluation of the biological variability in the system.

6.1.1 Benguela Variability

The ocean-atmosphere coupling plays a vital role in wind-driven upwelling systems like the Benguela. It would stand to reason that the climate variability within the system on inter-annual time scales is an important component in understanding the biological variability in the system. Unfortunately the study of the inter-annual: wind stress, surface heat fluxes and salt fluxes which could account for some of the environmental changes in the system are beyond the scope of this project. Additionally, the response of the coastal ocean to inter-annual or decadal wind regime shifts depends significantly on the topography and thermohaline stratification, which could be a separate study all on their own. These geographical factors induce physical processes, like internal Kelvin waves and local vorticity, which interact locally with the upwelling and could influence HAB formation and entrapment.

The primary driver of the system, the equatorward wind stress, has 3 main scales of variability (Shannon and Nelson, 1996):

- 2-8 day variability driven by atmospheric pressure systems which modulate upwelling intensity mainly in the southern Benguela.
- Seasonal variability which is controlled by the meridional shifts of the SAA which modulates upwelling-favourable winds. The upwelling-favourable winds are tempered to 10-25 day frequencies by eastward moving Rossby waves in the westerlies (Jury, 1998, Jury and Brundrit, 1992).

Central to the satisfactory functioning of the algorithms is the inter-annual variability of SSTs in the Benguela. In a comparative study, McClain et al., (1985) suggested that SST anomalies in the ecosystem are more persistent in time rather than space, in contrast to other upwelling regions. Anomalous warming events in the northern Benguela in 1963 and 1984 have been researched by Shannon et al., (1986) and related to southward incursions of equatorial waters. Low resolution data (9km) have been used to construct a climatology of SST and *chl a* concentrations for the Benguela and high resolution (1km) SST data have been used to investigate the effects of environmental variability on pelagic fish distribution in South Africa and Namibia (Agenbag, 1992).

6.1.2 Seasonal Scale Analysis

Further to examining the validity of the algorithms during dynamic variations in upwelling in the southern Benguela, is the development of a time series and the ability to quantify intra-seasonal variations. In order to discern the variability of different areas of the system, the focus of the study was where blooms are known to form and be transported within the physical and dynamic retention mechanisms of an area. By comparing the estimated NO_3 concentrations, Iso_{12} depths and upwelling in 3 varying zones in the southern Benguela, it should be possible to elucidate the response of the phytoplankton biomass from a basis of thermal and chemical changes due to upwelling, subsequent heating and stratification. The SST, wind and *chl a* data for the key zones were generated by extracting values from remotely sensed sources for the daily averaged 8 single year time series of the southern Benguela.

6.2 METHODS

6.2.1 Time Series Data

Wind

The remotely sensed wind used for the time series were daily averaged QuickScat seawinds data. The data used were extracted and processed in the same manner described in Chapter (4). The wind data were used in the estimation of the Iso_{12} depths and the calculation of the upwelling indices (described below) for each zone.

Bakun's Upwelling Index

An upwelling index, derived in Bakun, (1973) and later refined in Schwing et al., (1996), was calculated from QuikScat seawinds data:

$$M = \frac{1}{f} . (\rho_a C_d U_{10}^2) \tag{6.1}$$

Where M, is the Ekman transport and f is the Coriolis parameter. The term$(\rho_a C_d U_{10}^2)$ is the wind stress (τ), where ρ_a is the density of air, C_d is the drag coefficient and U_{10}^2 is a surface wind vector. U_{10} is given by the rotated meridional component of the wind vector. Bakun, (1973) defined C_d as a constant, however, Trenberth et al., (1990) redefined the term as a variable, the neutral drag coefficient (C_n) on the wind speed. The definition used in Trenberth et al., (1990) was used in this study, as the authors reported that C_d is dependant on "wind speed and atmospheric stability." The definition of the C_n term at differing U_{10} is shown below:

$$\begin{aligned} C_n &= 0.49 + 0.065U \quad for\ U > 10 m.s^{-1}\ (a) \\ &= 1.14 \quad for\ 3 \leq U \leq 10 m.s^{-1}\ (b) \\ &= 0.62 + 1.56U^{-1} \quad for\ U \leq 3 m.s^{-1}\ (c) \end{aligned} \tag{6.2}$$

Sea Surface Temperature

To derive the estimated NO_3 concentration and Iso_{12} depth time series the daily remotely-sensed MODIS Terra data were used. The daily SST data underwent the same processing techniques as those used in the event scale analysis (Chapter 5). In this chapter the seasonal and latitudinal variations in T_{up} were taken into account in the calculation of δT, unlike in Chapter 3 where T_{up} was constant. The T_{up} values used were as follows:

Area 1: T_{up} (30° S, autumn/summer) = 11°C (a) (6.3)

Area 2: T_{up} (33° S, autumn/summer) = 10.8°C (b)

Area 3: T_{up} (34° S, autumn/summer) = 10.4°C (c)

Chlorophyll a

The final, most difficult measure with regard to reconciling scales of variability, and vital components in the process of ecosystem investigation using earth observation is the biological aspect. Despite the well known issues of using *chl a* as a proxy for phytoplankton biomass (Cullen, 1982, Legendre and Michaud, 1999), it was used here because it is the biological variable most easily measured by satellite ocean colour (Morel and Berthon, 1989, Sathyendranath and Platt, 1993). Problems in the southern Benguela with measuring *chl a* are: the deficiencies in the atmospheric correction algorithms in the typically atmospherically complex and biologically turbid waters; the highly turbid waters in the ecosystem with concentrations commonly > 20 mg/m³ which the standard MERIS algorithms for Case 1 and Case 2 waters cannot accurately resolve.

Yearly time series *chl a* data (2003-2010) from the Medium Resolution Imaging Spectrometer (MERIS) on board Envisat 1 were obtained for the southern Benguela. The *chl a* data were derived from Level 2 reduced resolution data, processed using MERIS Level 2 ground segment (MEGS) version 8.0. Level 2 water leaving reflectance data were used as input to the Algal 0 processing algorithm (Bernard et al., 2006), with a spatial resolution of 1km. The Algal 0 algorithm applied is an empirical *chl a* algorithm specifically derived for bloom monitoring in the southern Benguela, where the algorithm utilizes band ratios at 665nm and 709nm (Bernard et al., 2006). The MERIS Level 2 flags applied to the data which take into account the different sources of possible errors on the pixel values can be found in

Appendix (II). The final product files were indexed and extracted for use in the thesis using Matlab.

6.2.3 Key Locations

The key locations selected for closer analysis are along the length of the coastline from the 1) Namaqua region in the northern part of the Greater St Helena Bay region, associated with the Namaqua upwelling cell,2)St Helena Bay, and 3) the Cape Peninsula area in the south (Fig. 6.1). The zones delineated are within areas where depths were shallower than 200m because upwelled water originates within the 0-200m fringe of the continental shelf (Carr and Kearns, 2003). Missing data does occur on some days due to cloud cover, incomplete coverage of the region by the satellites, or flagged data described in Appendix (II) and Chapter (5). On the occasional days when there was no 1km resolution MODIS or MERIS data available for any one of the 3 areas for various reasons, no spatial or temporal interpolation was made from the surrounding areas. In order to assess the annual comparisons of the 3 regions, the data were divided into 8 years and 2 seasons: early summer and late summer/autumn. Winter and spring data were not included as the characteristics required for bloom formation do not occur during these 2 seasons. Pitcher and Probyn, (2011) define three distinct physical periods in the ecosystem where: from November to the end of April the system is characterized by southerly upwelling favourable winds, considerable water column temperature variation and stratification; from the end of April to July, by a well mixed water column dominated by north-westerly storm events and from July to mid-October by cold water temperatures due to persistent upwelling. For this reason the physical characteristics during winter and spring were outside the NO_3/Iso_{12} derivation range and seasonal applicability for the system.

Analyses from 2005 and 2009 are focused in this chapter and further analyses from other years' are illustrated in Appendix (I). 2005 and 2009 were chosen as these years had significant and well-documented blooms in the St Helena Bay/ Cape Columbine region (Fawcett et al., 2007 and Pitcher and Probyn, 2011).

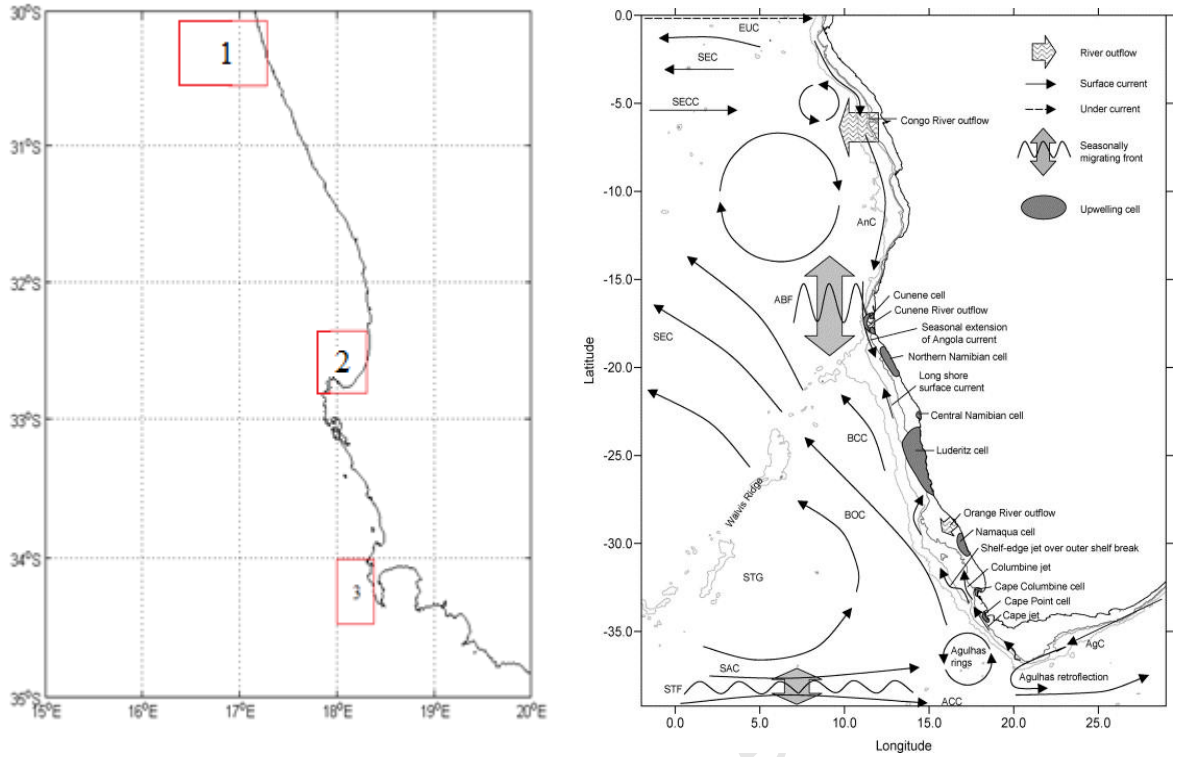

Figure 6.1 Location of the 3 sites. 1) Namaqua zone, 2) St Helena Bay zone and 3) Cape Peninsula zone (left panel). The location of the upwelling cells, bathymetry and circulation in the Benguela system. (right panel-figure adapted from Hardman-Mountford et al., 2003)

Statistics

For each of the zones daily data were calculated for: the estimated surface NO_3 concentrations, Iso_{12} depths, remotely sensed surface *chl a* and the Ekman transport. The final zone data value was the arithmetic mean of all the pixels within the box for each day. On days when less than 40% of the pixels in a zone were available the box was classified as empty and shown as having none available. There was a period during which a number of *chl a* images were missing, namely in 2007 and 2008. Only 36 images out of a possible 120 acquisition days for the early summer and late summer seasons were obtained meaning there were large *chl a* data gaps during those two years. Subsequent results obtained from those years with regards to *chl a* should therefore be considered with caution.

6.3 RESULTS

6.3.1 Zone 1 (Namaqua; Dimensions: 30.1°S to 30.6°S; 16.4°E to 17.3°E)

For the Namaqua zone the time series of the estimated surface NO_3, Iso_{12} depth, surface *chl a* and upwelling index were computed for 2005 and 2009. These set of variables allow for the analysis of the sub-seasonal variability trends of different upwelling dynamics and biological responses across several inner shelf regions in the southern Benguela.

The estimated surface NO_3 variability in 2005 and 2009 reveals strong event scale patterns, presenting the highest concentrations in the early upwelling season for both years (November-December) (Fig. 6.2). It is not entirely surprising that the concentrations decrease in the mid summer and rise again in the autumn period. The concentrations during this period show trends to be expected of the system where values average between ~ 15 and 25µmol/l during upwelling events with slightly higher peaks in the early summer of ~30µmol/l (Carr and Kearns, 2003). Between the two different years the trends are similar but surface NO_3 are maintained for longer periods in 2009 for both the early summer and autumn periods. The zonally averaged values exhibit similar event scale variability for the NO_3 algorithm products, indicating acceptable synoptic and temporal upscallings.

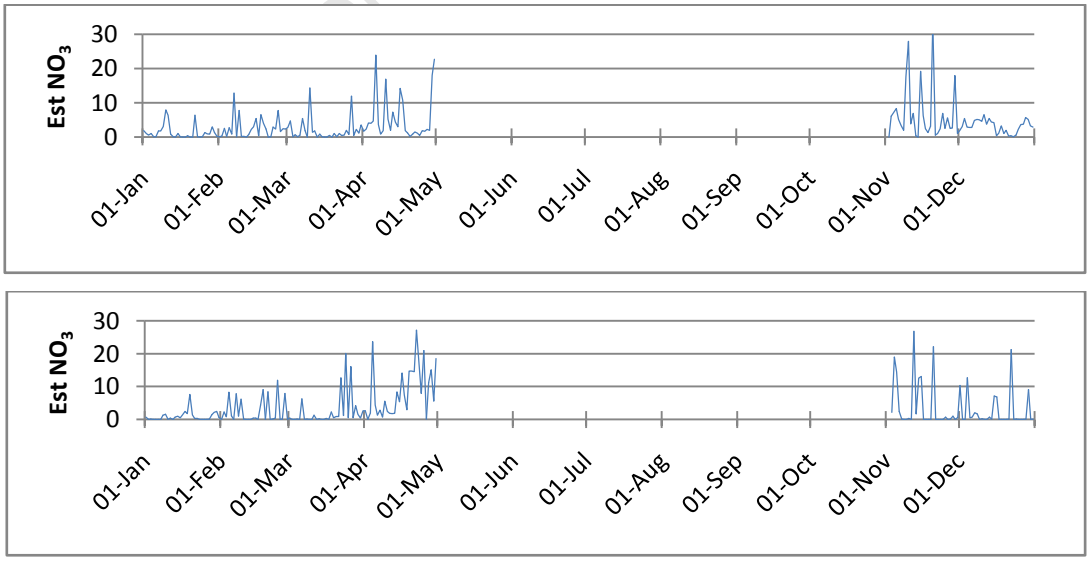

Figure 6.2 Daily averages of the estimated NO_3 (µmol/l), for the Namaqua zone in 2005(top panel) and 2009(bottom panel).

The estimated Iso_{12} depths in 2005 and 2009 show inversely proportional patterns to the estimated NO_3 concentrations in the same zone, and display similar high frequency to the NO_3 products (Fig. 6.3). However, there are differences between the years where during the mid-summer/autumn period in 2005 there is a larger variance in the depths and slight decrease in the mean depth of the isotherm through the upwelling season. In 2009, however the declining trend and consistent shoaling of the isotherm is more pronounced from January-May. The differences between the years in the early summer are small but it is interesting to note is there is a lack of appreciable upwelling in 2005 during December where the zonally averaged Iso_{12} is estimated not to break the surface.

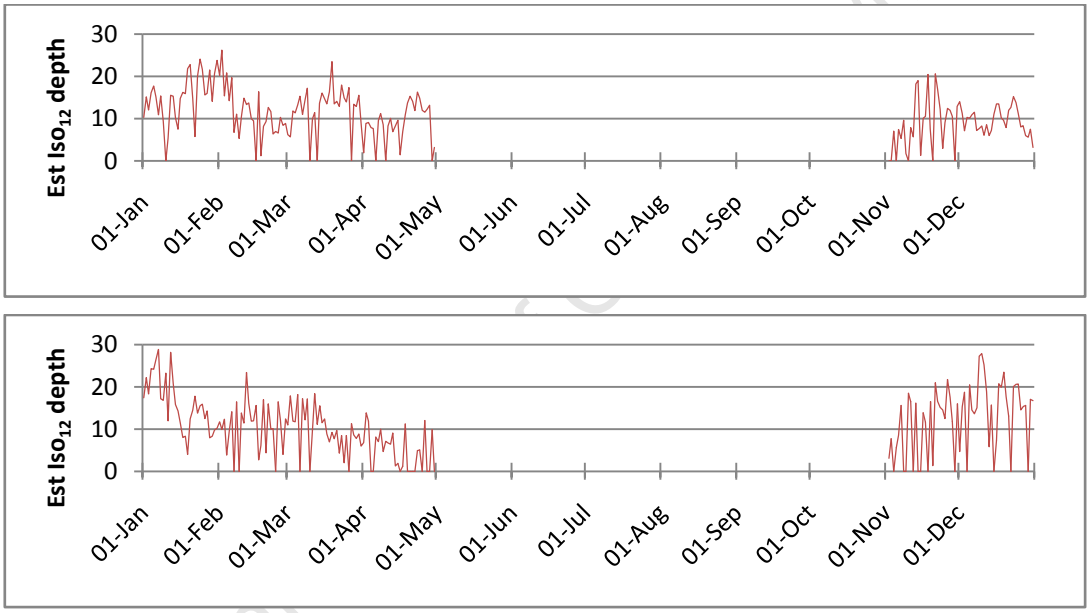

Figure 6.3 Daily averages of the estimated Iso_{12} depths (m), for the Namaqua zone in 2005(top panel) and 2009(bottom panel).

The daily zonal averages of the *chl a* concentrations in 2005 and 2009 reveal lower concentrations in the late autumn in 2005 and early summer in 2009 (Fig. 6.4). Increased concentrations are found in 2005 relative to 2009, where during the same time periods the corresponding estimated NO_3 concentrations follow the expected relationship where an increase in NO_3 concentrations are matched by lower average *chl a* values. The expected relationship is due to the lack of stratification when NO_3 concentrations are high. Immediately after upwelling where NO_3 concentrations in the euphotic zone are high, excessive water column turbulence results in increased mixing to depth (Carr and Kearns,

2003) which would inhibit phytoplankton growth resulting in the lower biomass exhibited by the *chl a* values.

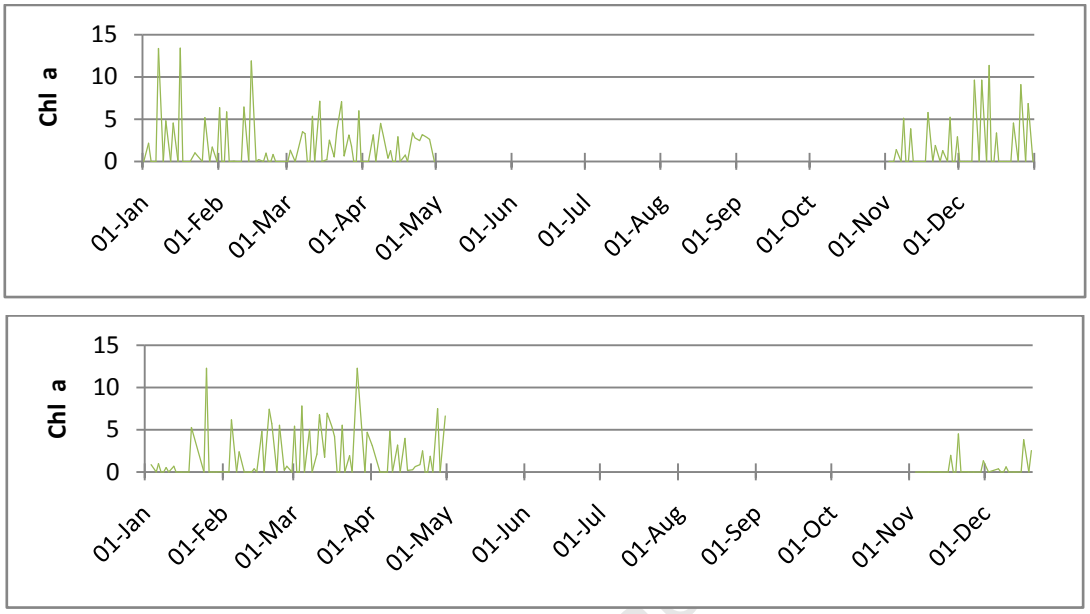

Figure 6.4 Daily averages of the *chl a* concentrations (mg/m^3), for the Namaqua zone in 2005(top panel) and 2009(bottom panel).

The Ekman offshore transport reveals the succession of active upwelling events (positive values) and slight downwelling (negative values) during the two years (Fig. 6.5). The low variability of this parameter in the Namaqua box is due to the fact that the area is in a designated upwelling cell (Weeks et al., 2006, Pitcher et al., 2008, SC) and relatively weak downwelling phases occur. The Namaqua zone does display periods of quiescence: the upwelling is not perennial as in the northern Bengela Luderitz zone, and oscillations between positive and neutral Ekman transport are not uncommon. The strong signal in November 2005 shows the expected physical, chemical and biological variability of a strongly pulsed wind driven upwelling cell, where mass transport of ~100m^3/s was accompanied by high nutrient availability, extensive rapid shoaling of the isotherm and relatively low concentrations of *chl a* because of the excessive mixing to depth during the period. In 2009 there was a decrease in the Ekman transport in the January-May interval, resulting in greater zonally averaged *chl a* concentrations, when biomass proliferation was possible due to dampened turbulence, excessive nutrients and the oscillation of the isotherm between the 0-10m depth range.

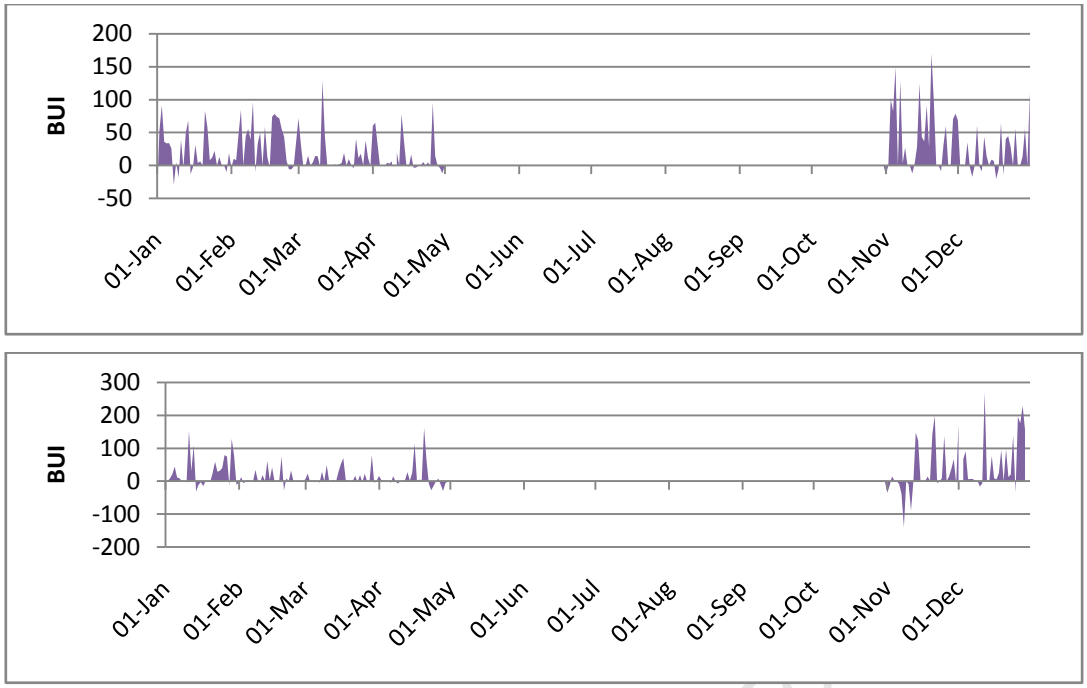

Figure 6.5 The daily averages of the Bakun Upwelling Index (BUI) (m^3/s) for the Namaqua zone in the 2005 (top panel) and 2009 (bottom panel).

6.3.2 Zone 2 (St Helena Bay; Dimensions: 32.0°S to 32.5°S; 17.75°E to 18.3°E)

The same daily zonal averaging was done in the St Helena Bay region as with the Namaqua region for 2005 and 2009. The area is of particular interest due to the retentive characteristics of the area arising from the pronounced cape and resulting recirculation, and the resulting predominance of resident high biomass blooms (Pitcher and Nelson, 2006, Weeks et al., 2006).

The estimated surface NO_3 exhibited very little variability between the two years for both the early summer and late summer/autumn periods (Fig. 6.6). During the early part of the summer months in both years, the concentrations were strongly bimodal, with NO_3 peaks of ~30µmol/l separated by low concentrations (<5µmol/l). However during December for both years, the strongly pulsed nature of the signal is not as readily apparent. Quiescence is far more prevalent in the mid summer period (January-March) with lower concentrations (<5µmol/l) present for a greater number of days. However maximum concentrations (~30µmol/l) similar to the early summer period in 2005 and 2009 are still achieved.

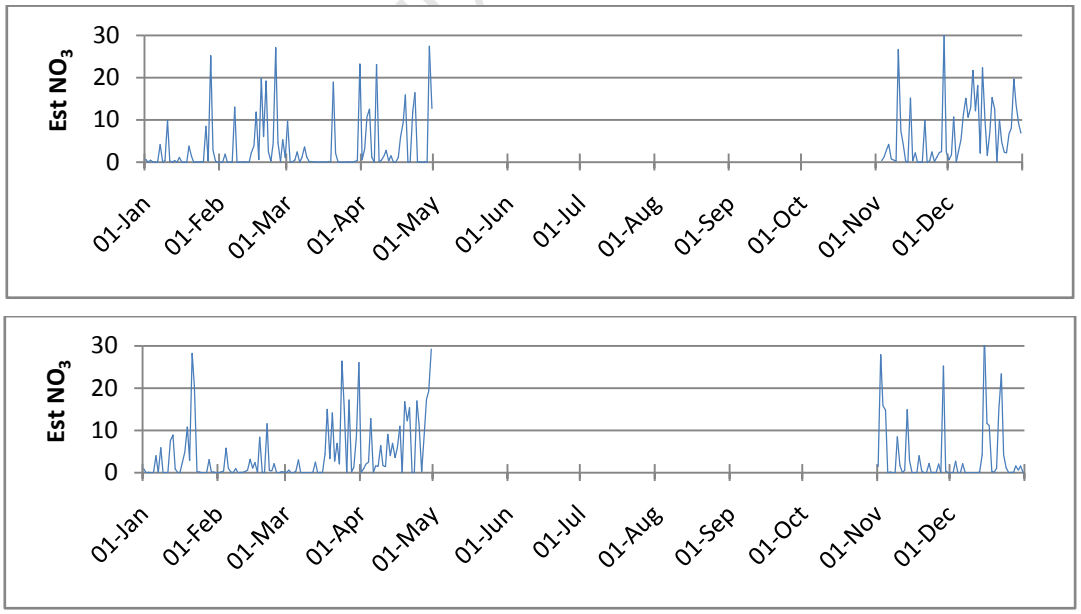

Figure 6.6 Daily averages of the estimated NO_3 (µmol/l), for the St Helena Bay zone in 2005(top panel) and 2009(bottom panel).

Upwelled water in the southern Benguela has a temperature of ~10°C (Demarcq et al., 2003, Carr, 2003, Hutchings et al., 2009). The estimated Iso_{12} depth during this period should therefore shoal extensively and this can be seen in figure. 6.7. The Iso_{12} depth could be consequently modified by surface processes such as solar heating, evaporation and precipitation. But due to the seasonal atmospheric climatology of the zone, precipitation and evaporation have little or no effect on the Iso_{12} movement but the solar heating due to high insolation does. However the surface warming is only responsible for the short term variability in the estimated Iso_{12} depths in 2005 and 2009. During the autumn (March-April) period in 2005 (Fig 6.7) there was a consistent balance between the upwelling and quiescent phases with extensive upwelling (depth~0m) and warming periods (depth~30m). However in 2009 during the corresponding period the isotherm showed a decreasing trend and longer periods of extensive shoaling where phases allowed for the oscillation of the Iso_{12} around the 0-10m depth range.

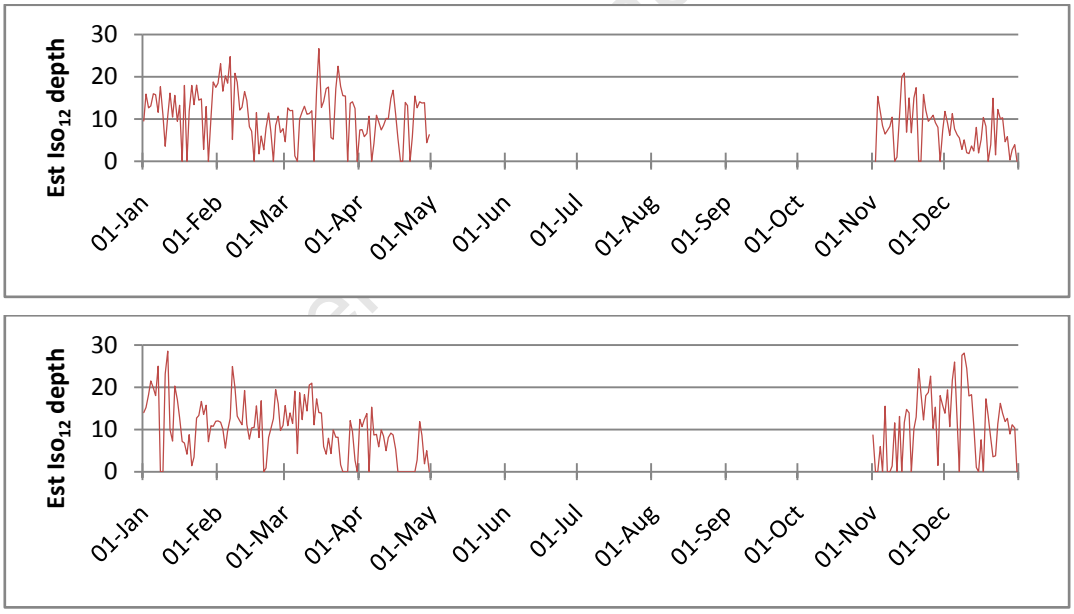

Figure 6.7 Daily averages of the estimated Iso_{12} depths (m), for the St. Helena Bay zone in 2005(top panel) and 2009(bottom panel).

The *chl a* data present a similar trend in the surface waters to both the isotherm and NO_3 patterns, with minimal concentrations during upwelling and increased biomass activity during quiescent phases (Fig. 6.8). The low concentrations during the early summer period for both 2005 and 2009 were due to the extensive upwelling during this time. During this period *chl a*

concentrations were < 10mg/m^3 which was far less than the concentrations experienced during the autumn periods in both years. The greater concentrations between January and May are consistent with Calder and Pitcher, (2000) who demonstrated that blooms occur commonly during this period in the southern Benguela.

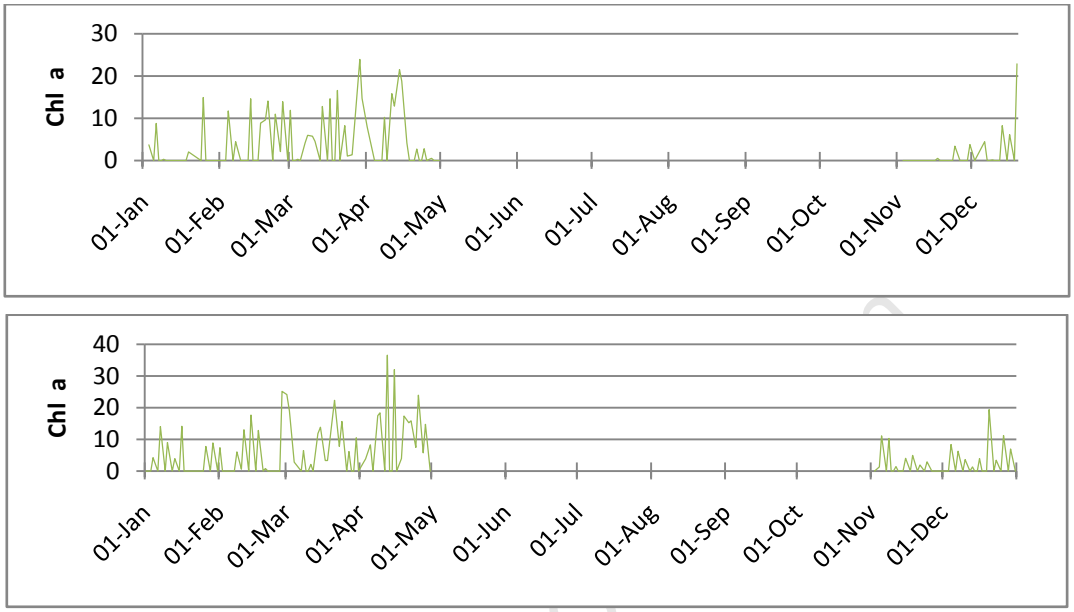

Figure 6.8 Daily averages of the *chl a* concentrations (mg/m^3), for the St. Helena zone in 2005(top panel) and 2009(bottom panel).

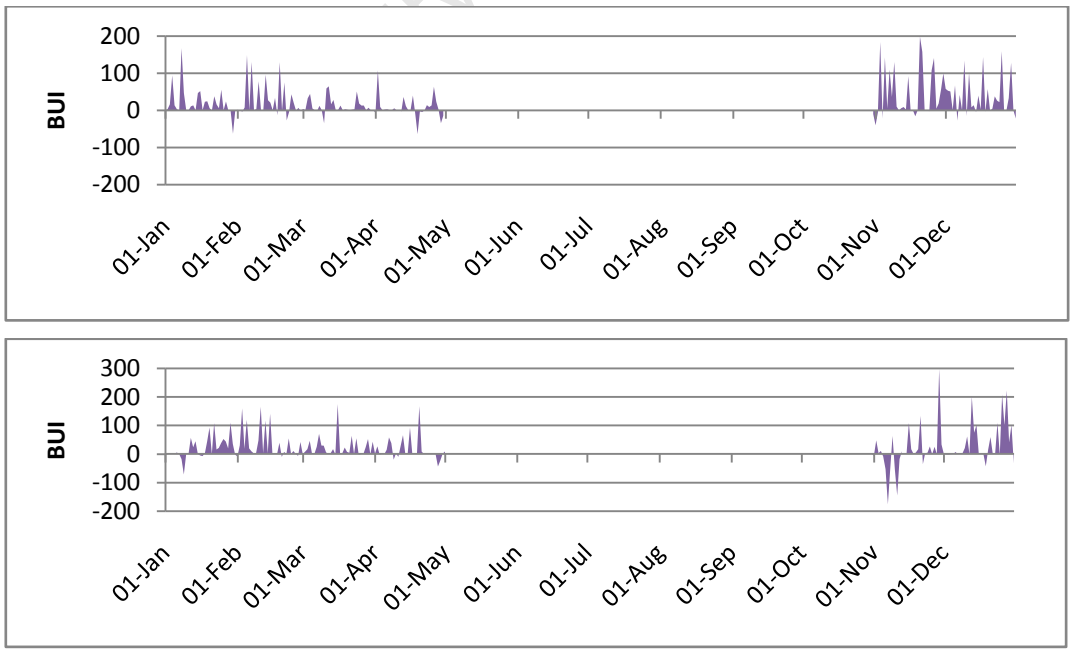

Figure 6.9 The daily averages of the Bakun Upwelling Index (BUI) (m^3/s) for the St. Helena Bay zone in the 2005 (top panel) and 2009 (bottom panel).

Figure 6.9 show the BUI for the zone in 2005 and 2009. The strong upwelling during November and December in both years is reinforced by the extensive NO_3 concentrations and rapid rise and fall of the Iso_{12} depth. In contrast the upwelling was erratic with weak to moderate transport and sporadic strong downwelling events namely in 2009. This is due to the increased episodic nature of the upwelling favourable winds during the late summer/ autumn period at this latitude during both the years.

6.3.3 Zone 3 (Cape Peninsula; Dimensions: 34.0°S to 34.5°S; 17.8°E to 18.3°E)

The Cape Peninsula zone is similar to the narrow inner shelf area of the Namaqua box, in contrast to the moderately broad inner shelf area of St Helena Bay, giving it a similarly strong upwelling signal to the Namaqua zone.

Most dominant in the Cape Peninsula zone is the consistently high (>20µmol/l) estimated NO_3 in the autumn and early summer for 2005 and 2009 (Fig. 6.10). Variability between the two years is not clearly visible: NO_3 concentrations above 10µmol/l are infrequent during both 2005 and 2009 in the mid-summer period. In November of both years there is a single extensive period where there is little NO_3 at the surface. Interestingly, during both years intense upwelling can be seen around the end of April.

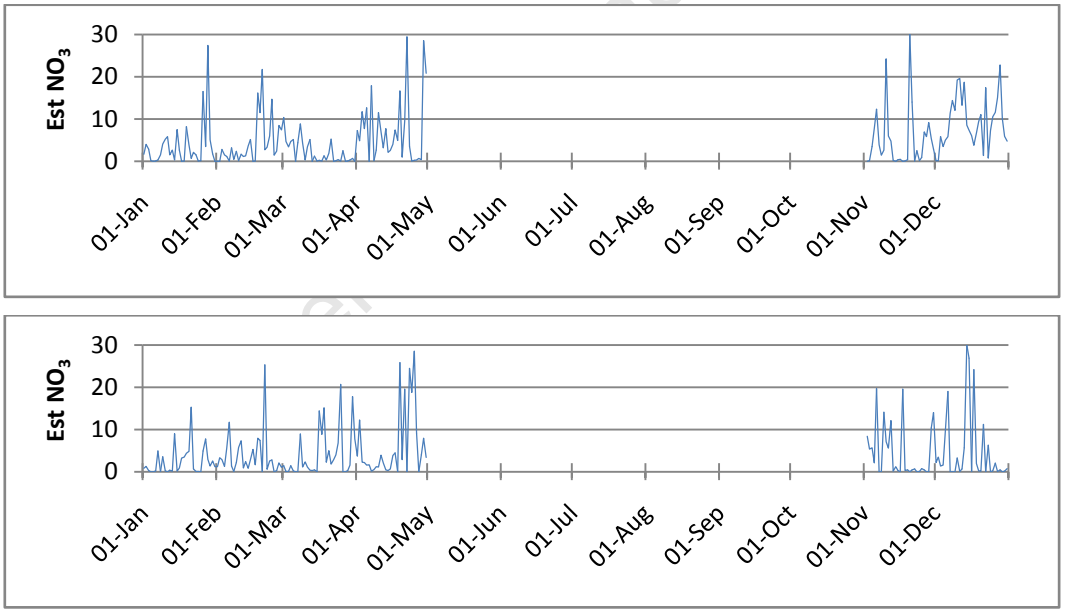

Figure 6.10 Daily averages of the estimated NO_3 (µmol/l), for the Cape Peninsula zone in 2005(top panel) and 2009(bottom panel).

The estimated Iso_{12} depth does show a similar variability to the associated NO_3 and is influenced by the rapid frequency of the upwelling and the subsequent heating/stratification thereafter (Fig. 6.11). The isotherm depth exhibits a strong localised, seasonal signal both in 2005 and 2009, where the excessive upwelling inside the Cape Peninsula zone during the

summer/autumn seasons is clearly evident. At such times the estimated Iso_{12} depth is at 0m, coincidental with freshly upwelled waters on the inner shelf. Slightly elevated or deeper depths (~5m) are observed for prolonged periods during 2005 when at the corresponding period in 2009 the Iso_{12} depth was consistently reaching the surface, consistent with the more pulsed characteristics of 2005 seen in the St Helena Bay zone.

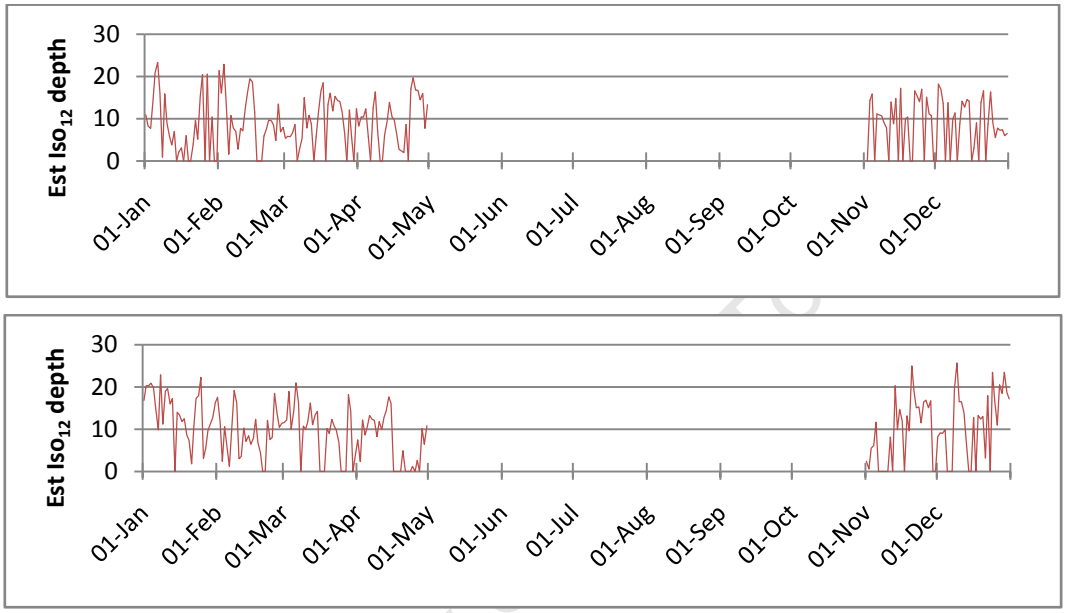

Figure 6.11 Daily averages of the estimated Iso_{12} depths (m), for the Cape Peninsula zone in 2005(top panel) and 2009(bottom panel).

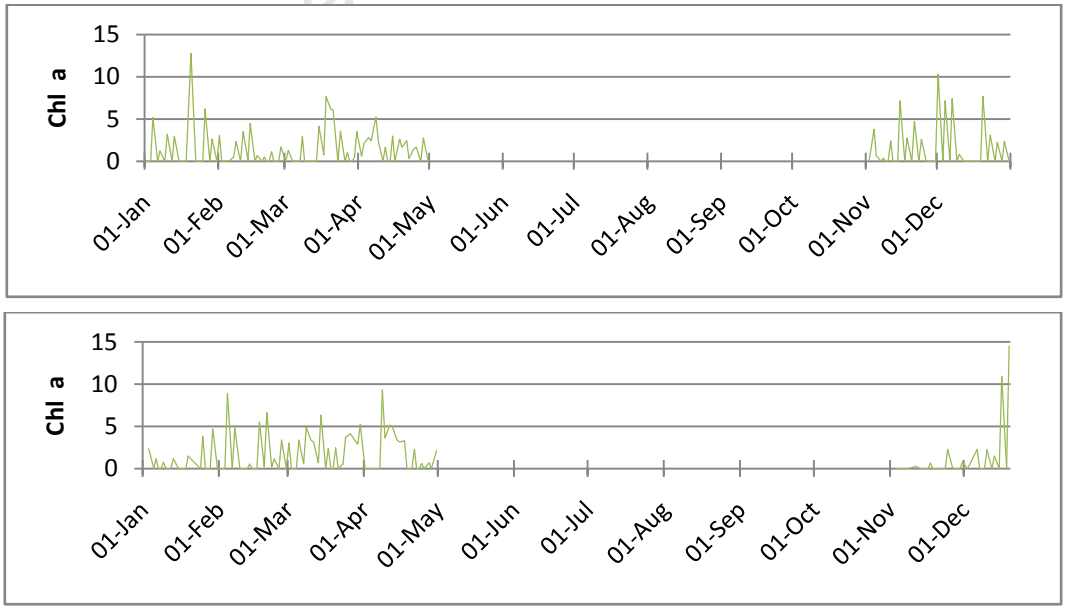

Figure 6.12 Daily averages of the *chl a* concentrations (mg/m^3), for the Cape Peninsula zone in 2005(top panel) and 2009(bottom panel).

The *chl a* concentrations in the Cape Peninsula box are on average much lower for both 2005 and 2009 than for the St. Helena Bay zone (Fig. 6.12). *Chl a* concentrations (generally < 10mg/m^3) in the Cape Peninsula zone are typically a third of those exhibited in the St. Helena Bay zone during the same time periods. Higher *chl a* concentrations (~10-15mg/m^3) are only apparent on two occasions during the two years, in January 2005 and December 2009. These locally elevated *chl a* concentrations appear to be associated with NO_3 concentrations of between 0 and 10µmol/l and Iso_{12} depths >10m.

In contrast to the other two areas the upwelling index shows much higher transport during 2005 and 2009 (Fig. 6.13). Correspondingly there is also a stronger downwelling signal for the Cape Peninsula zone with instances of between -100 and -200 m^3/s which is much larger than the ~-50m^3/s exhibited in the Namaqua and St Helena Bay zones. The presence of upwelled water is still clearly evident on the event scale and reinforced by the corresponding NO_3 and Iso_{12} values. Some differences between 2005 and 2009 are generally apparent with stronger transport in the January-May period for 2005 and the inverse for 2009 (November-December).

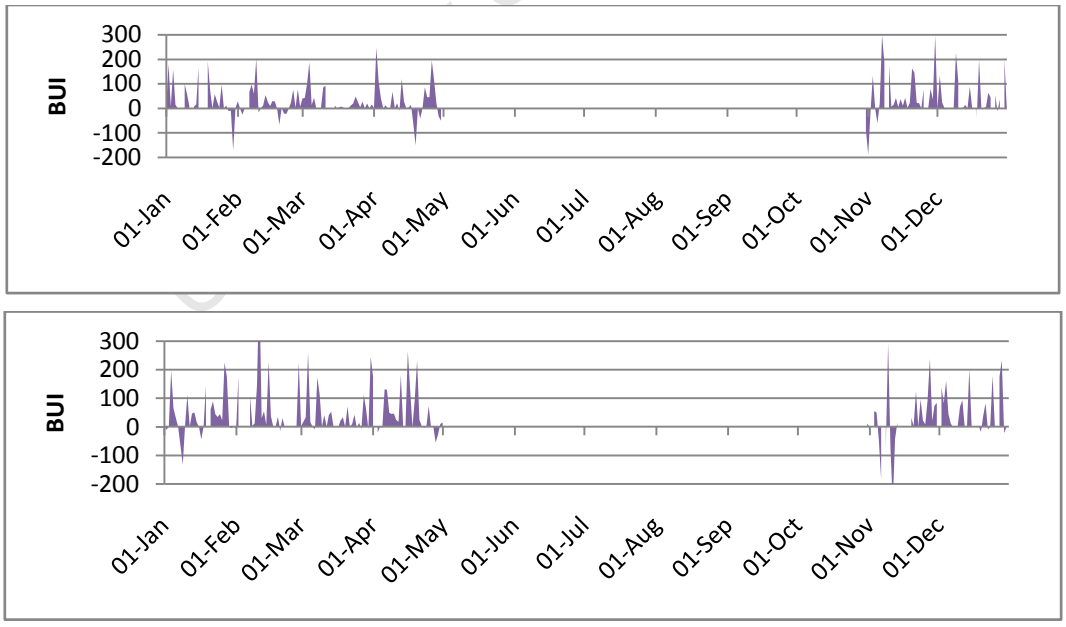

Figure 6.13 The daily averages of the Bakun Upwelling Index (BUI) (m^3/s) for the Cape Peninsula zone in the 2005 (top panel) and 2009 (bottom panel).

6.4 DISCUSSION

6.4.1 Event Scale NO_3 and Iso_{12} Algorithm Performance

The *in situ* surface measurements made during 2005, 2006 and 2007 (from which the algorithms are derived) allow an assessment of the algorithm application in representing the event scale physical and chemical variability of the surface waters in the southern Benguela, particularly in the St Helena Bay area. For the chosen algorithms presented in Chapters (3) and (4), the estimated NO_3 concentrations and Iso_{12} depths were compared to the *in situ* measured values. The data set is the same one that was used in the derivation of the algorithms making this not a validation technique for the algorithms but rather a means at evaluating their local, meso and synoptic scale performances.

Local Scale

The different algorithms derived both in Chapters (3) & (4) showed an improvement when the temperature of upwelled water was considered in Chapter (3) and the inclusion of the remotely sensed wind data in Chapter (4). Several factors may contribute to the increased scatter shown between the estimated and measured NO_3 values between 10 and 20µmol/l, and the estimated and measured Iso_{12} values at depths > 10m. For the NO_3 returns the inclusion and estimation of the δT term is an attempt at estimating the temperature of upwelled water which is based on a gross assumption that upwelled water moves from the coast westwards. The inclusion and explicit description of the latitudinal variation in the δT term is done with the assumption that there is no cross shelf variation in the term. The circulation of water masses from the on-shelf physics in other directions induces some noise in the δT term, and some perturbations in the NO_3- δT relationships (SC). The estimated Iso_{12} algorithm is not without its own deficiencies, where the inclusion of the remotely sensed wind improves the determination coefficients but increases the standard error between the estimated and *in situ* Iso_{12} depths. The low spatial resolution wind values were not entirely beneficial in resolving the scatter above 10m, where perhaps higher resolution *in situ* winds would better define the estimated Iso_{12} depth. However there was a reluctance in only utilizing temperature as the sole independent variable when it is known that wind is the primary driver of the system (Armstrong et al., 1987, Fawcett et al., 2007, Shillington et al., 2006) and the fact that the *in*

situ isotherm depth is derived from the said temperature. What is clearly evident is the satisfactory performance of the estimated NO_3 and Iso_{12} depth algorithms on a local scale where: (i) using the δT term as a signal of the age of upwelled water in an attempt to lessen the scatter between the NO_3-temperature relationship is beneficial, and (ii) the ability at picking up the upwelling and quiescent phase signals from both the estimated variables was satisfactory.

6.4.2 Synoptic Scale NO_3 and Iso_{12} Algorithm Performance

The match between *in situ* and the satellite derived surface NO_3 concentrations and Iso_{12} depths indicates that the algorithms are good at capturing the physics and variability of the system, with the remotely sensed estimations in the *in situ* region within +/-5µmol/l for the NO_3 and +/-2m for the Iso_{12} depth of the *in situ* values for all the years. Using the δT term and incorporating the wind signal into the derivation of the algorithms appears to work well with the expected on-shelf physics judging from the clear differences in values during upwelling and quiescent phases.

Using the examples in Chapter (5) (Figs. 5.4-5.12) to test the performance of the algorithms on a system wide synoptic event scale, the examples show the major role of the high resolution SST for both the estimation of the surface NO_3 and estimated Iso_{12} depths, and the secondary role played by the lower resolution remotely sensed winds in estimating the Iso_{12} depths. It is possible to resolve the signals associated with the main upwelling cells in the system during the upwelling phase in the NO_3 fields, namely in 2005 and 2006. The influence of the wind vectors on the estimated Iso_{12} depths seems small, with the isotherm field closely resembling the thermal structures shown in the SST images. The algorithms' performance are only as useful on a synoptic scale as the high resolution SST data; which, on a positive note regarding algorithm performance, do at least appear able to resolve the temporal and spatial upwelling variability in the system.

Across shelf values: The examples showed increased on-shelf NO_3 concentrations during upwelling days and non-detectable values during the quiescent phase. The significant concentrations cease at the upwelling and shelf break fronts in the system during upwelling, where both the fronts can co-exist because their dynamics are not mutually exclusive

(Mooers et al., 1978, Shannon and Nelson, 1996). The upwelling front is highly variable and shifts temporally whereas the shelf break front is usually stationary (Hutchings et al., 1986). The NO_3 gradients at the fronts during upwelling are not as exaggerated as the corresponding temperature gradients (14ºC to 17ºC) with only a ~2µmol/l difference. The spatial distribution of the concentrations between the frontal zone and coast is large in 2005 and 2006, with the difference between inshore upwelled waters and offshore nutrient-poorer waters of ~10µmol/l, following the expected trend of the southern Benguela of a decreasing gradient as one moves offshore (Armstrong et al., 1987, Probyn and Waldron, 1992, Tyrell and Lucas, 2002). Estimated Iso_{12} depths also display the cross-shelf variability during upwelling and to a lesser degree during quiescent phases.

St Helena Bay: On 24thMarch, 2005, coccolithophorids dominated the phytoplankton assemblage off Lamberts Bay in the highly stratified period associated with poleward flow from 16 March-24 March, 2005 (Fawcet et al., 2007). The highly stratified conditions experienced at the *in situ* location are unfortunately not captured by the estimated Iso_{12} depth image (Fig. 5.5, centre panel) due to no wind pixel in that region on that particular day. It is safe to assume though that the depth of the isotherm was probably >15m due to the high surface temperatures in the region on the day and the Iso_{12} depths in the local vicinity of the site. The Iso_{12} depth algorithm was however able to estimate the period of intermediate stratification of the Iso_{12} of between ~5-12m, where at the site southward currents and slight upwelling-favourable winds resulted in a large phytoplankton population shown in the *in situ* ~170mg/m^3*chl a* concentrations. The phytoplankton assemblage was dominated by the dinoflagellate *Prorocentrum triestinum* (Fawcett et al., 2007).

A comparison between the estimated NO_3 concentrations in the study area and *in situ* data confirms the satisfactory performance of the estimated NO_3 concentration algorithm in capturing the expected low surface concentrations in aged upwelled water in the southern Benguela during periods of increased thermal stratification (Fig 5.4, left panel) (Hutchings et al. 2009, Joyce and Pitcher, 2004). The influence of the light upwelling favourable winds off the coast of the system was revealed where estimated NO_3 levels in surface waters in St Helena Bay were initially undetectable on 24th March but increased slightly downstream of the site to ~2µmol/l. The slight nutrient input on 30th March would have aided in the growth or maintenance of the dinoflagellate bloom already present at the locale. The extent of the upwelling in the system in 2005 is portrayed by the variable increases of surface NO_3 on the

shelf due to the different strengths of upwelling plumes of cold water (~10ºC)(Fig.5.4, right panel) governed by the topographical variations in the southern Benguela (Armstrong et al., 1987;Pitcher and Nelson, 2006; Weeks et al., 2006). The estimated concentrations off Elands Bay were between 10 and 15µmol/l where the algorithm is able to illustrate recently upwelled waters through the increased surface concentrations.

The extent and frequency of upwelling during 2006 was greater than in 2005 culminating in the strongest *in situ* upwelling on 23rd March. In the days preceding the upwelling peak the water column was relatively moderately mixed (Fig. 2.3) and was associated with surface *in situ chl a* levels of between 10 and 50mg/m^3. The Iso_{12} depth illustrated the moderately mixed nature of the water column with depths of ~5m off the coast around Lamberts Bay on 8th March, 2006. Unfortunately on 19th March there was no SST image to apply the estimated Iso_{12} depth algorithm to, which was classified as a moderately mixed day according to the *in situ* temperature data. On this day the surface *in situ chl a* levels displayed concentrations ~100mg/m^3 in 13ºC water. The phytoplankton assemblage on this day was dominated by diatoms, accompanied by a low abundance of flagellates (Fawcett et al., 2007). It would have been of particular interest to see the estimated Iso_{12} depth in the area on this date and gauge the depth of the thermocline. The estimated NO_3 plot (Fig. 5.7, left panel) showed concentrations ~20µmol/l around the site almost matching with *in situ* surface value of 22µmol/l.

Most notable in the performance of the algorithms in 2007 is the ability to pick up the small changes in temperature, particularly on 27th March where the on-shelf upwelled water displayed varying temperatures. The estimated NO_3 concentrations algorithm was sensitive to these temperature changes due to the small interval where the algorithm is able to show appreciable NO_3. The estimated NO_3 concentrations in the *in situ* area on 27th March showed the single failure of the algorithm which is the persistent under sampling it gives during upwelling events of ~+/-5µmol/l, although this is partially explained by the +/-2µmol/l. standard error of the algorithm. Other variability could be explained by the warm bias of the satellite data, and its inaccurate definition and application on the MODIS Terra data. The solution to dealing with the inconsistency in the warm bias would require sensor specific validation studies aimed at categorizing a dynamic bias at different temperatures, which is beyond the scope of this study.

The dynamic event scale variability of the southern Benguela is sufficiently captured by the robust algorithms. The estimates of both the NO_3 and Iso_{12} depths reproduced satisfactory and consistent values during the quiescent phases with a larger variance in the upwelling periods.

6.4.3 Annual Comparisons and Intra-Seasonal Scale NO_3 and Iso_{12} Algorithm Performance

The annual average and variability patterns of the southern Benguela are illustrated in Chapter (6) with the investigation of three locations along the ecosystem. The zonal daily averaged plots allow a clear identification of the latitudinal and annual variability in the upwelling, NO_3 concentrations, Iso_{12} depths and *chl a* concentrations of the system.

The Cape Peninsula and Namaqua zones, which are within designated upwelling cells (Weeks et al., 2006, Hutchison et al., 2009), are identified by strong upwelling indicated by the index, with particular strength during the early summer. Upwelling strength is generally intense at these two locations with a peak during October where the high wind-stress at this time of year leads to greater upwelling strength and not necessarily frequency (Risien et al., 2004). The most distinguishable phenomena between the three areas is the rapidly pulsed nature of the upwelling in the system, with the event scale nature of the occurrence clearly evident. Significant downwelling episodes only seem evident during 2009 for the St Helena Bay and Cape Peninsula boxes. The data values derived by the index range between 300 and -250 m^3/s per 100m, which is similar to the ranges reported by Bakun (1973) and Schwing et al., (1996) for the California system.

The dominant pattern of estimated NO_3 concentrations is one of higher values at all the three sites during the early summer period. This is consistent with the increase in upwelling events during this time of year, where the sustained upwelling consistently replenishes the euphotic zone with new NO_3. During the late summer/autumn period the NO_3 average concentrations are tempered by the increase in the duration of the quiescent periods. The increase of the NO_3 variability during this time of year is common in the southern Benguela (Pitcher et al., 1989, Probyn and Waldron., 1992). Whilst the temporal relationship between the upwelling and NO_3 is non linear (Stoens et al., 1999), a positive relationship exists.

The estimated Iso_{12} depths obviously also show strong links with the event scale pulsing of the upwelling and associated variability. During 2005 and 2009 in the St Helena Bay zone the isotherm seems to shoal slightly and oscillate between ~8 and ~15m over a few days. It is not coincidental that these oscillation corresponds with recorded large blooms in the St Helena Bay area, where big blooms of predominantly *Prorocentrum triestinum* were seen in 2005 (Fawcett et al., 2007) and *Ceratium balechii* in 2009 (Pitcher and Probyn, 2011). This isotherm level allows the swim strategy adopted by certain species of dinoflagellate to be utilized by the migration to the thermocline boundary in search of nutrients. The results of the estimated NO_3 and Iso_{12} depths clearly demonstrate that boom formation is dependent upon two things in the southern Benguela: the system being primed with sufficient NO_3, and a period of quiescence and stratification. This is well known and reported on for the ecosystem (Pitcher et al., 1996, Pitcher and Joyce, 2004, Pitcher and Nelson, 2006, Fawcett et al., 2007, Pitcher and Probyn, 2011), but it is very encouraging to see it clearly shown in the data and it is a good starting point towards the path of bloom prediction in the system.

Chl a concentrations at all three sites to a large degree mirror the estimated Iso_{12} depth variability, similarly dominated by the event scale processes. What is clearly evident is the link between turbulence and cell growth, where in the strong upwelling, high turbulence environments such at the Cape Peninsula and Namqua zones the average *chl a* concentrations are markedly lower than those in the more variable and stratified zone of St Helena Bay. Two distinct periods of elevated *chl a* values are seen and coincide with the blooms in March/April, 2005 and March 2009 with concentrations >20mg/m^3, and instances of markedly higher than maximum concentrations quoted in Barlow, (1982) of aged water of 30mg/m^3. Weeks et al., (2006) also showed relatively high on-shelf *chl a* concentrations (>10mg/m^3) for St Helena Bay for the late summer/autumn period. In general the *chl a* patterns show a correlation with turbulence and shelf width, where during the early summer concentration averages are low when upwelling is at its peak and high late summer concentrations when wind relaxation and reversals play a larger role in the system physics.

Overall the algorithm performances display very little annual differences between 2005 and 2009 in the respective zones but a good intra-seasonal signal within the zones and relative to each other.

6.3.4 A Qualitative Application of the Algorithms in a Key Area for Bloom Formation

Further to examining the dynamic variations in upwelling and phytoplankton response in the southern Benguela is the analysis and a test of the algorithms in a key area susceptible to bloom formation. The central theme of this study is to identify the relationship between nutrient availability, turbulence and phytoplankton assemblages according to Margalef's mandala (Margalef, 1978) using earth observation. According to Margalef, (1978) the general succession of phytoplankton functional groups are based on an ecological place which is defined by a continuum from r-selected (diatoms) to K-selected (dinoflagellate) organisms, which is largely controlled by turbulence, which provides a proxy for nutrient and light availability. This implied that certain taxa are adapted to particular environments.

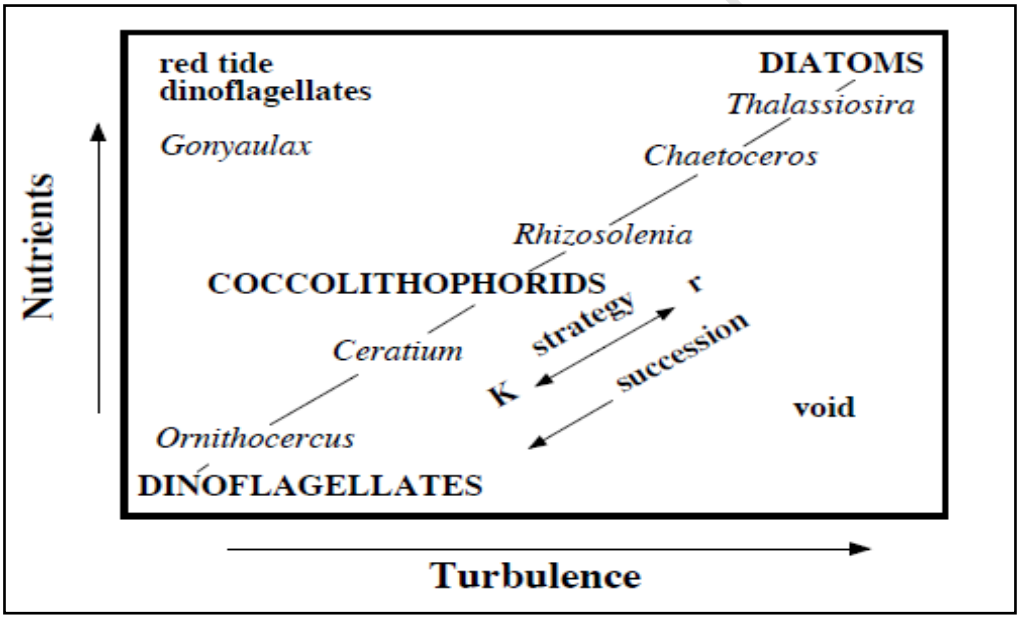

Figure 6.14 A graphic representation of Margalef's Mandala which shows the main phytoplankton life forms in an ecological space defined by nutrient concentration and turbulence (Adapted from Estrada and Berdalet, 1997).

According to the mandala (Fig 6.14) major taxonomic groups of phytoplankton occupy different spaces within the mandala and the diagonal approximates the main succession sequence in a system.

Diatoms: They are non-motile, fast potential growth cells, which adopt a "sink" strategy under sub-optimal conditions (Kudela et al., 2005, Pitcher and Nelson, 2006) and thrive in relatively turbulent, nutrient-rich waters.

Dinoflagellates: The growth of phytoplankton requires sufficient supplies of light and nutrients. Post upwelling as the water is heated there is a succession pattern from r-selected (diatoms) to K-selected (dinoflagellates) organisms as the turbulence and nutrients decrease (Margalef, 1978).

Red Tide Dinoflagellates: The ecological space where the mandala positions red tide blooms- in high nutrients, low turbulence regions is not practically possible in upwelling systems. Smayda and Reynolds, (2003) state that in order for a red tide bloom to happen according to that ecological space there would need to be an external input (i.e. terrestrial) of nutrients because low turbulence is a poor nutrient-pump. The above stated event would be somewhat of an anomaly from the expected succession patterns (Bernard et al., 2006).

In terms of the mandala typical phytoplankton succession would follow a trend from the high turbulence-high nutrient corner to the opposite low-turbulence-low nutrient corner. In the Benguela this conceptual model is useful in defining phytoplankton assemblages, not only temporally in the upwelling zone, but also spatially across the shelf.

The central aim of this thesis is to use earth observation methods to define the physical-biological ecosystem state along Margalef's general approach to the systematization of phytoplankton life-forms. A strong focus has been placed on establishing the confidence and constraints in the derived nutrient and turbulence proxies, and their relative applicability on the event, annual and intra-seasonal scales. By assessing the algorithms' performances in the context of the mandala it is expected it should be possible to predict the phytoplankton functional groups using the estimated NO_3 and Iso_{12} products.

Ecological Niche

The NO_3 and Iso_{12} products were tested for their gross functionality at defining an ecological niche where the survival of phytoplankton populations are the result of a temporary equilibrium between success in remaining afloat and inevitable sinking. During the study the

12ºC isotherm has been utilized as a proxy for the thermocline depth. The relative depth of the thermocline in the water column can then be directly related to the stratification of the water column, provided the surface temperature is known. The turbulence, as one of the two primary mandala variables, allows us to hypothesize the different taxa present in the system according to the state of the environment. The turbulence index in this thesis is derived from the zonally averaged daily Iso_{12} depths from the St Helena Bay zone during 2005 and is defined as follows:

$$Turbulence\ Index = \frac{1}{Stratification\ \ (Est.Isotherm\ depth)} \tag{6.4}$$

The second variable, the nutrient proxy, is derived from the zonally averaged daily NO_3 concentrations from the St Helena Bay zone during 2005. The two proxies were plotted against each other (Fig. 6.15) according to the mandala (Margalef, 1978), with the remotely sensed zonally averaged daily *Chl a* concentrations included in an attempt at defining the taxa in the St Helena Bay zone during 2005. The data sets are identical to those used earlier in Chapter (6).

According to the mandala, major taxonomic groups of phytoplankton occupy different spaces within the mandala and the diagonal approximates the main succession sequence in a system. The ecological space hypothesized by the mandala to have increased diatom occupation doesn't seem to materialize with very low *chl a* concentrations in the high turbulence-high nutrient region (Fig. 6.15). The expected conditions where the major taxonomic group would be diatoms, is immediately post upwelling where they thrive in turbulent, nutrient-rich water (Margalef, 1978, Kudela et al., 2005). The biomass position within the ecological space does seem rather low with *chl a* values expected higher up the nutrient axis. There could be a few possible reasons for the suppressed nutrient concentrations:1) The already mentioned inherent under sampling of the estimated NO_3 concentrations algorithm, specifically at cold water temperatures immediately after upwelling or 2) there simply wasn't any significant diatom bloom in 2005 but rather cells which didn't reach bloom levels.

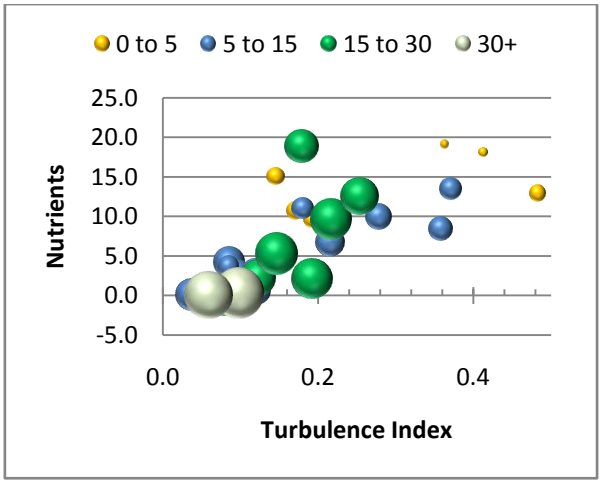

Figure 6.15 A bubble plot of the estimated NO_3 concentrations (µmol/l)(nutrients) vs. turbulence index (dimensionless). The colour scale refers to the *chl a* concentration interval (mg/m^3) in the St Helena Bay zone for 2005. Relative bubble sizes depict the biomass scale related to the *chl a* concentration (Right panel).

The observations of the estimated surface NO_3, turbulence and *chl a* concentrations show large concentration patches of dinoflagelletes in the ecological space defined by the mandala. These patches most likely correspond to the autumn period in 2005, where several quiescent phases associated with the relaxation of upwelling-favourable winds resulted in poleward nearshore currents and decreased levels of turbulence (Fawcet et al., 2007). Fawcett et al., (2007) states that the HAB that was present during this period in St Helena Bay was associated with dinoflagellates *Dinophysis spp*. and *Protoceratium reticulatum* which produced toxins associated with DSP. The ecological space where the dinoflagellates are found are in a low turbulence-low nutrient environments. This might lead to the expectation that dinoflagellate species have a monotonous habitat preference according to the mandala. It is at this juncture where Smayda and Reynolds, (2001) express that observational evidence leads to the contrary and recognize nine different habitats where dinoflagellates can bloom. In continuing with the classic stratification-HAB paradigm articulated by Margalef, (1978), where dinoflagellates dominate in nutrient poor stratified environments, the conditions where inshore poleward flow in St Helena Bay promote retentive circulation and the stratification were available in 2005. The motile nature of dinoflagellates due to their flagella, allows them to regulate their position in the water column, where in low turbulence conditions they can migrate to preferential habitats (Kudela et al., 2005) for nutrients in aid of sustained growth. The high biomass illustrated in the *Ornithocercus* and *Ceratium* ecological space confirms what observational evidence in the southern Benguela has established where there are a large

number of *Ceratium* species which play a role in HABs within the ecosystem (Pitcher and Probyn, 2011; Kudela et al., 2005). The relative biomass concentrations of *coccolithophorids* from the mandala, where they appear to occupy intermediate positions mostly correspond to the period in mid March, 2005, where concentrations of *coccolithophorids* increased in stratified conditions. One should expect higher NO_3 concentrations at the dinoflagellate/*ceratium* ecological space and this was not shown in Fig 6.15, where the biomasses were at concentrations below 5µmol/l. This is because of the scale difference between the biology and physics in system where the absolute NO_3 concentrations (nutrients) are different from the assimilated NO_3 which has a direct correlation to the phytoplankton growth.

Quantifying the ecological niche

One of the difficulties in the application of the mandala to real data is the quantification of the nutrients and turbulence. Bowman et al., (1981), Jones and Gowen (1990) attempted to do this by using the potential growth rates of organisms and representing them in a diagram defined by optical depth and turbulence intensity, as expressed by the stratification index developed by Simpson and Hunter (1974). In this present study no attempt was made to quantify the niche were a bloom is possible but what was evident from the experimental data was that organisms seem to develop at depths where the Iso_{12} depth (i.e. thermocline) is between 5 and 15m. This however is not empirical proof of the values where a bloom will develop but just an observation.

7. 1 CONCLUSIONS

This study aimed to utilize earth observation and our current understandings of phytoplankton succession theory in an attempt to articulate Margalef's mandala (Margalef, 1978) of: "*...different life-forms of phytoplankton are functionally interpreted as adaptations to survival in an unstable and turbulent environment*" using nutrients and turbulence proxies. This was done to contribute towards real-time bloom prediction and management efforts for the southern Benguela system. Four major questions were asked with regard to finding an ecological niche where phytoplankton succession can be hypothesized.

7.1.1 *Are the algorithms adapted from Silió-Calzada et al., (2008) valid on local scales in the southern Benguela? If not, are the newly locally derived algorithms able capture the events and seasonal scale coupling of the physics and biology of the system?*

Estimated surface NO_3 concentrations

Silió-Calzada et al., (2008) developed a new approach that allows the seasonal estimation of surface NO_3 concentrations in the Benguela system, based on the correlation between *in situ* NO_3 and an indicator of the water temperature based on time elapsed since upwelling, δT. The new approach was an attempt at reducing the traditional dispersion in the NO_3-temperature relationships by accounting for the latitudinal and seasonal variability in the δT term. In this thesis the mesoscale derived algorithms from Silió-Calzada et al., (2008) and the locally derived algorithms from the current study were both tested against the current *in situ* data.

In the thesis there was an improvement in the surface NO_3 concentration predictions using the technique initially proposed by Silió-Calzada et al., (2008), where the locally derived algorithms had higher determination coefficients and lower standard errors in the predicted values, than the mesoscale derived algorithms used in Silió-Calzada et al., (2008). These

results were as to be expected due to the fact that the thesis algorithms were derived from the current *in situ* data which was used to test the accuracy of both algorithms. The utilization of the algorithms in Silió-Calzada et al., (2008) first with: NO_3 as a function of the *in situ* surface temperature (SST_{depth}) and then NO_3 as a function of the *in situ* surface temperature (δT) and *chl a* concentration proved unsatisfactory at estimating surface NO_3 off the coast of Lamberts Bay, with large standard errors between the estimated and *in situ* NO_3 values. However using the thesis derived algorithms yielded satisfactory concentrations at the same site with tighter correlations and lower standard errors between the estimated and *in situ* NO_3. The introduction of the, δT, term in place of the surface temperature in an attempt at indicating the time elapsed since upwelling helped to resolve the scatter in the NO_3-temperature relationship at the location. The inclusion of a *chl a* term allowed for the evaluation of the influence phytoplankton have on the accuracy of the estimated surface NO_3 concentrations in the Silió-Calzada et al., (2008) algorithm. The inclusion of the *chl a* term in this thesis was found to be detrimental in the scatter of the NO_3-temeprature relationship due to the physical-biological decoupling of the system on a local, event scale. It must be noted that the thesis derived algorithms were not explicitly validated due to the lack of an independent data set and the comparison between the estimated and *in situ* variables is only for assessment purposes.

Estimated Iso_{12} depth

The current study proposed using the Iso_{12} depth as a proxy for the thermocline depth in the southern Benguela ecosystem. The performance of the locally derived estimated Iso_{12} depth algorithm based on the *in situ* surface temperature (SST_{depth}) was satisfactory when the estimated Iso_{12} depths were compared to *in situ* values. The further inclusion of the remotely sensed meridional QuickScat seawinds in the derivation of the algorithm yielded a stronger determination coefficient but an increase in the standard error. The decision was taken to persist with the algorithm which took into consideration the remotely sensed wind even with the associated increase in the errors. The Iso_{12} depth results should be considered with caution due to this.

Event and meso scale algorithm performances

The robust algorithms performances were good when applied to MODIS Terra data, which was the purpose they were developed for. A major problem which was discovered upon the application of the algorithms on the SST data was the larger than expected warm bias

between the *in situ* surface and remotely sensed temperatures. The problem was exacerbated by the small temperature interval where the algorithms were applicable, where during cold events (i.e. upwelling) there was a large warm bias which resulted in low estimated surface NO_3 concentrations and deep Iso_{12} depths (described in detail in Chapter 5). An attempt was made to define the dynamic bias using a robust method which was successful at reducing the temperature difference between *in situ* and remotely sensed temperatures. The resultant derived NO_3 and Iso_{12} depth fields were able to capture the event and mesoscale variability, with the ability to resolve the upwelling variability along the southern Benguela caused by topographical variations within the system (Hutchings et al., 2009) and the on-shelf physics.

Annual and intra-seasonal algorithm performances

The annual and intra-seasonal analysis of the algorithms shows a clear signal in all the zones chosen, where during the early summer due to the increased wind-stress the upwelling strength and frequency are raised and the estimated NO_3 concentrations and estimated Iso_{12} depths change accordingly. The intra-seasonal variability shows the expected longer periods between upwelling episodes, where NO_3 concentrations are limiting in the system in the latter part of the upwelling season. The algorithms further capabilities are the ability to resolve the ecosystem upwelling variability with a relative change in the estimated NO_3 and Iso_{12} values, where the two upwelling cells (Cape Peninsula and Namaqua) show consistently high NO_3 concentrations and high variability in Iso_{12} depths in response to the increased divergence in those regions. The annual comparisons seem limited with only a clear signal shown in the Iso_{12} depths where they shoal consistently more in 2009 than in 2005.

7.1.2 Can the principles with regards to phytoplankton life forms based on the optimum ecological niche apply to the southern Benguela and further more can it be extrapolated to the system as a whole?

Using the NO_3 and Iso_{12} products as the nutrient and turbulence proxies in an attempt at classifying the ecosystem according to Margelef's Mandala was satisfactory as a first attempt at defining the ecosystem using earth observation. The proxies were reasonably able to model the environments in 2005 and thus create the ability to predict phytoplankton life forms according to the habitats. Even with the satisfactory performance of the algorithms at defining the phytoplankton functional types there was an issue with the different time scales

between the nutrient availability and biomass growth. As previously discussed, NO_3 availability and biomass are intimately linked, as the NO_3 limits the biomass in the system. However, not all NO_3 is necessarily consumed, or at least not at the same rate, as a function of time by different phytoplankton functional types. It is at this point where there is a disconnect between the explicit NO_3 concentrations estimated by the algorithm and the NO_3 assimilation which in part controls where the biomass appears in the ecological space within the mandala. For this reason the results from the ecological niche analysis must be interpreted with some caution. Even with minor issues between the physical and biological time scales of the proxies, the system is known to follow the conceptual model of the mandla. Various *in situ* based studies within the southern Benguela have been able to that show that the biology follows the conceptual model of the mandala (Pitcher et al., 1989; Pitcher and Nelson, 2006; Fawcett et al., 2007) but this was the first time it was done using earth observation explicitly and it revealed mixed results at defining an ecological niche.

The ability to extrapolate the proxies across the southern Benguela and keep their relative accuracy should be possible because of the proven ability of the algorithms at resolving the ecosystem event mesoscale variability. An extrapolation to the northern sector of the Benguela would be a different proposition as the physical and biological couplings work differently to those in the southern Benguela and the influence of the topography on the biology is not as dominant. The lack of a pulsing nature in the upwelling would need accomodation and potentially a new algorithm that could be used in the northern Benguela. The proposal by Silió-Calzada et al., (2008) to include the δT term was an attempt at having a single algorithm that could be applied across the entire Benguela instead of multiple algorithms which may provoke discontinuities or artefacts along the boundaries and imply the use of interpolation procedures. The concern with using the algorithms derived in Silió-Calzada et al., (2008) for the southern Benguela is the lack of recently upwelled 10ºC water which is endemic to the system which was flagged out in the remotely sensed data, so the algorithms' usefulness in this sector were tested but results remain inconclusive.

7.1.3 Does a broad, simplistic approach in the analysis of the physical and biological interactions on the continental shelf capture the spatial and temporal variability of the system?

The simplistic, robust approach hypothesized in this study at using real-time earth observation in an attempt at predicting bloom formation or the potential for bloom formation and creating an ecosystem management approach of HABs in the region was satisfactory as a first attempt at the task. The algorithms had the desired sensitivity to the ecosystem spatial and temporal variability even though the values of the estimated NO_3 concentrations predicted showed an inherent under sampling during and immediately after upwelling when compared with *in situ* values.

7.1.4 *Improvements and Closing Notes*

Two major improvements that need to be made the in the future are:

1) The further validation of the algorithms in the St Helena Bay area and other parts of the ecosystem. The algorithms derived could also be incorporated with circulation models of the system so as to take into account the direction of water displacement after upwelling.
2) Investigations and the definition of the dynamic warm bias between the MODIS Terra SST and the *in situ* bulk temperature in the southern Benguela must be done. The differences between the *in situ* and remotely sensed temperatures have a direct influence on the validity of the algorithms in the ecosystem, where a subtle change in the remotely sensed component yields a strong change in the estimated algorithm values. Due to the complexity of upwelling regions and their unique thermal signals the process of defining the bias may be an arduous and expensive task where radiometer validation studies would need to be undertaken for an accurate interpretation of the warm bias.

The influence of using data from different satellite sensors (MODIS and MERIS) run by different programs in the definition of the phytoplankton functional types in the system is unknown. It would be of particular interest in the future to do this study again with data from the upcoming Sentinel 3 program by ESA, with co-acquired data from where the new OLCI

ocean colour sensor (MERIS quality data) and the new SLSTR SST sensor (AATSR quality data).

The most important aspect of this study to note is that satellite NO_3 and Iso_{12} depths cannot be expected to and will not match the accuracy of *in situ* measurements, but will at best represent "potential" NO_3 and thermocline values. This is potentially true as long as satellite SST estimates have errors and the warm bias in the southern Benguela is not defined. For this reason the algorithms are not and should not be considered as a substitute for *in situ* data but rather a tool for providing synoptic information on variability on surface NO_3 and thermocline depths where *in situ* data cannot.

With regard to the ecological window approach at defining the ecosystem biology, presently the prediction of the precise synoptic community composition is unlikely without using temporally threadbare MERIS data but the formulation of functional groups using the mandala does provide the potential for limited prediction because of the distinctive ecophysiological properties of various life forms (Pitcher and Nelson., 2006) and the stability of the SST dataset.

References

Adrian, R., J., 1991. Particle-imaging techniques for experimental fluid mechanics. *Annual Review of Fluid* Dynamics 23, 261-304.

Armstrong, D., A., Mitchell-Innes, B., A., Verheye, F., Waldron, H., Hutchings, L., 1987. Physical and biological features across an upwelling front in the southern Benguela. *South African Journal of Marine Science* 5 (1987), 171-190.

Bakun, A., 1973. Coastal upwelling indices, west coast of North America, 1946-71. U.S. Department of Commerce, *NOAA Technical Report*, NMFS SSRF-693, 114.

Bakun, A., Nelson, C., S., 1991. Wind stress curl in subtropical eastern boundary current regions. *Journal of Physical Oceanography* 21, 1815-1834.

Barlow, R., G., 1982. Phytoplankton ecology in the southern Benguela current. 1. Biochemical composition. *Journal of Experimental Marine Biology and Ecology* 63. 239-248.

Berger, W., H., Smetacek, V., S., Wefer, G., 1989. Ocean productivity and paleoproductivity-an overview. *Productivity of the ocean: present and past*. Berger, W., H., Smetacek, V., S., Wefer, G., eds., John Wiley and Sons, New York, 1-34.

Bernard, S., Kudela, R., M., Franks, P., Fennel, W., Kemp, A., Fawcett, A., Pitcher, G., C., 2006. The Requirements for Forecasting Harmful Algal Blooms in the Benguela. [Eds] Shannon, L., V., Hempel, P., Malanotte-Rizzoli, P., Moloney, C., Woods., J. *Large Marine Ecosystems* 14, 281-302.

Bode, A., Botas, J., A., Fernandez, E., 1997. Nitrate storage by phytoplankton in a coastal upwelling environment. *Marine Biology* 129, 399-406.

Broeker, W., S., Peng, T., H., 1982. The anthropogenic invasion: the movement of water through the oceanic thermocline. *Tracers in the sea*. Lamont-Doherty Geological Observatory, New York. 383-444.

Brown, O., B., Minnett, P., J., 1999. MODIS Infrared Sea Surface Temperature Algorithm-Algorithm Theoritical Basis Document Version 2.0. *University of Miami*. 1-98.

Burchard, H., Craig, P., D., Gemmrich, J., R., van Haren, H., Mathieu, P., Markus Meier, H., E., Alex, W., Nimmo Smith, M., Prandke, H., Rippeth, T., P., Skyllingstad, E., D., Smyth, W., D., Welsh, D., J., S., Wijesekera, H., W., 2008. Observational and numerical modelling methods for quantifying coastal ocean turbulence and mixing. *Progress in Oceanography* 76, 399-442.

Bowman, M., J., Esaias, W., E., Schnitzer, M., B., 1981. Tidal stirring and the distribution of phytoplankton in Long Island and Block Island Sounds. Journal of Marine Research 39, 587-603.

Calvert, S., Price, N., B., 1971. Upwelling and nutrient regeneration in the Benguela Current, October 1968. *Deep-Sea Research* 18, 505-523.

Carr, M., 2002. Estimation of potential productivity in Eastern Boundary Currents using remote sensing. *Deep-Sea Research II* 49 (2002), 59–80.

Carr, M., E., Kearns, E., J., 2003. Production regimes in four Eastern Boundary Current systems. *Deep-Sea Research Part II* 50, 3199-3221.

Chaen, M., Wyrtki, K., 1981. The 20°C Isotherm Depth and Sea Level in the Western Equatorial Pacific. *Journal of the Oceanographic Society of Japan* 37, 198-200.

Chapman, P., Shannon, L., V., 1985. The Benguela ecosystem: Chemistry and related processes. *Oceanographic Marine Biology Annual Review* 23, 183-251.

Chavez, F., P., Barber, R., T., 1987. An estimate of new production in the equatorial Pacific. *Deep Sea Research* 34, 1229-1243.

Chavez, F., P., Toggweiler, J., R., 1995. Upwelling in the ocean: Modeling processes and ancient records. Summerhayes, C., P., ed., Wiley, New York, 313-320.

Chavez, F., P., Service, S., K., Buttrey, S., E., 1996. Temperature-Nitrate relationships in the central and eastern tropical Pacific. *Journal of Geophysical Research* 101, 20553-20563.

Codispoti, L., A., 1989. Phosphorus vs. Nitrogen limitation of new (export) production. *Productivity of the ocean: present and past*. Berger, W., H., Smetacek, V., S., Wefer, G., eds., John Wiley and Sons, New York, 1-34.

Collos, Y., Vaquer, A., Souchu, P., 2005. Acclimatation of nitrate uptake by phytoplankton to high substrate levels. *Journal of Phycology*, 41. 466-478

Crowley, T., J., 2000. Causes of climate change over the last 1000 years. *Science* 289. 270-277.

Curry, P., Roy, C., 1989. Optimal environmental window and pelagic fish recruitment success in upwelling areas. *Canadian Journal of Fisheries and Aquatic Science* 46, 670-680.

Demarcq, H., Barlow, R., G., Shillington, F., A., 2003. Climatology and variability of sea surface temperature and surface chlorophyll in the Benguela and Agulhas ecosystems as observed by satellite imagery**.** *African Journal of Marine Science* 25, 363–372.

Denman, K., L., 1973. A time-dependant model of the upper ocean. *Journal of Physical Oceanography* 3, 173-174.

Donlon, C., J., Robinson, I., S., 1997. Observations of the oceanic thermal skin in the Atlantic Ocean. *Journal of Geophysical Research* 102, 18585-18606,

Donlon, C., J., Minnett, P., J., Gentemann, C., Nightingale, T., J., Barton, I., J., Ward, B., Murray, M., J., 2002. Toward Improved Validation of Satellite Sea Surface Skin Temperature Measurements for Climate Research. *American Meteorological Society*, 353-369.

Dowset, H., Willard, D., 1996. Southeast Atlantic marine and terrestrial response to middle Pliocene climate change. *Marine Micropaleontology* 27. 181-193.

Ducklow, H., Steinberg, D., K., Buessele, K., 2001. Upper Ocean Carbon Export and the Biological Pump. *U.S. Joint Global Ocean Flux Study* 14, 4.

Dugdale, R., C., Goering, J., J., 1967. Uptake of new and regenerated forms of nitrogen in primary productivity. *Limnology and Oceanography* 12, 196-206.

Dugdale, R., C., Morel, A., Bricaud, A., Wilkerson, F., P., 1989. Modelling new production in upwelling centres: A case study of modelling new production from remotely sensed temperature and colour. *Journal of Geophysical Research* 94, 18119-18132.

Dugdale, R., C., Wilkerson, F., P., Morel, A., 1990. Realization of new production in coastal upwelling areas: A means to compare relative performance. Limnology and Oceanography 35, 822-829

Dugdale, R., C., Wilkerson, F., P., Barber, R., Chavez, F., 1992. Estimating new production in the equatorial Pacific Ocean at 150°W. Journal of Geophysical Research 97, 681-686.

Dugdale, R., C., Wilkerson, F., P., Minas, H., J., 1995. The role of a silicate pump in driving new production. *Deep-Sea Research I* 42, 697-719.

Duncan, C., P., Nell, J., H., 1969. Surface currents off the Cape coast. *Invest Rep Div Sea Fish S Afr* 76, 1-19.

Durand, M., H., Mendelssohn, R., 1998. How to detect a change both on global and local scale in oceanographic time series. Global Versus Local Changes in Upwelling, Durand, M., H., et al, eds, 45-78. Ed. De L'Orstom, Paris.

Emery, W., J., Lee, W., G., Magaard, L., 1984. Geographic and Seasonal distributions of Brunt-Väisälä frequency and Rossby radii in the North Pacific and North Atlantic. *Journal of Physical Oceanography* 14, 294-317.

Eppley, R., Renger, E., H., Harrison, W., G., 1979. Nitrate and Phytoplankton Production in Southern California Coastal Waters. *Limnology and Oceanography*, 24. 483-494.

Estrada, M., Berdalet, E., 1997. Phytoplankton in a turbulent world. *Scientia Marina* 61, 125-140.

Esaias, W., E., Abbott, M., R., Barton, I., Brown, O., B., Campbell, J., W., Carder, K., L., Clark, D., K., Evans, R., H., Hoge, F., E., Godon, H., R., Balch, W., M., Letelier, R, Minnett, P., J., 1998. An Overview of MODIS Capabilities for Ocean Science Observations. *IEEE Transactions on Geoscience and Remote Sensing* 36, 1250- 1266.

Ettwein, V., J., Stickley, C., E., Maslin, M., A., Laurie, E., R., Rosell-Mele, A., Vidal, L., Brownless., M., 2001. Fluctuations in productivity and upwelling intensity at site 1083 during the intensification of Northern Hemisphere Glaciation (2.4-2.65 Ma). *Proceedings of the Ocean Drilling Program. Scientific Results* 175, 1-24.

Falkowski, P., G., Scholes, R., J., Boyle, E., Canadell, J., Canfield, D., Elser, J., Gruber, N., Hibbard, K., Högberg, P., Linder, S., MacKenzie., F., T., Moore., B., Pedersen, T., Rosenthal, Y., Seitzinger, S., Smetacek, V., Steffen, W., 2000. The global carbon cycle: A test to our knowledge of earth as a system. *Science* 290, 291

Fawcett, A., Pitcher, G., C., Bernard, S., Cembella, A., D., Kudela, R., M., 2007. Contrasting wind patterns and toxigenic phytoplankton in the southern Benguela upwelling system. *Marine Ecology Progress Series* 348, 19-31.

Ferziger, J., H., Perić, M., 2001. Computational methods for fluid dynamics. *Springer*, Berlin, Heidelberg, New York.

Field, C., B., Behrenfeld, M., J., Randerson, J., T., Falkowski, P., G., 1998. Primary production of the biosphere: Integrating terrestrial and oceanic components. *Science* 281, 237-240.

Freeland, H., Denman, K., Wong, C., S., Whitney, F., Jacques, R., 1997. Evidence of change in the winter mixed layers in the north-east Pacific Ocean. *Deep-Sea Research* 44A, 2117-21219.

Fung, I., Doney, S., C., Lindsay, K., John, J., 2005. Evolution of carbon sinks in a changing climate. *Proc. Nat. Acad. Sci. (USA)* 102, 11201-11206.

Garzoli, S., L., Gordon, A., L., 1996. Origins and Variability of the Benguela Current. *Journal of Geophysical Research* 101, 897-906.

Gazeau, F., Quiblier, C., Jansen, J., M., Gattuso., JP., Middelburg, J., J., Heip, C., H., R., 2007. Impact of elevated CO_2 on Shellfish Calcification. *Geophysical Research Letters* 34.

Gentemann, C., L., Donlon, C., J., Stuart-Menteth, A., Wentz, F., J., 2003. Diurnal signals in satellite sea surface temperature measurements. *Geophysical Research Letters* 30, 401-404.

Gentemann, C., L., Minnett, P., J., Le Borgne, P., Merchant, C., J., 2008. Multi-satellite measurements of large diurnal warming events. *Geophysical Research Letters* 35, 1-6.

Gerkema, T., 2001. Internal and interfacial tides: beam scattering and local generation of solitary waves. *Journal of Marine Research* 59, 227-255.

Goes, J., I., Saino, T., Oaku, H., Jiang, D., L., 1999. Method for estimating sea surface nitrate concentrations from remotely sensed SST and chlorophyll a: A case study for the North Pacific Ocean using OCTS/ADEOS data. *IEEE Transactions on Geoscience and Remote Sensing*, 37, 1633-1644

Gordon, A., L., 1985. Indian-Atlantic transfer of thermocline water at the Agulhas Retroflection. *Science* 227, 1030-1033.

Guastella, L., A., 1992. Sea surface heat exchange at St Helena Bay and implications for the southern Benguela upwelling system. *South African Journal of Marine Science* 12, 61-70.

Hart, T., J., Currie, R., I., 1960. The Benguela Current. *Discovery Report* 31, 123-298.

Hasse, L., 1971. The sea surface temperature deviation and the heat flow at the air-sea interface. *Boundary Layer Meteorology* 1, 369-379.

Hoegh-Guldberg, O., Mumby, P., J., Hooten, A., J., Stenek, R., S., Greenfield, P., Gomez, E., Harvell, C., D., Sale, P., F., Edwards, A., J., Caldeira, K., Knowlton, N., Eakin, C., M., Iglesias-Priento, R., Muthiga, N., Bradbury, R., H., Dubi., A., Hatziolos, M., E., 2007. Coral Reefs Under Rapid Climate Change and Ocean Acidification. *Science* 318, 1737-1742.

Hodgkiss, I., J., Ho, K., C., 1997. Are changes in N:P ratios in coastal waters the key to increased red tide blooms? *Hydrobiologia* 352, 141-147.

Holden, C., J., 1987. Observations of low frequency currents and continental shelf-waves along the west coast of South Africa. In the Benguela and Comparable ecosystems. [Eds] Payne, A., I., L., Gulland, J., A., Brink., K., H. *South African Journal of Marine Science* 5, 197-208.

Holmes, M., E., Muller, P., J., Schneider, R., R., Segl, M., Patzold, J., Wefer, G., 1996. Stable nitrogen isotopes in Angola Basin surface sediments. *Marine Geology* 134 , 1-12.

Holmes, M., E., Muller, P., J., Schneider, R., R., Wefer, G., 1997. Reconstruction of past nutrient utilization in the eastern Angola Basin based on sedimentary $^{14}N/^{15}N$ ratios. *Paleoceanography* 4, 604-614.

Hosoda, K., Murakami, H., Sakaida, F., Kawamura, H., 2007. Algorithm and Validation of Sea Surface Temperature using MODIS sensors aboard Terra and Aqua in the Western North Pacific. *Journal of Oceanography* 63, 267-280.

Houry, S., Dombrowski, E., De Mey, P., Minster, J., 1987. Brunt-Väisälä frequency and Rossby radii in the South Atlantic. *American Meteorological Society* 7, 1619- 1626.

Hutchings, L., van der Lingen, C., D., Shannon, L., J., Crawford, R., J., M., Verheye, H., M., S., Bartholomae, C., H., van der Plas, A., K., Louw, D., Kreiner, A., Ostrowski, M., Fidel., Q., Barlow., R.,G., Lamont, T., Coetzee, J., Shillington, F., Veitch, J., Currie, J., C., Monteiro, P., M., S., 2009. The Benguela Current: An ecosystem of four components. *Progress in Oceanography* 83, 15-32.

Johnson, M., Sanders, R., Avgoustidi, V., Lucas, M., Brown, L., Hansell, D., Moore, M., Gibb, S., Liss, P., Jickells, T., 2007. Ammonium accumulation during a silicate-limited diatom bloom indicates the potential for ammonia emission events. *Marine Chemistry* 106, 63-75.

Joiris, C., Billen, G., Lancelot, D., Daro, M., H., Mommaerts, J., P., Bertels, A., Bossicart, M., Nijs, J., Hecq, J., H., 1982. A budget of carbon recycling in the Belgian coastal zone: Relative roles of zooplankton, bacterioplankton and benthos in the utilization of primary production. *Netherlands Journal of Sea Research* 16, 260-275.

Jones, K., J., Gowen, R., J., 1990. Influence of stratification and irradiance regime on summer phytoplankton composition in coastal and shelf areas of the British Isles. Estuarine and Coastal Shelf Science 30, 557-567.

Joyce, L., B., Pitcher, G., C., 2004. Encystment of *Zygabikodimium lenticulatum* (Dinophyceae) during a summer bloom of dinoflagellates in the southern Benguela upwelling system. *Estuarine Coastal and Shelf Science* 59, 1-11.

Jury, M., R., 1988. Case studies of the response and spatial distribution of wind-driven upwelling off the coast of Africa: 29-34ºS. *Continental Shelf Research* 8, 1257-1271.

Jury, M., R., Brundrift, G., B., 1992. Temporal organization of upwelling in the southern Benguela ecosystem by resonant coastal trapped waves in the ocean and atmosphere. *South African Journal of Marine Science* 12, 219-224.

Kamykowski, D., Zentara, S., 1985. Nitrate and silicic acid in the world ocean: patterns and process. *Marine Ecology Progress Series* 26, 47-59.

Kamykowski, D., Zentara, S., 1986. Predicting plant nutrient concentrations from temperature and sigma-t in the world ocean. *Deep Sea Research* 33, 89-105.

Kierstead, H., Slobodkin, L., B., 1953. The size of water masses containing plankton blooms. *Journal of Marine Research* 12, 141-147.

Koeve, W., 2001. Wintertime nutrients in the North Atlantic-new approaches and implications for new production estimates. *Marine Chemistry* 74, 245-260.

Kraus, E., B., Turner, J., S., 1967. A one dimensional model of the seasonal thermocline, II. The general theory and its consequences. *Tellus* 19, 98-105

Kudela, R., M., Dugdale., R., C., 1996. Estimation of new production from remotely-sensed data in the coastal upwelling regime. *Advances in Space Research* 18, 91-97.

Kudela, R., M., Cochlan, W., P., Dugdale, R., C., 1997. Carbon and nitrogen uptake response to light by phytoplankton during an upwelling event. *Journal Plankton Research* 19, 609-630.

Kudela, R., M., Chavez, F., P., 2000. Modelling the impact of the 1992 El Nino on new production in Monterrey Bay, California. *Deep-Sea Research II* 47, 1055-1076

Kudela, R., Pitcher, G., C., Probyn, T., Figueiras, F., Moita, T., Trainer, V., 2005. Harmful Algal Blooms in Coastal Upwelling Systems. *Oceanography* 18, 184-197.

Kudela, R., M., Seeyave, S., Cochlan, W., P., 2010. The role of nutrients in regulation and promotion of harmful algal blooms in upwelling systems. *Progress in Oceanography* 85, 122-135.

Kurz, K., D., Maier-Reimer, E., 1993. Iron fertilization of the Austral Ocean: the Hamburg Model assessment. *Global Biogeochemical Cycles* 7, 229-244.

Margalef, R., 1978. Life-forms of phytoplankton as survival alternatives in an unstable environment. *Oceanoligica Acta* I. 493-509.

Margalef, R., Estrada, E., Blasco, D., 1979. Functioonal Morphology of organisms involved in red tides, as adapting turbulence. Taylor, D., L., Seliger, H., H., eds., *Toxic Dinoflagellate Blooms*, New York, Elsevier, 89-94.

Lamberth, R., Nelson, G., 1987. Field and analytical drogue studies applicable to the St Helena Bay of South Africa's west coast. Payne, A., L., L., Gulland, J., L., Brink, K., H., eds, The Benguela and comparative ecosystems. *South African Journal of Marine Science* 5, 163-169.

Large, W., G., Gent, P., R., 1999. Validation of vertical mixing in an equatorial ocean model using Large Eddy Simulations and Observations. *Journal of Physical Oceanography* 29, 449-464.

Longhurst, A., 1998a. Ecological biogeography of the pelagial. In A. C. Pierrot-Bults & S. van der Spoel (Eds). *Pelagic Biogeography. IOC workshop* 142, Paris: UNESCO, 239-249.

Longhurst, A., 1998b. *Ecological geography of the sea*. San Diego: Academic Press.

Lu, Y., Lueck, R., G., 1999. Using a broadband ADCP in a tidal channel. Part II: Turbulence. *Journal of Atmospheric and Oceanic Technology* 16, 1568-1579.

Lucas, A., J., Pitcher, G., C., Probyn, T., A., Kudela, R., M., 2013. The influence of diurnal winds on phytoplankton dynamics in a coastal upwelling system. *Deep-Sea Research II*, http://dx.doi.org/10.1016/j.dsr2.2013.01.016

Lutjeharms, J., R., E., Meeuwis, J., M., 1987. The extent and variability of South-East Atlantic upwelling. *South African Journal of Marine Science* 5, 51-62.

Lutjeharms, J., R., E., Stockton, P., L., 1987. Kinematics of the upwelling front off southern Africa. *South African Journal of Marine Science* 5, 35-50.

McClain, E., P., Pichel, W., G., Walton, C., C., 1985. Comparative performance of AVHRR-based multi-channel sea surface temperatures. *Journal of Geophysical Research* 90, 11587-11601.

Minnett, P., J., Evans, R., H., Kearns, E., J., Brown, O., B., 2002. Sea-surface temperature measured by the Moderate Resolution Imaging Spectroradiometer (MODIS). *IEEE Transactions on Geoscience and Remote Sensing*. 1177-1179.

Munk, W., H., 1966. Abyssal Recipes. *Deep Sea Research* 13, 707-703

Mooers, C., N., K., Flagg, C., N., Boicourt, W., C., 1978. Prograde and retrograde fronts. Oceanic Fronts in Coastal Processes. Bowman, M., J., W., E., Esaias [Eds]. *New York: Springer*, 43-58.

Morel, A., Berthon, J., F., 1989. Surface pigments, algal biomass profiles, and potential production of the euphotic layer: Relationships reinvestigated in view of remote sensing applications. *Limnology and Oceanography* 34, 1545-1562.

Morin, P., Wafar, M., V., M., Le Corre, P., 1993. Estimation of nitrate flux in a tidal front from satellite-derived temperature data. *Journal of Geophysical Research* 98, 4689-4696.

Nees, J., C., Dugdale, R., C., Dugdale, V., A., Goering, J., J., 1962. Nitrogen metabolism in lakes. Measurement of nitrogen fixation with N^{15}. Limnology and Oceanography 7, 163-169.

Nelson, G., Hutchings, L., 1983. The Benguela upwelling area. *Progress in Oceanography* 12, 333-356.

New, A., L., 1988. Internal tidal mixing in the Bay of Biscay. *Deep-Sea Research* 35, 691-1624.

New, A., L., Da Silva, J., C., B., 2002. Remote-sensing evidence for the local generation if internal soliton packets in the central Bay of Biscay. *Deep-Sea Research I* 49, 915-934.

Nimmo Smith, W., A., M., Atsavapranee, P., Katz, J., Osborn, T., R., 2002. PIV measurements in the botton boundary layer of the coastal ocean. *Experiments in Fluids* 33, 962-971.

Nimmo Smith, W., A., M., Osborn, T., R., Katz, J., 2004. PIV measurements in the bottom boundary layer of the coastal ocean. Gru, J., Lui, P., L., F., Pedersen, G., K., eds, PIV and Water Waves, Coastal and Ocean Engineering 9. *World Scientific Publishers*, 51-79.

O'Toole, M., J., J., 1980. Seasonal distribution of temperature and salinity in the surface waters off south-west Africa, 1972-1974. *Investigational Reports of the South Africa Sea Fisheries Institute* 121, 1-25.

Oschilies, A., Garçon, V., 1998. Eddy-induced enhancement of primary production in a model of the North Atlantic Ocean. Nature 394, 263-269.

Palacios, D., M., Bograd, S., J., Mendelssohn, R., Schwing, F., B., 2004. Long-term and seasonal trends in stratification in the California Current, 1950-1993. *Journal of Geophysical Research* 109, 1-12.

Papadakis, J., E., 1981. Determination of the wind mixed layer by an extension of Newton's method. *Pacific Marine Science Report* 81-9, Institute of Ocean Sciences, Sydney, British Columbia, Canada, 1-32.

Papadakis, J., E., 1985. Determination of the wind mixed layer by an extension of Newton's method: On a class of form oscillators. *Speculations Science and Technology* 8, 291-303.

Parsons, T., R., Muita, Y., Lalli, C., 1984. A manual of Chemical and Biological Methods of Seawater Analysis. *Pergamon Press*, Oxford.

Pauly, D., Christensen, V., 1995. Primary production required to sustain global fisheries. *Nature* 374, 255–257.

Peters, H., Gregg, M., C., Toole, J., M., 1988. On the parameterization of equatorial turbulence. *Journal of Geophysical Research* 93, 1199-1218.

Pitcher, G., C., Walker, D., R., Mitchell-Innes, B., A., 1989. Phytoplankton sinking rate dynamics in the southern Benguela upwelling system. *Marine Ecology Progress Series* 55, 261-269.

Pitcher, G., C., Brown, P., C., Mitchell-Innes, B., A., 1992. Spatio-temporal variability of phytoplankton in the southern Benguela upwelling system. *South African Journal of Marine Science* 12, 439-456.

Pitcher, G., C., Boyd, A., J., 1996. Across-shelf and alongshore dinoflagellate distributions and the mechanisms of red tide formation withing the southern Benguela upwelling system. Yasumoto, T., Oshima, Y., Fukuyo, Y., (Eds), *Harmful and Toxic Algal Blooms. Intergovernmental Oceanographic Commission of UNESCO.* Paris, 243-246.

Pitcher, G., C., Boyd, A., J., Horstman, D., A., Mitchell-Innes, B., A., 1998. Subsurface dinoflagellate populations, frontal blooms and the formation of red tide in the southern Benguela upwelling system. *Marine Ecological Progress Series* 172, 253–264.

Pitcher, G., C., Calder, D., 2000. Harmful algal blooms of the southern Benguela current: a review and appraisal of monitoring from 1989 to 1997. *South African Journal of Marine Science* 22, 255–271.

Pitcher, G., C., Nelson, G., 2006. Characteristics of the Surface Boundary Layer Important to the Development of Red Tide on the Southern Namaqua Shelf of the Benguela Upwelling System. *Limnology and Oceanography* 51. 2660-2674

Pitcher, G., C., Bernard, S., Ntuli, J., 2008. Contrasting Bays and Red Tides in the southern Benguela Upwelling System. *Oceanography* 21, 82-91

Pitcher, G., C., Probyn, T., A., 2011. Anoxia in southern Benguela during the autumn of 2009 and its linkage to a bloom of the dinoflagellate *Ceratium balechii*. *Harmful Algae* (2011), doi 10.1016/j.hal.2011.07.001.

Platt, T., Harrison, W., G., 1985. Biogenic fluxes of carbon and oxygen in the ocean. *Nature* 318, 55-58.

Platt, T., Harrison, W., G., Lewis, M., R., Li, W., K., W., Sathyendranath, S., Smith, R., E., Vézina, A., F., 1989. Biological production of the oceans: the case for a consensus. *Marine Ecology Progress Series* 52, 77-88

Porter, D., L., Thompson, D., R., 1996. Estimation of thermocline depths from SAR imagery and a two layer density model. *Remote Sensing for a Sustainable Future*. IGARSS 1996.

Powles, S., B., 1984. Photoinhibition of photosynthesis induced by visible light. *Annual Review of Plankton Physiology* 35, 15-44.

Price, J., F., Weller, R., A., Pinkel, R., 1986. Diurnal cycling: Observations and models of the upper ocean response to diurnal heating, cooling and wind mixing. *Journal of Geophysical Research*, 91, 8411-8427.

Probyn, T., A., 1985. Nitrogen uptake by size-fractionated phytoplankton populations in the southern Benguela upwelling system. Marine Ecology Progress Series 22, 249-258.

Probyn, T., A., 1992. The inorganic Nitrogen nutrition of phytoplankton in the southern Benguela: New production, phytoplankton size and implications for pelagic foodwebs. *South African Journal of Marine Science* 12, 411-420.

Probyn, T., A., Pitcher, G., C., Monteiro, P., M., S., Boyd, A., J., Nelson, G., 2000. Physical processes contributing to Harmful Algal Blooms in Saldanha Bay, South Africa. *South African Journal of Marine Scienc*e 22, 285-297.

Raven, J., A., Falkowski, P., G., 1999. Oceanic sinks for atmospheric CO_2. *Plant, Cell and Environment* 22, 741-755

Redfield, A., C., Ketchum, B., H., Richards, F., A., 1963. The influence of organisms on the composition of seawater. Hill, M., N., ed, *The Sea*. Interscience, New York.

Rees, W., G., 2001. Physical Principles of Remote Sensing. *Cambridge University Press* 2nd Edition, 1-33.

Reynolds, R., W., Rayner, N., A., Smith, T., M., Stokes, D., C., Wang, W., 2002. An improved in *in situ* and satellite SST analysis for climate. *Journal of Climate* 15. 1609-1625.

Rippeth, T., P., Williams, E., Simpson, J., H., 2002. Reynolds stress and turbulent energy production in a tidal channel. *Journal of Physical Oceanography* 32, 1242-1251.

Rippeth, T., P., Williams, E., Simpson, J., H., Inall, M., E., 2003. Measurement of the rates of production and dissipation of turbulent kinetic energy in an energetic tidal flow: Red Wharf Bay Revisited. *Journal of Physical Oceanography* 33, 1889-1901.

Risien, C., M., Reason, C., J., C., Shillington, F., A., Chelton, D., B., 2004. Variability in satellite winds over the Benguela upwelling system during 1999-2000. *Journal of Geophysical Research* 109, C0310.

Robinson, C., L., K., Ware, D., M., 1994. Modeling pelagic fish and phytoplankton trophodynamics off southwestern Vancouver Island, British Columbia. *Canadian Journal of Fisheries and Aquatic Science* 51, 1737-1751

Sabine, C., L., Feely, R., A., Gruber, N., Key, R., M., Lee, K., 2004. The oceanic sink for anthropogenic CO_2. *Science* 305, 367-371.

Sarmiento, J., L., Siegenthaler, U., 1992. New Production and the global cycle. *Primary Productivity and Biogeochemical Cycles in the Sea*. P. Falkowski, ed., Plenum Press, New York, 317-332.

Sarmiento, J., L., Gruber, N., Brzezinski, M., A., Dunne, J., P., 2004. High-latitude controls of thermocline nutrients and low latitude biological productivity. *Nature* 427, 56-60.

Sarnthein, M., Winn, K., Duplessy, J. C., Fontugne, M., R., 1988. Global variations of surface ocean productivity in low and mid latitudes: Influence on CO_2 reservoirs of the deep ocean and atmosphere during the last 21000 years. *Paleoceanography* 3 (1988), 361-399.

Savtchenko, A., Ouzounov, D., Ahmad, S., Acker, J., Leptoukh, G., Koziana, J., Nickless, D., 2004. Terra and Aqua MODIS products available from NASA GES DAAC. *Advances in Space Research* 34, 710-714.

Saunders, P., 1967. The temperature at the ocean-air interface. *Journal of Atmosphere Science* 24, 269-273.

Schneider, N., Muller, P., 1990. The meridional and seasonal structures of the mixed-layer depth and its diurnal amplitude observed during the Hawaii-to-Tahiti Shuttle experiment. *Journal of Physical Oceanography* 20, 1395-1404.

Sharples, J., Mark Moore, C., Ripperth, T., P., Holligan, P., M., Hydes, D., J., Fisher, N., R., Simpson, J., H., 2001. Phytoplankton distribution and survival in the thermocline. *Limnology and Oceanography* 46, 486-496.

Schwing, F., B., O' Farrell, M., Steger, J., M., Baltz, K., 1996. Coastal upwelling indices west coast of North America 1946-95. *NOAA Techinical Memorandum NMFS*.

Schwing, F., B., Mendelssohn, R., 1997. Increased coastal upwelling in the California Current System. *Journal of Geophysical Research* 102, 3421-3438.

Semina, H., J., 1997. An outline of the geographical distribution of oceanic plankton. *Advances in Marine Biology* 32, 527-563.

Shannon, L., V., 1985. The Benguela ecosystem. Part I: Evolution of the Benguela, physical features and processes. *Oceanography and Marine Biology Annual Review* 23, 105-182.

Shannon, L., V., Boyd, A., J., Brundrit, G., B., Taunton-Clark, J., 1986. On the existence of an El Nino type phenomenon in the Benguela system. *Journal of Marine Research* 44, 495-520.

Shannon, L., Nelson, G., 1996. The Benguela: large scale features and processes and system variability. Wefer, G., Berger, W., H., Siedler, G., Web, D., J., eds, The South Atlantic: present and past circulation. *Springer*, Berlin, Heidelberg.

Sherman, K., 2006. Forecasting Within the Context of Large Marine Ecosystems Programs [Eds] Shannon, L., V., Hempel, P., Malanotte-Rizzoli, P., Moloney, C., Woods., J. *Large Marine Ecosystems* 14, 281-302.

Shillington, F., A., 1998. The Benguela upwelling system off Southwestern Africa, coastal segment (16°E). *The Sea II: The Global Coastal Ocean*, 332-340

Silió-Calzada, A., 2008. Estimation of new primary production in upwelling areas from multi-sensor satellite data: application to the Benguela system, and study of its seasonal and interannual variability. *Doctor of Philosophy in Science*. 1-246

Silió-Calzada, A., Bricaud, A., Gentili, B., 2008. Estimates of sea surface nitrate concentrations from sea surface temperature and chlorophyll concentration in upwelling areas: A case study for the Benguela System. *Remote Sensing of Environment* 112, 3173-3180.

Simpson, J., H., Rippeth, T., P., Williams, E., Betteridge, K., F., E., 2005. Acoustic Doppler techniques. Baumert, H., Simpson, J., H., Sündermann, J., eds., Marine Turbulence Theories, Models and Observations, Results of the CARTUM Project. *Cambridge University Press*, Boston, 127-138.

Skyllingstad, E., D., Smyth, W., D., Moum, J., N., Wijesekera, H., 1999. Upper- ocean turbulence during a westerly wind burst: A comparison of large-eddy simulation results and microstructure measurements. *Journal of Physical Oceanography* 29, 5-28.

Smayda, T., J., 1990. Phytoplankton species succession. In: Morris I (ed) The physiological ecology of phytoplankton. *Studies in Ecology* 7. Blackwell, Oxford, 493-570.

Smayda, T., J., Reynolds, C., S., 2001. Strategies of marine dinoflagellate survival and some rules of assembly. Journal of Sea Research 49, 95-106.

Smayda, T., J., 2002. Turbulence, water mass stratification and harmful algal blooms: an alternative view and frontal zones as "pelagic seed banks". *Harmful Algae* I, 85-112.

Smith, R., E., Kalf, J., 1983. Competition for phosphorus among co-occuring freshwater plankton. *Limnology and Oceanography* 28, 448-464.

Smyth, W., D., Hebert, D., Moum, J., N., 1996a. Local ocean response to a multiphase westerly wind burst. Part 1: The dynamic response. *Journal of Geophysical Research* 101, 22495-22512

Smyth, W., D., Hebert, D., Moum, J., N., 1996b. Local ocean response to a multiphase westerly wind burst. Part 2: Thermal and freshwater responses. *Journal of Geophysical Research* 101, 22513-22533.

Stacey, M., T., Monismith, S., G., Burau, J., R., 1999. Mesurements of Reynold's stress profiles in unstratified tidal flow. *Journal of Geophysical Research* 104, 10993-10949.

Steidinger, K., A., Haddad, K., 1981. Biologic and Hydrographic Aspects of Red Tides. *BioScience* 31 (1981), 814-819.

Stewart, R., H., 2007. Introduction into Physical Oceanography. *Department of Oceanography-Texas A&M University*, 88.

Stickland, J., D., H., Solarzano, L., Eppley, R., W., 1970. Part One: General introduction into the hydrography and chemistry, in the ecology of the plankton off La Jolla, California, in the period April through September, 1967. Strickland, J., D., H., ed., *Scripps Institution of Oceanography Bulletin* 17, 1-22.

Strub, P., T., Shillington, F., A., James, C., Weeks, S., 1998. Satellite comparison of the seasonal circulation in the Benguela and California current systems. *South African Journal of Marine Science 19*, 99-112.

Stoens, A., Menkes, C., Radenac, M., H., Dandonneau, Y., Grima, N., Eldin, G., Memery, L., Navarette, C., André, J., M., Moutin, T., Raimbault, P., 1999. The coupled physical new production system in the equatorial Pacific during the 1992-1995 El Niño. *Journal of Geophysical Research* 104, 3323-3339.

Stuart-Menteth, A., C., Robinson, I., S., 2003. A global study of diurnal warming using satellite-derived sea surface temperature. *Journal of Geophysical Research* 108, 241-257.

Tauton-Clark, J., 1985. The formation growth and decay of upwelling tongues in response to the mesoscale wind field during summer. *South African Ocean Colour Experiment*. [Ed] Shannon, L., V. Sea Fisheries Research Institute, 47-61.

Touratier, F., Field, J., G., Moloney, C., L., 2003. Simulated carbon and nitrogen flows of the pplanktonic food web during and upwelling relaxation period in St Helena Bay (southern Benguela ecosystem). *Progress in Oceanography* 58, 1-41

Traganza, E., D., Silva, V., M., Austin, D., M., Hanson, W., L., Bronsink, S., H., 1983. Nutrient mapping and recurrence of coastal upwelling centres by satellite remote sensing: Its implication to primary production and the sediment record. Suess, E., Thiede, J., eds., *Coastal Upwelling. Its sediment record, part* A. 61-83.

Trenberth, K., Large, W., Olson, J., 1990. The mean annual cycle in global ocean wind stress. *Journal of Physical Oceanography* 20. 1742-1760.

Turk, D., McPhaden, M., J., Busalacchi, A., J., Lewis, M., R., 2004. Remotely Sensed Biological Production in the Equatorial Pacific. *Science* 293, 471-474.

Tyrrell, T., Lucas, M., I., 2002. Geochemical evidence of denitrification in the Benguela upwelling system. *Continental Shelf Research* 22 (2002), 2497–2511.

Tyson, P., D., Preston-Whyte. R., A., 2000. The weather and Climate of Southern Africa. *Oxford University Press-Cape Town* (2000), 396.

Waldron, H., N., Probyn., T., A., 1992. Nitrate supply and potential new production in the Benguela upwelling system. In the *Benguela Trophic Functioning*. Payne, A., I., L., Brink, K., H., Mann, K., H., and R. Hilborn (Eds). *South African Journal of Marine Science* 12, 29-39.

Waldron, H., N., Probyn, T., A., Brundrit, G., B., 1997. Preliminary annual estimates of regional nitrate supply in the Southern Benguela using coastal sea level fluctuations as a proxy for upwelling. *South African Journal of Marine Science* 18, 93-105.

Walton, C., C., 1988. Nonlinear multichannel algorithms for estimating sea-surface temperature with AVHRR satellite data. *Journal of Applied Meteorology* 27. 115-124.

Wang, D., McWilliams, J., C., Large, W., G., 1998. Large-eddy simulation of the diurnal cycle of deep equatorial turbulence. Journal of Physical Oceanography 28, 129-148.

Ward, B., Minnett, P., J., 2001. An autonomous profiler for near surface temperature measurements. Gas Transfer at Water Surfaces. *Geophysical Monography* 127, American Geophysical Union. 167-172

Weeks, S., J., 2004. Specific Applications of Satellite Remote Sensing to the Benguela Ecosystem. Submitted as requirement for a Doctor in Philosophy degree.

Weeks, S., J., Barlow, R., Roy, C., Shillington, F., A., 2006. Remotely sensed variability of temperature and chlorophyll in the southern Benguela: upwelling frequency and phytoplankton response. *African Journal of Marine Science* 28, 493-509.

Wijesekera, R., W., Gregg, M., C., 1996. Surface layer response to weak winds, westerly bursts, and rain squalls in the western Pacific warm pool. Journal of Geophysical Research 101, 977-997

Wijffels, S., Firing, E., Bryden, H., 1994. Direct observations of the Ekman balance at 10°N in the Pacific. *Journal of Physical Oceanography* 24, 1666-1679.

Yool, A., Martin, A., P., Fernanadez, C., Clark, D., R., 2007. The significance of nitrification of oceanic new production. *Nature* 447, 999-1002.

Zentara, S., J., Kamykowski, D., 1977. Latitudinal relationships among temperature and selected plant nutrients along the west coast of North and South America. *Journal of Marine Research* 35, 321-337.

Zhang, J., Gilbert, D., Gooday, A., J., Levin, L., Naqvi, S., W., A., Middelburg, J., J., Scranton, M., Ekau, W., Pena, A., Dewitte, B., Oguz, T., Monteiro, P., M., S., Urban, E., Rlabais, N., N., Ittekkot, V., Kemp, W., M., Ulloa, O., Elmgren, R., Escobar-Briones, E., Van Der Plas, A., K., 2010. Natural and human-induced hypoxia and consequences for coastal areas: synthesis and future development. *Biogeosciences* 7, 1443-1467.

Zimmerman, R., Kremer, J., N., Dugdale, R., 1987. Acceleration of nutrient uptake by phytoplankton in a coastal upwelling ecosystem: A modelling analysis. *Limnology and Oceanography* 32, 359-367.

Appendix I

The daily zonally averaged variables for 2003, 2004, 2006, 2007, 2008 and 2010.

2003

a)

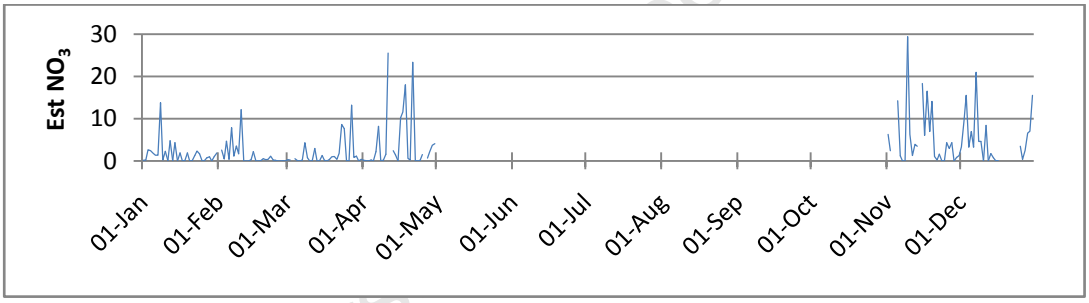

b)

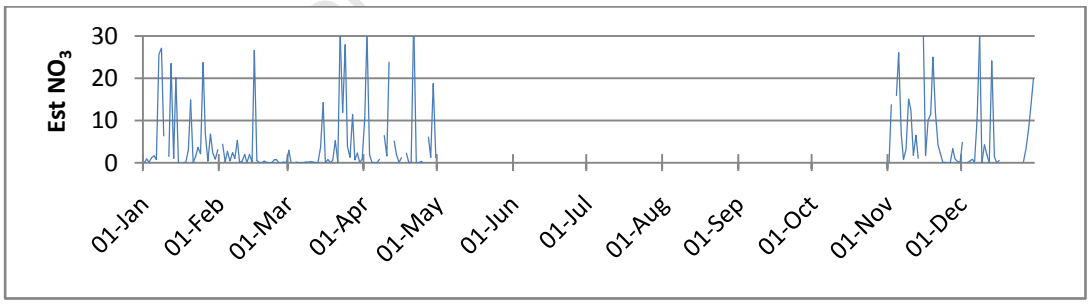

c)

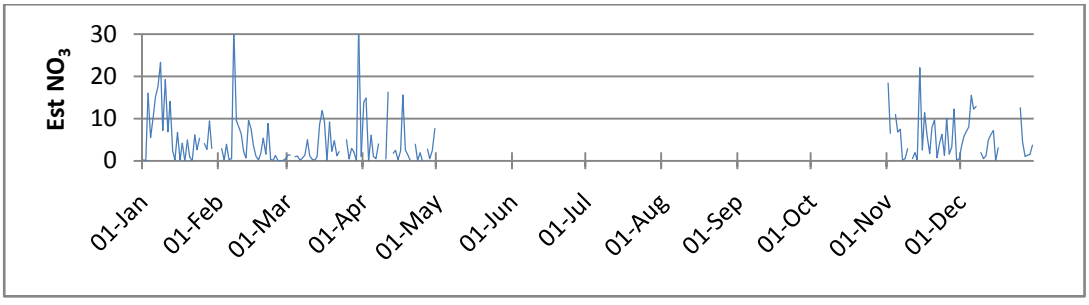

Figure A.I Daily averages of the estimated NO_3 (µmol/l), for the Namaqua zone (top panel), St Helena Bay zone(middle panel) and Cape Columbine zone (bottom panel) for 2003.

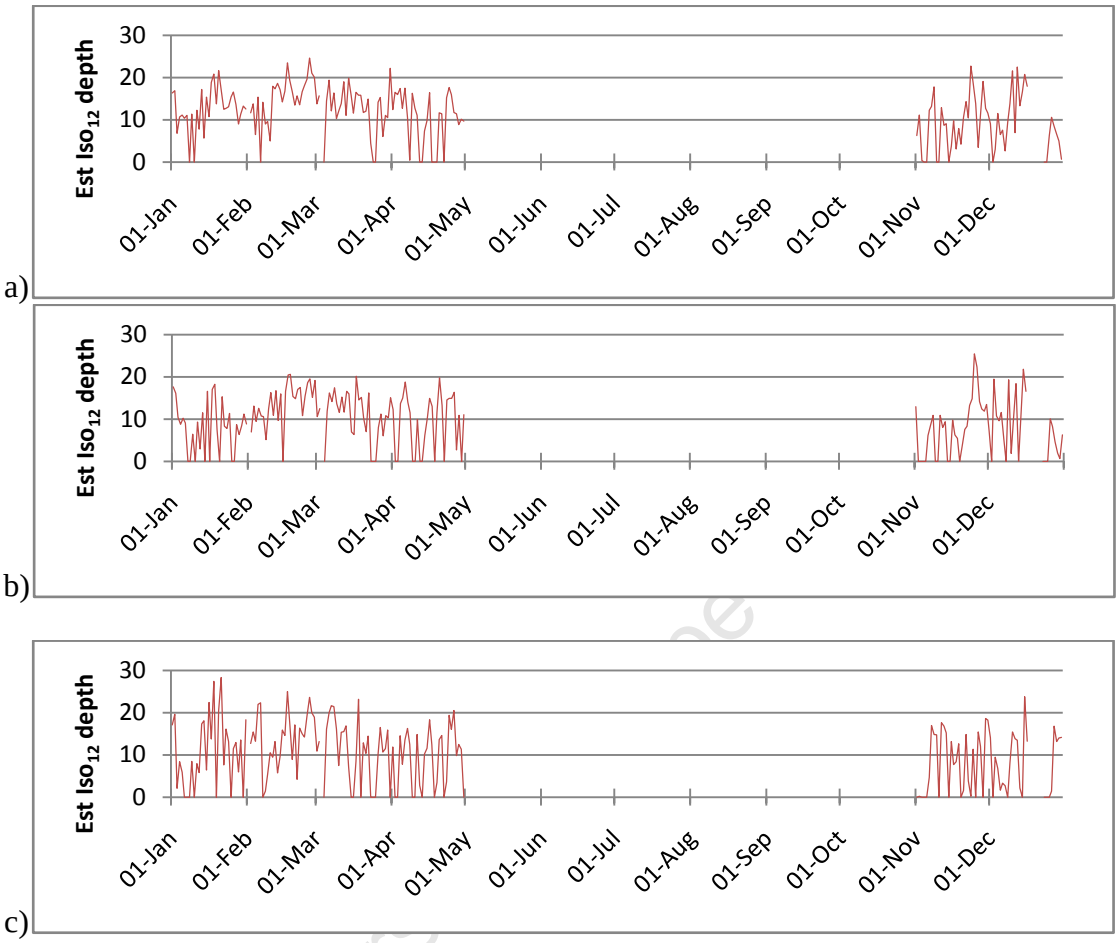

Figure A.2 Daily averages of the estimated Iso_{12} depths (m), for Namaqua zone (top panel), St Helena Bay zone(middle panel) and Cape Columbine zone (bottom panel) for 2003.

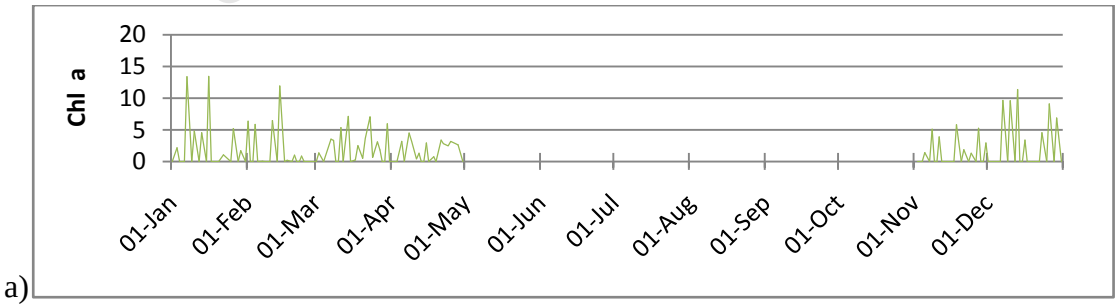

b)

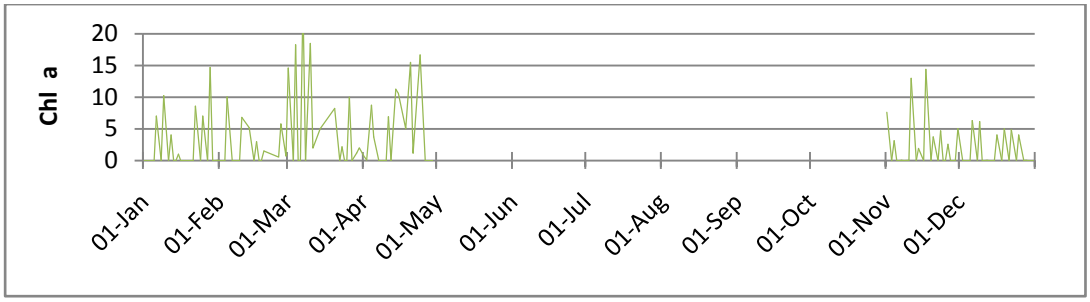

c)

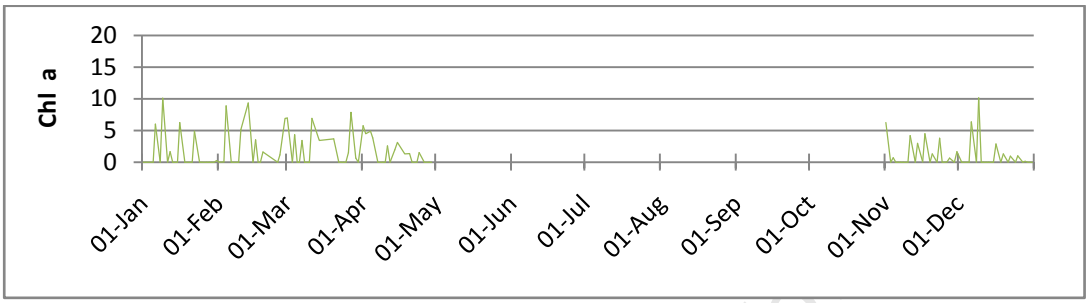

Figure A.3 Daily averages of the *chl a* concentrations (mg/m^3), for Namaqua zone (top panel), St Helena Bay zone(middle panel) and Cape Columbine zone (bottom panel) for 2003.

2004

a)

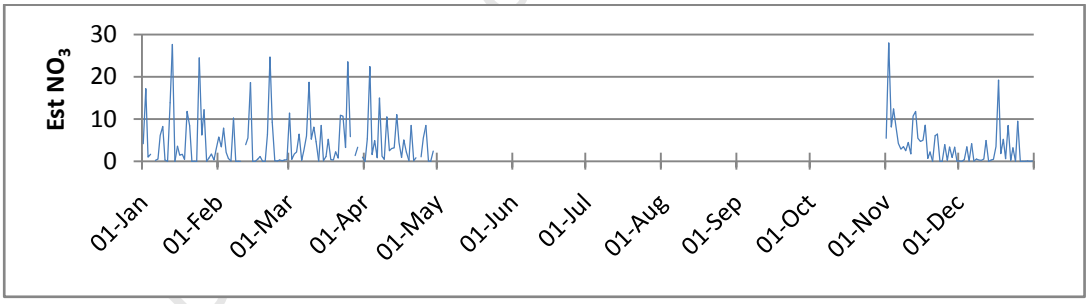

b)

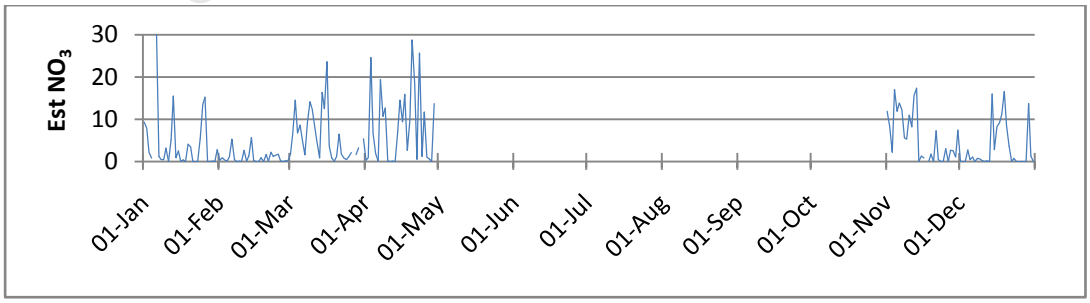

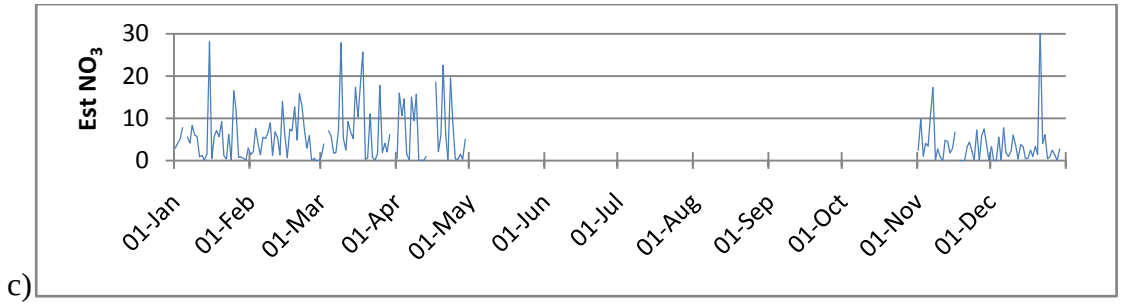

c)

Figure A.4 Daily averages of the estimated NO_3 (µmol/l), for the Namaqua zone (top panel), St Helena Bay zone(middle panel) and Cape Columbine zone (bottom panel) for 2004.

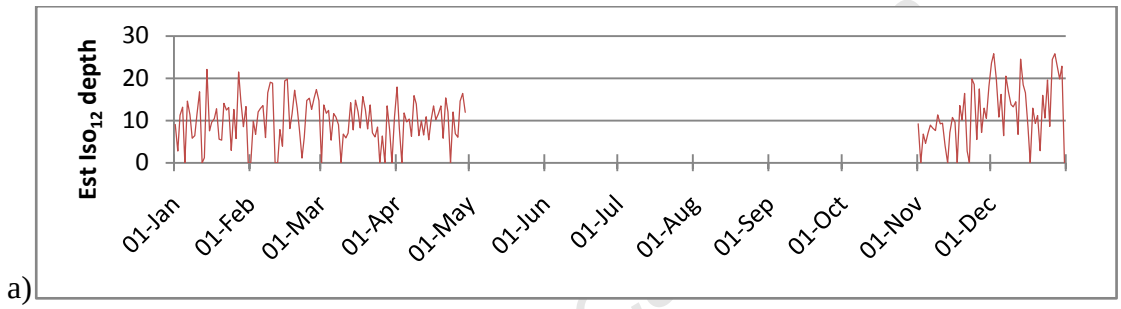

a)

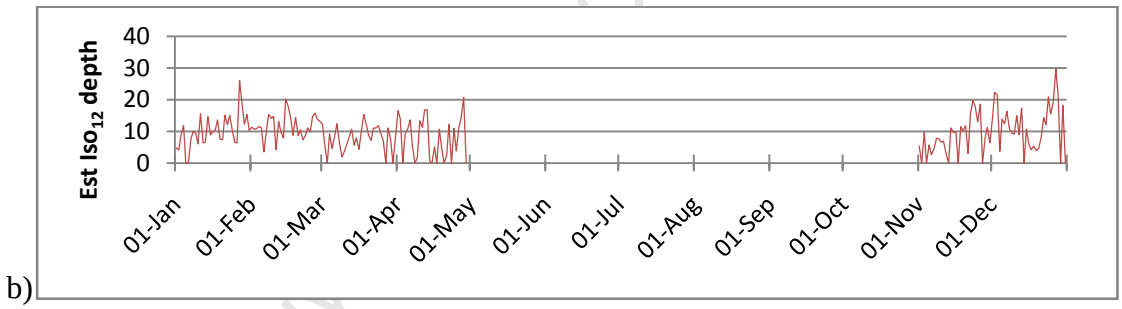

b)

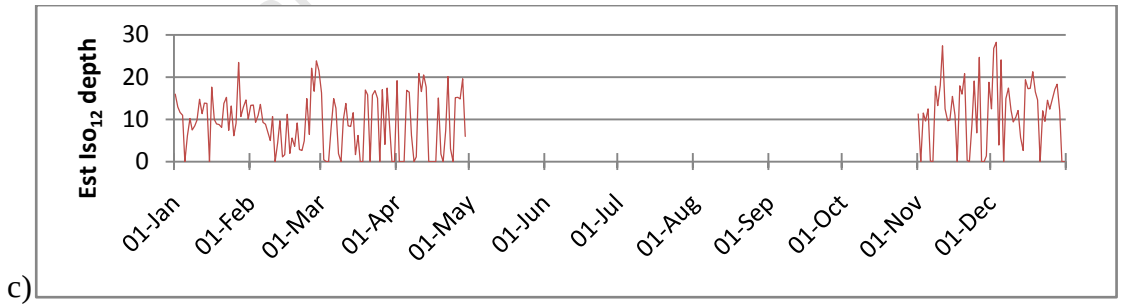

c)

Figure A.5 Daily averages of the estimated Iso_{12} depths (m), for Namaqua zone (top panel), St Helena Bay zone(middle panel) and Cape Columbine zone (bottom panel) for 2004.

a)

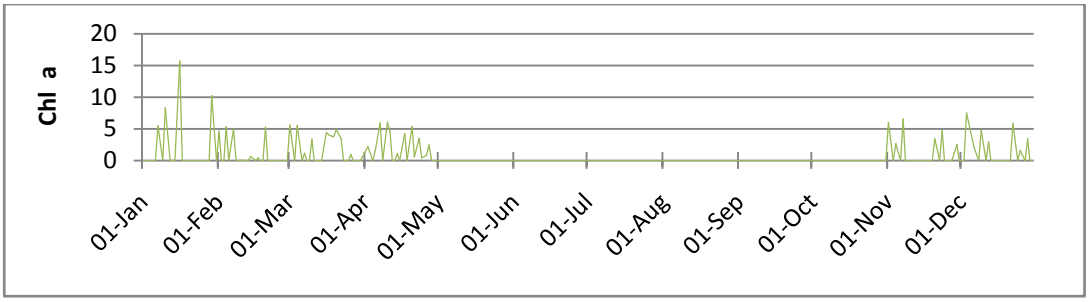

b)

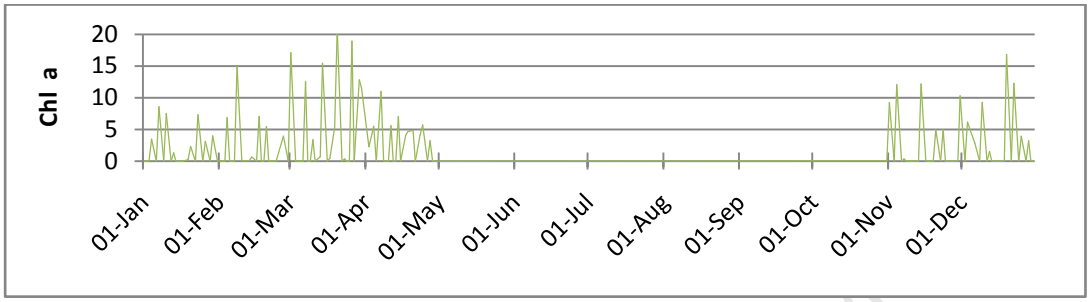

c)

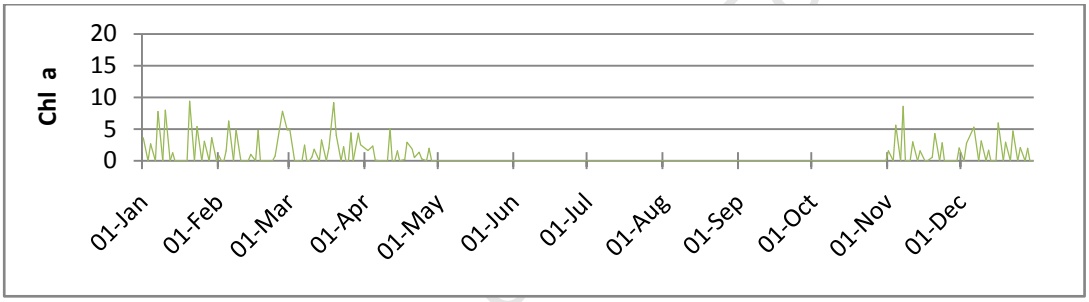

Figure A.6 Daily averages of the *chl a* concentrations (mg/m^3), for Namaqua zone (top panel), St Helena Bay zone (middle panel) and Cape Columbine zone (bottom panel) for 2004.

2006

a)

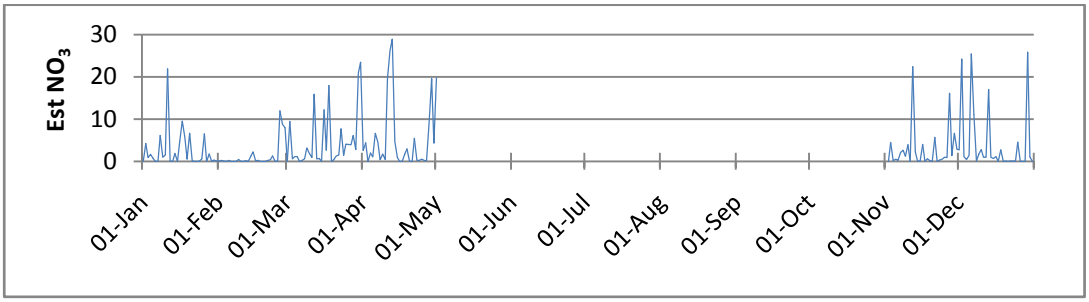

b)

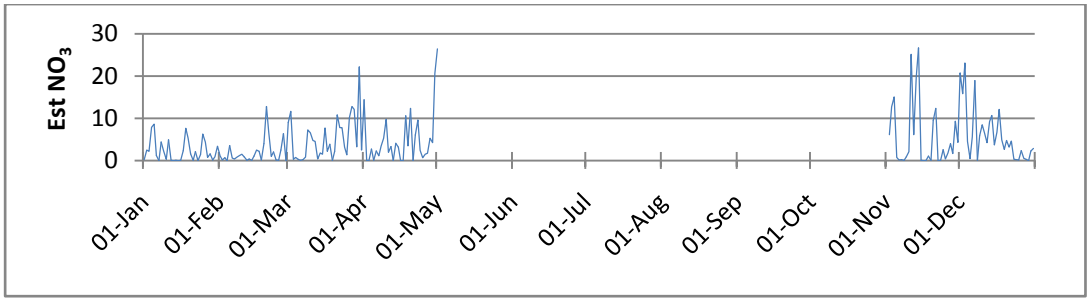

c)

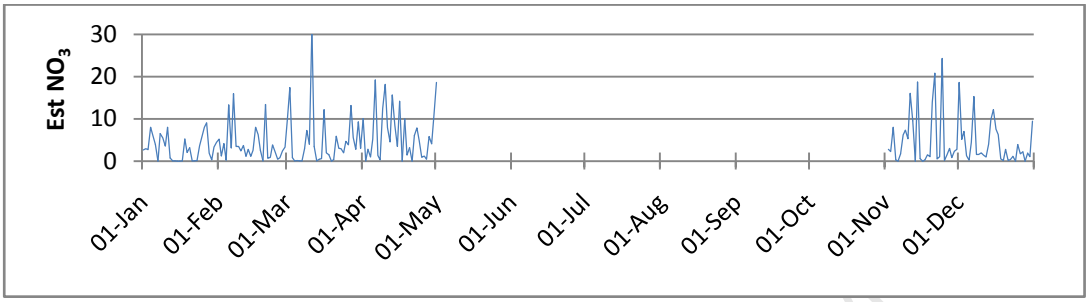

Figure A.7 Daily averages of the estimated NO_3 (µmol/l), for the Namaqua zone (top panel), St Helena Bay zone(middle panel) and Cape Columbine zone (bottom panel) for 2006.

a)

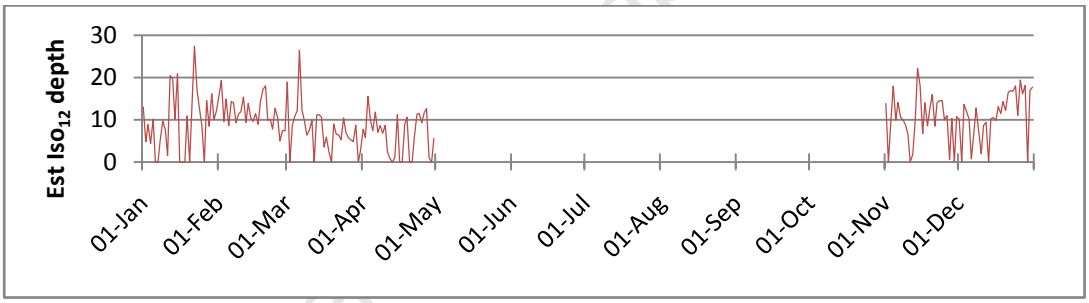

b)

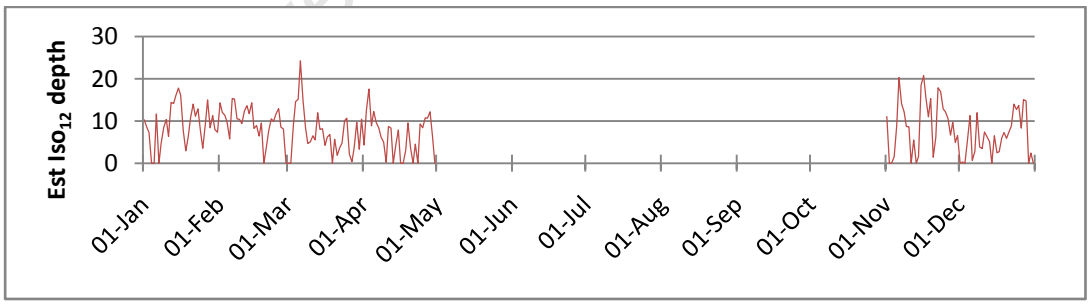

c)

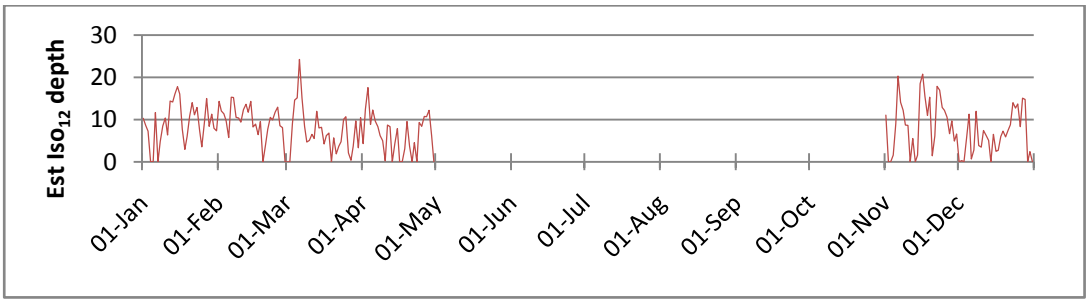

Figure A.8 Daily averages of the estimated Iso_{12} depths (m), for Namaqua zone (top panel), St Helena Bay zone(middle panel) and Cape Columbine zone (bottom panel) for 2006.

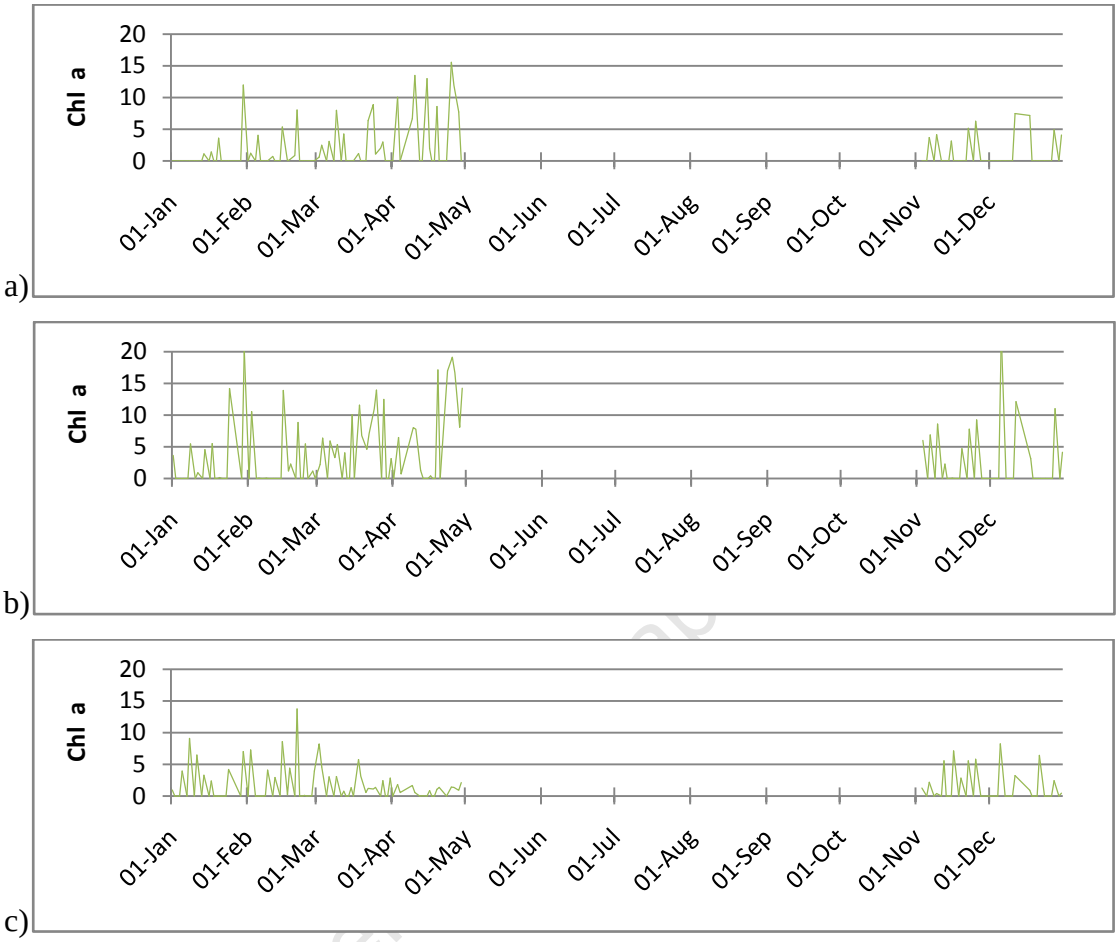

Figure A.9 Daily averages of the *chl a* concentrations (mg/m^3), for Namaqua zone (top panel), St Helena Bay zone (middle panel) and Cape Columbine zone (bottom panel) for 2006.

2007

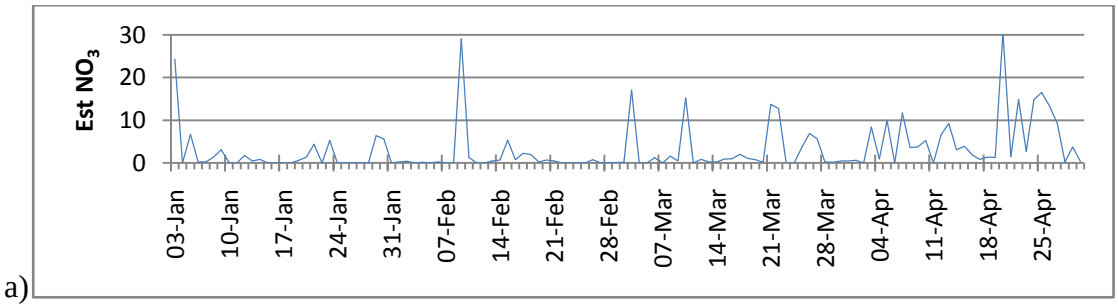

b)

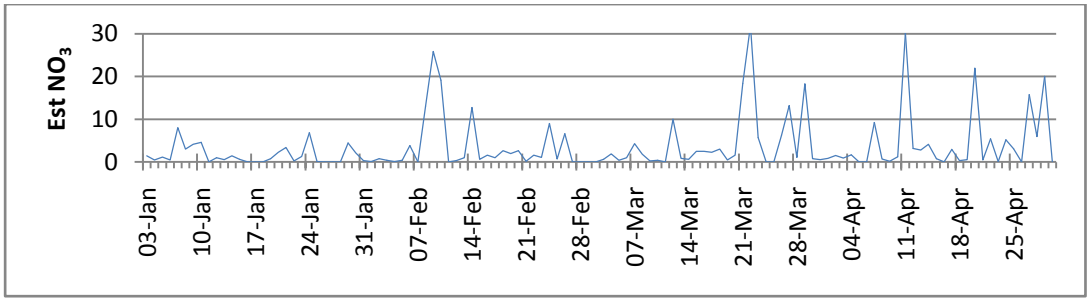

c)

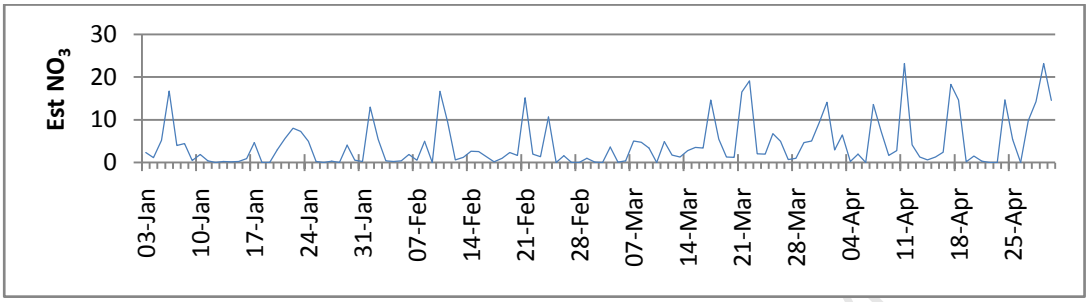

Figure A.10 Daily averages of the estimated NO_3 (µmol/l), for the Namaqua zone (top panel), St Helena Bay zone(middle panel) and Cape Columbine zone (bottom panel) for 2007.

a)

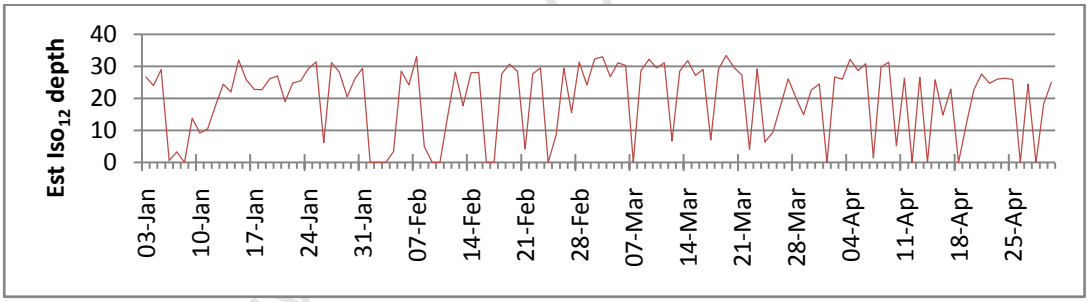

b)

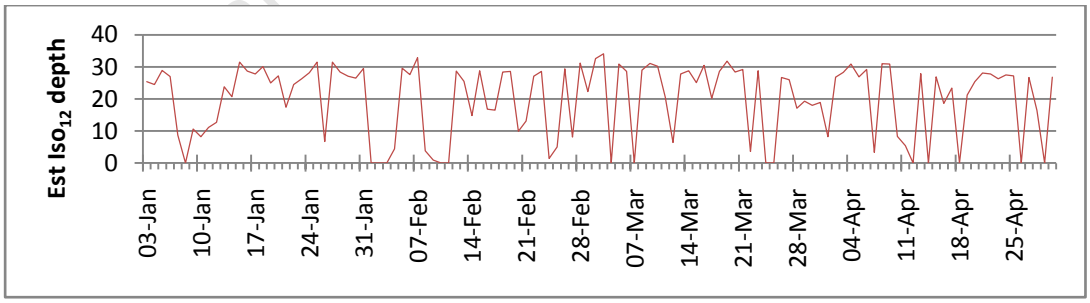

c)

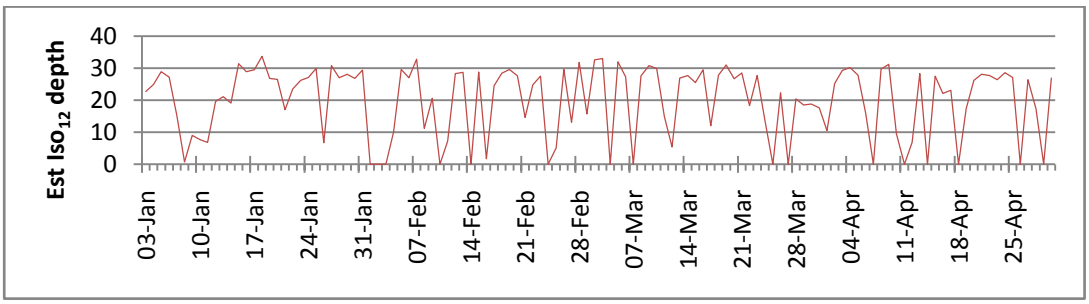

Figure A.11 Daily averages of the estimated Iso_{12} depths (m), for Namaqua zone (top panel), St Helena Bay zone(middle panel) and Cape Columbine zone (bottom panel) for 2007.

a)

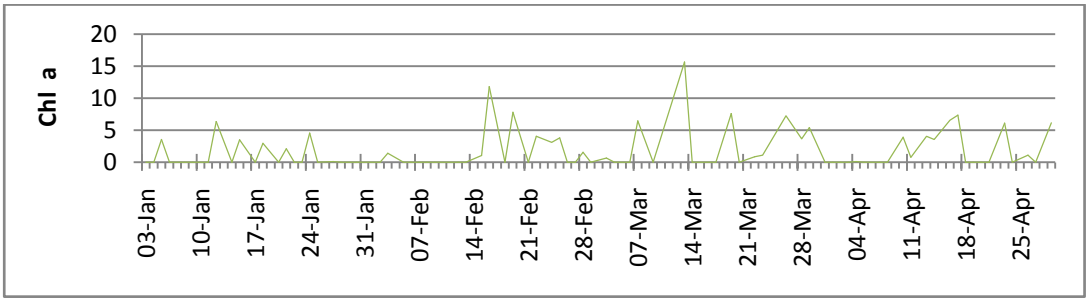

b)

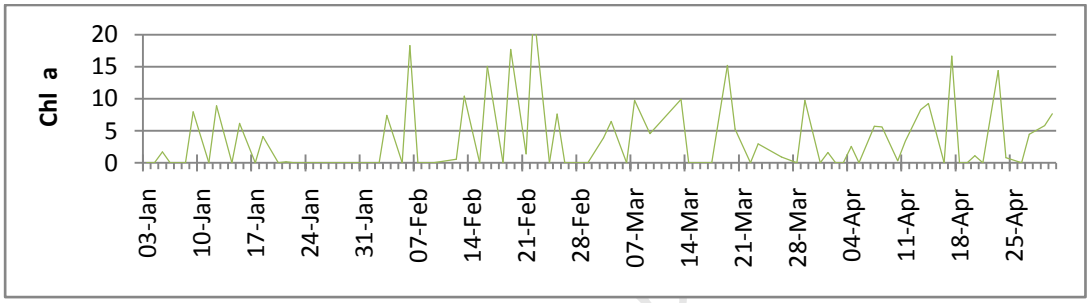

c)

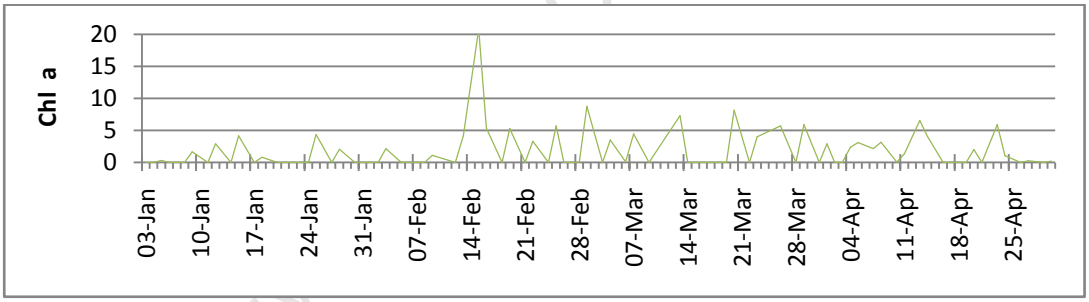

Figure A.12 Daily averages of the *chl a* concentrations (mg/m^3), for Namaqua zone (top panel), St Helena Bay zone (middle panel) and Cape Columbine zone (bottom panel) for 2007.

2008

a)

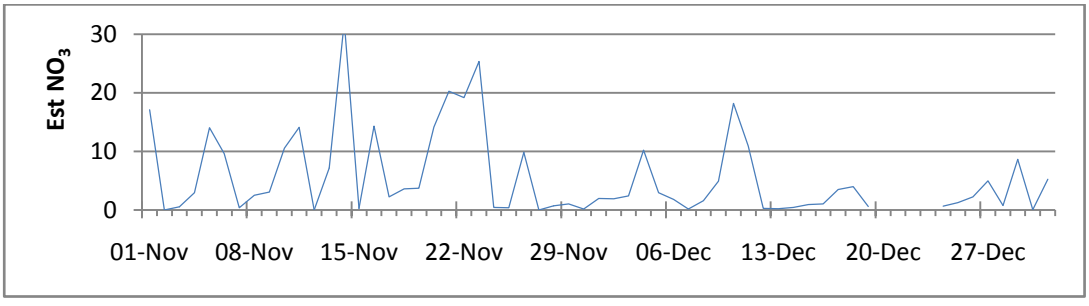

b)

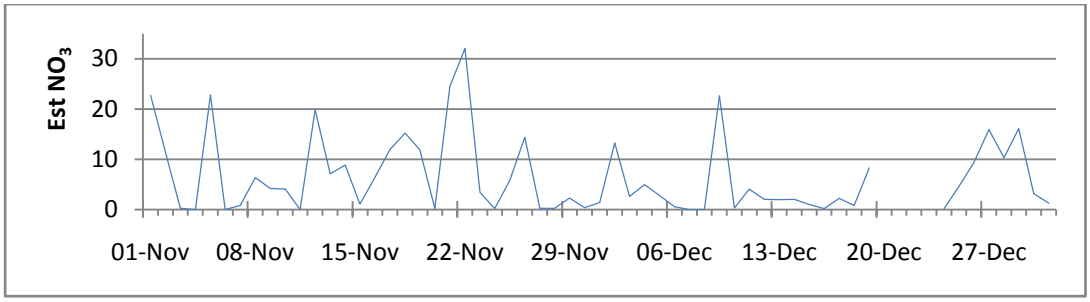

c)

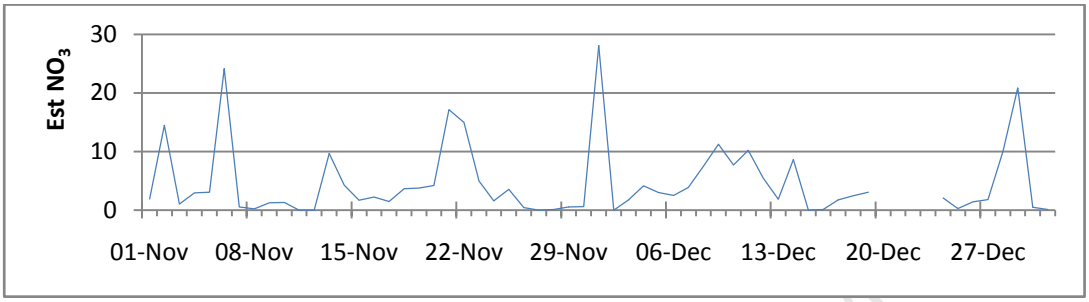

Figure A.13 Daily averages of the estimated NO_3 (µmol/l), for the Namaqua zone (top panel), St Helena Bay zone(middle panel) and Cape Columbine zone (bottom panel) for 2008.

a)

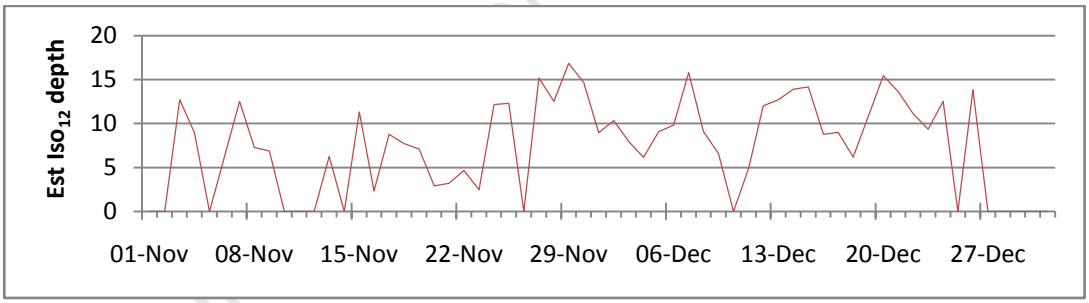

b)

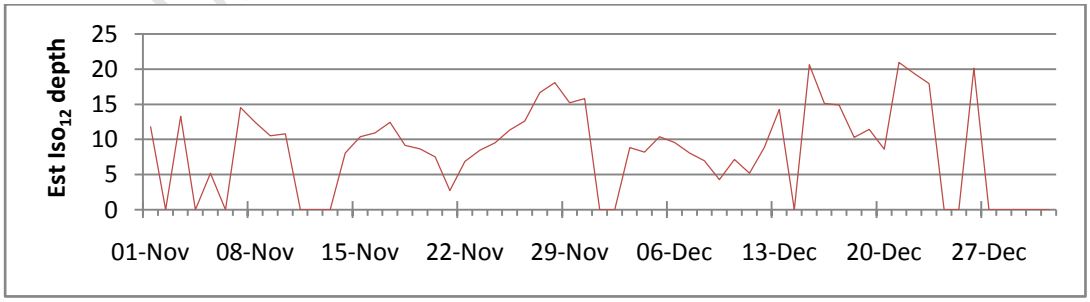

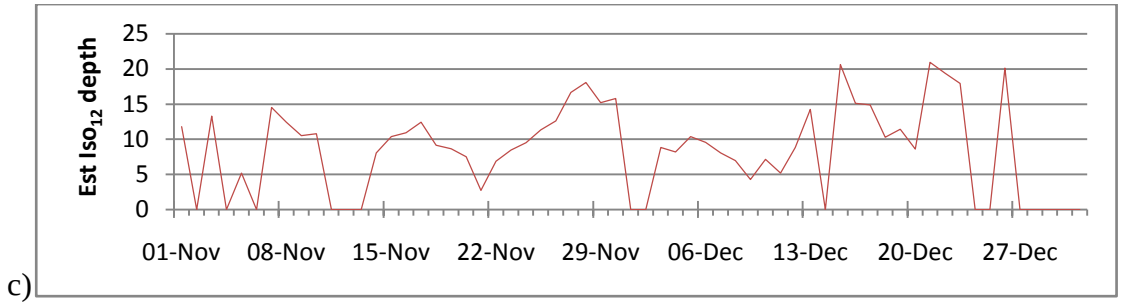

c)

Figure A.14 Daily averages of the estimated Iso_{12} depths (m), for Namaqua zone (top panel), St Helena Bay zone(middle panel) and Cape Columbine zone (bottom panel) for 2008.

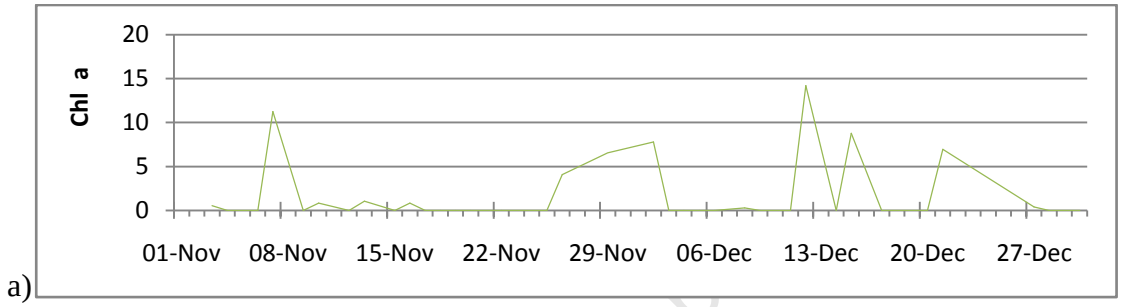

a)

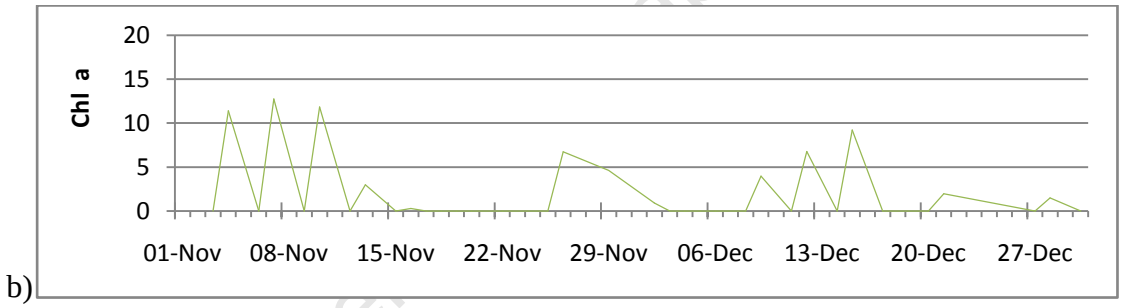

b)

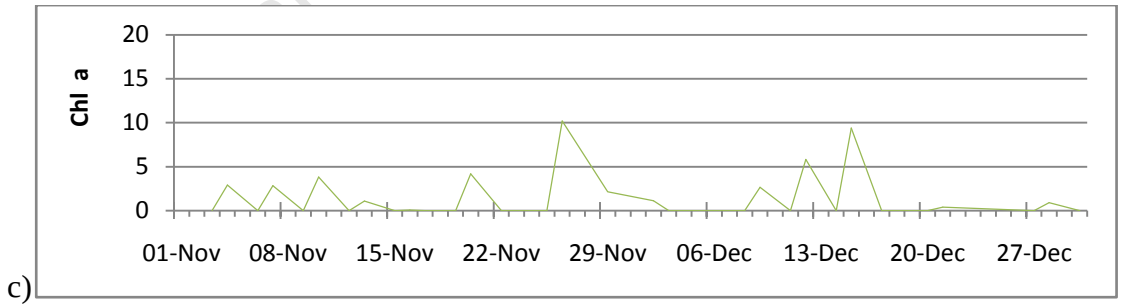

c)

Figure A.15 Daily averages of the *chl a* concentrations (mg/m^3), for Namaqua zone (top panel), St Helena Bay zone (middle panel) and Cape Columbine zone (bottom panel) for 2008.

2010

a)

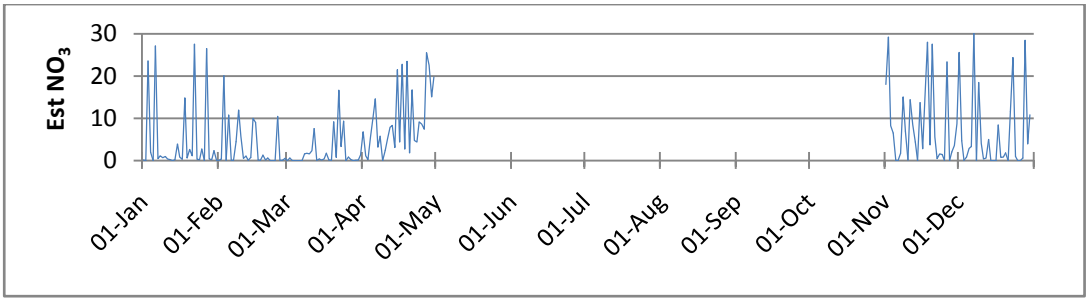

b)

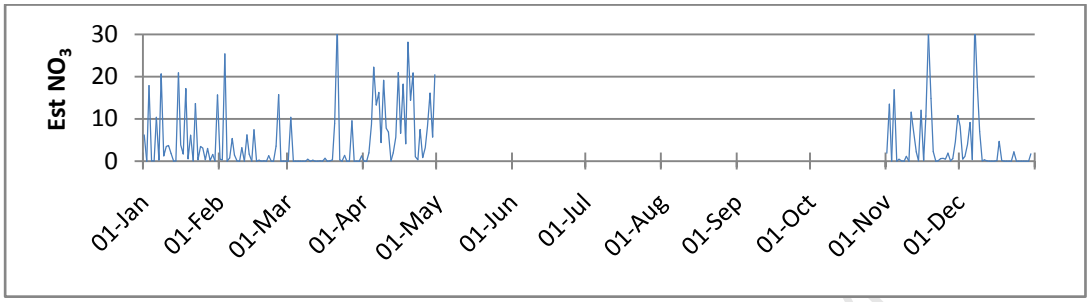

c)

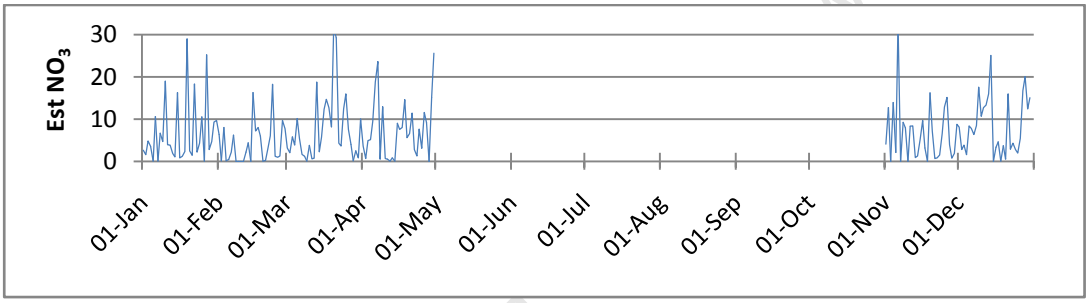

Figure A.16 Daily averages of the estimated NO_3 (µmol/l), for the Namaqua zone (top panel), St Helena Bay zone(middle panel) and Cape Columbine zone (bottom panel) for 2010.

a)

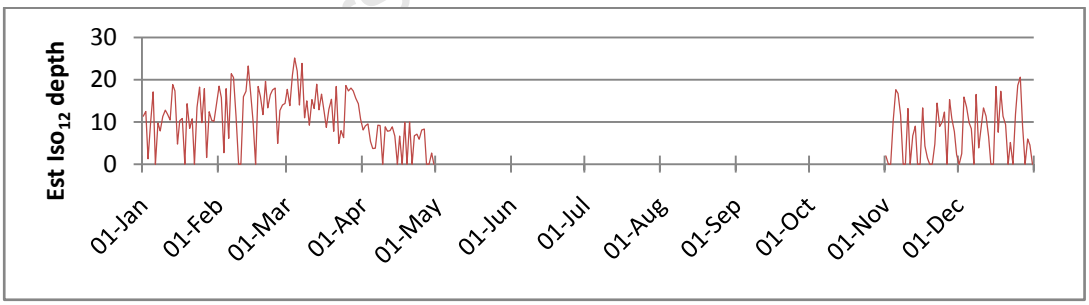

b)

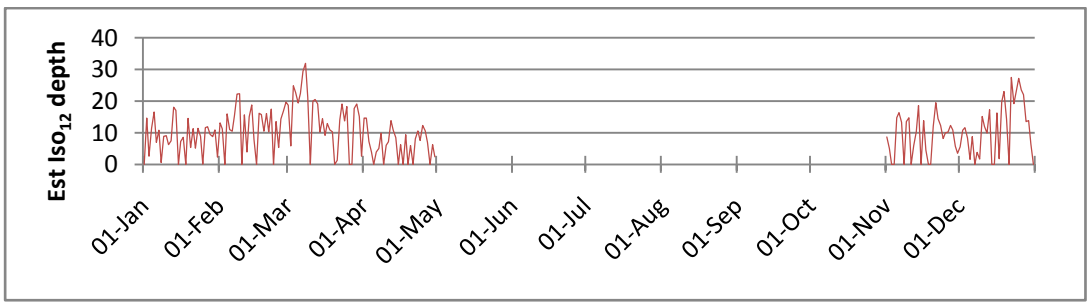

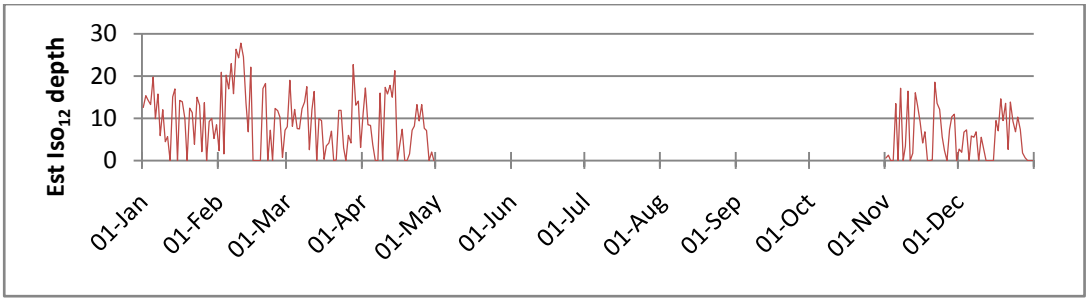

c)

Figure A.17 Daily averages of the estimated Iso_{12} depths (m), for Namaqua zone (top panel), St Helena Bay zone(middle panel) and Cape Columbine zone (bottom panel) for 2010.

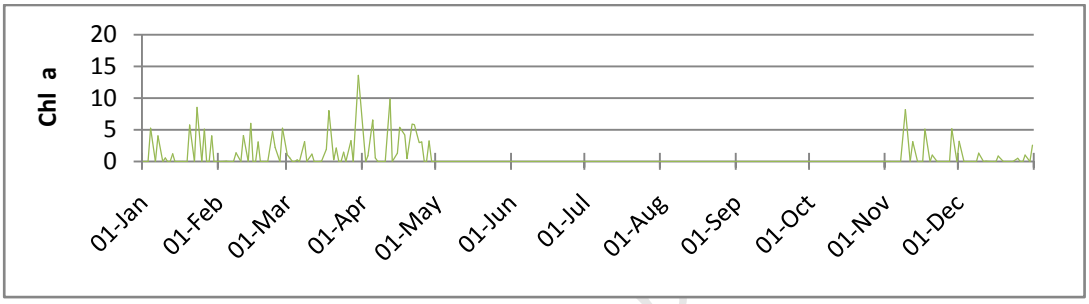

a)

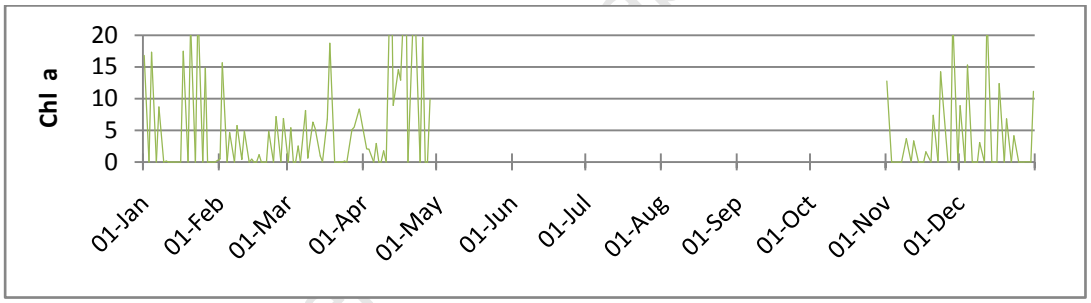

b)

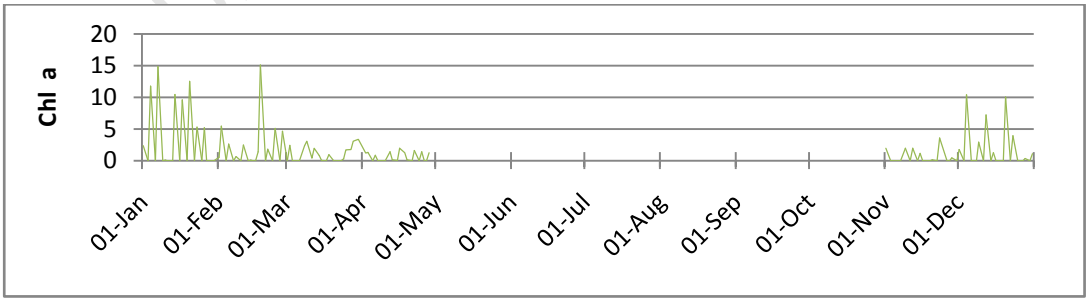

c)

Figure A.18 Daily averages of the *chl a* concentrations (mg/m^3), for Namaqua zone (top panel), St Helena Bay zone (middle panel) and Cape Columbine zone (bottom panel) for 2010.

Appendix II

MERIS FLAGS APPLIED

Name	Bit*	Brief Description
TOAVI_INVAL_REC	23	
ABSOA_DUST	9	Dust-like absorbing aerosol
MEDIUM_GLINT	21	Pixel corrected for medium level glint.
SUSPECT	11	Suspect flag (from level 1b): Transmission errors means measurements may be unreliable.
ABSOA_CONT	10	Continental absorbing aerosol
LAND	23	Pixel classified as land in L1B, adjusted radiometrically during L2 pixel classification to allow for geocorrection errors and tidal changes.

COASTLINE	13	Coastline flag
CLOUD	22	Pixel classified as cloud by the L2 cloud screening algorithm.
TOAVI_CSI	23	
HIGH_GLINT	21	Pixel with high sun-glint, which has not been corrected.
PCD_19	14	Confidence flag for MDS 19 (aero_epsilon, aero_opt_thick_). Raised when atmospheric correction fails, when there is whitecaps, or high yellow substance.
PCD_18	15	Confidence flag for MDS 18 (phoyosyn_rad). Raised when atmospheric correction fails, when there is whitecaps, or high yellow substance.
PCD_17	16	Confidence flag for MDS 17 (algal_2). Raised when PCD_13 is raised, or when the algorithm input or output is outside the expected range.
PCD_16	17	Confidence flag for MDS 16 (yellow_subs/total_susp). Raised when PCD_13 is raised, or when the algorithm input or output is outside the expected range.
PCD_15	18	Confidence flag for MDS 15 (algal_1). Raised when atmospheric correction fails, when there is whitecaps, or high yellow substance.
COSMETIC	12	Cosmetic flag (from L1B). Missing data filled by interpolation.
DDV	3	Dark dense vegetation.
CASE2_Y	21	Yellow substance loaded water.
CASE2_S	8	Turbid water, nominally TSM > 0.3 g/m^3.
P_CONFIDENCE	2	The two atmospheric pressure estimates do not compare successfully.
LOW_PRESSURE	0	Pressure computed from data lower than ECM/WF pressure.
ICE_HAZE	21	Pixel with high radiance in the blue, likely to be caused by ice or high aerosol load.
PCD_1_13	20	Confidence flag for MDS 1 to 13 (reflectance's).
CASE2_ANOM	21	Bright water pixel, anomalous scattering water. Flags the presence of Case 2 water.
TOAVI_WS	23	
TOAVI_BRIGHT	23	Bright land pixel, suspect vegetation index.

TOAVI_BAD	23	Top of atmosphere vegetation index is no good.
WATER	21	Pixel classified as ocean in L1B, adjusted radiometrically during L2 pixel classification to allow for geo-correction errors and tidal changes in land/ water boundary.

*Binary position when containing 1 when the flag is set.